

POLITECNICO DI TORINO

Collegio di Ingegneria Civile

**Corso di Laurea Magistrale
in Ingegneria Civile**

Tesi di Laurea Magistrale

Displacement based seismic vulnerability analysis of steel frame buildings



Relatori

KU Leuven

prof. Geert Degrande
prof. Barbara Rossi

Politecnico di Torino

prof. Rosario Ceravolo

Candidato

Hicham Argane

Marzo 2018

Preface

First of all, I would like to extend my genuine thanks to my main supervisor Professor Geert Degrande for his guidance, constructive support and valuable advice throughout my thesis studies at KU Leuven.

I would like also to express my gratitude to my co-supervisor Doctor Hernan Garcia for his constant support, availability and helpful suggestions.

A special thanks to Professor Barbara Rossi and Engineer Tom Molken for their collaboration and the useful material provided.

My sincere thanks go also to Professor Rosario Ceravolo for his help as supervisor at the Politecnico di Torino and to Professor Cecilia Surace for her continuous support and encouragement during my stay at the host institution.

Hicham Argane

Contents

Preface	i
Abstract	iv
List of Figures	v
List of Tables	ix
1 Introduction	1
1.1 Background	1
1.2 Scope	1
1.3 Objective	2
1.4 Outline of the content	3
2 State of the art of seismic vulnerability assessment	5
2.1 Introduction	5
2.2 Empirical methods	7
2.2.1 Damage probability matrices	8
2.2.2 Continuous Vulnerability Curves	9
2.3 Analytical methods	9
2.3.1 Displacement-Based Methods	11
2.3.2 General Remarks on Analytical Methods	14
3 Non-linear static procedures	15
3.1 Introduction	15
3.2 Modal Pushover Analysis	16
3.2.1 MDOF to SDOF transformation	16
3.2.2 Step-By-Step Procedure	19
3.3 N2 Method in CSM format	22
3.3.1 Capacity Curve	22
3.3.2 Seismic Demand	23
3.3.3 SDOF displacement demand	25
3.3.4 MDOF system seismic demand	29
3.4 Conclusion	29
4 Case studies	31
4.1 SAC-9 Building	31
4.2 Modeling of SAC-9 building	33
4.2.1 Concentrated plasticity model	35

4.2.2	Seismic input	39
4.2.3	Modal Pushover Analysis	39
4.2.4	N2 Method	46
4.2.5	Results Discussion	50
4.3	Helix parking	52
4.3.1	Overview	52
4.3.2	Loads	52
4.3.3	Structural behaviour	55
4.3.4	Modelling of the Helix-Parking	55
4.3.5	Seismic Assessment Features	56
4.3.6	Results discussion	62
4.3.7	Displacement-based control of damage	63
5	Fragility curves	65
5.1	Introduction	65
5.2	Fragility Curves	65
5.2.1	Performance Levels	68
5.2.2	Seismic input	69
5.3	Results Discussion	70
5.3.1	SAC-Building	70
5.3.2	Helix Parking	76
5.4	Accuracy of MPA-based fragility curves	82
6	Conclusion	87
A	The First Appendix	91
A.1	Pushover curves parameters	91
A.1.1	SAC-9	91
A.1.2	Helix-Parking	91
A.2	IDA results	94
A.2.1	SAC-9	94
A.2.2	Helix-Parking	106
	Bibliography	119

Abstract

The seismic vulnerability defines susceptibility of a building or group of buildings to undergo damage due to seismic ground motion. It is a common practice to represent vulnerability information by way of fragility curves. The analytical curves are derived by numerically reproducing seismic response by means of structural dynamic analysis. Although the most rigorous analytical method consists in the use of full non-linear response history analysis, the inherent high computational cost of this tool appears to be a relevant obstacle for its wide use in the professional practice. The pursuit of a reliable and more efficient alternative led to the development and the increasing interest in the simplified non linear analysis, referred to generally as the Non-linear Static Procedures (NSP). In line with this tendency, this thesis considers a practicable method for deriving fragility curves by using the NSPs for two steel structures with different lateral bearing systems. To this end, responses for different ground motion scenarios are preliminary evaluated by the most common non-linear static methods, namely the Capacity Spectrum Method, the N2 method and the Modal Pushover Analysis, and are compared with those by the response history analysis. Based on this analysis, approximate NSP-based fragility curves for both case studies are derived and are examined in contrast with those by response history analysis. The comparison indicates NSP-based approximate fragility curves are fairly accurate over the entire range of ground motion intensity and damage, even close to collapse.

List of Figures

2.1	The different methodologies for the seismic vulnerability assessment.(Adapted from (Calvi et al. 2006))	6
2.2	The different components of the evaluation of analytical vulnerability functions and DPMs (adapted from Dumova (2004))	10
2.3	Fitted analytical fragility curves for different damage levels	11
2.4	Simplified scheme for the transformation from an MDOF system to an equivalent SDOF system.	12
2.5	Distributed damage/ ductile failure mechanism (left) and soft-storey failure mechanism (right).	12
2.6	In-plane deformed shapes for different masonry limit states	13
2.7	Intersection of the reduced demand spectrum and the capacity area for different building typologies	13
2.8	Vulnerability curves for a bridge model for State of Minor Damage (a) and for State of Major Damage (b), from Shinozuka,2001	14
3.1	Schematic representing the generation of an equivalent SDOF system by pushover analysis from FEMA 440	16
3.2	Idealization of the pushover curve using the equal energy principle.	19
3.3	Flow chart depicting simplified SDOF nonlinear analysis process.(from (FEMA 440))	20
3.4	Flow chart depicting simplified SDOF non-linear analysis with the seismic demand estimated from elastic response spectrum from FEMA 440.	21
3.5	Comparison of base shear coefficients from elastic design spectrum and <i>International Building Code</i> . From (Chopra 1998)	23
3.6	Elasto-plastic system and its corresponding linear system. From (Chopra 1998)	24
3.7	Ductility-dependent reduction factor R_μ spectrum	25
3.8	Demand spectra for constant ductilities	26
3.9	Demand spectra for constant ductilities in ADRS format	27
3.10	Illustration of the main steps of the iterative procedure.	27
3.11	Demand and capacity spectra for two illustrative examples from Fajfar 1999	28

LIST OF FIGURES

3.12	Torsional effects in terms of normalized top displacements obtained by N2 method as the envelop of the results obtained by modal analysis and pushover analysis, from Fajfar 2005.	29
4.1	Los Angeles 9-storey SAC building adapted from Chopra et al 2002. . .	32
4.2	Typical column-beam welded connection with panel zone strengthened with doublers.	34
4.3	Principles of the use of a dummy column to include P- Δ effects.	35
4.4	Modelling interior (gravity) columns to include P-Delta effects.	36
4.5	Model with concentrated non linear zones at extremes of frame members	36
4.6	Description of chord rotation, adapted from FEMA356.	38
4.7	Generalized element moment-rotation relations for modelling and acceptance criteria, adapted from FEMA356.	38
4.8	North-South component of El Centro ground motion from PEER's database.	39
4.9	Elastic response spectrum of El-Centro ground motion.	40
4.10	Mode 1	40
4.11	Mode 2	40
4.12	Mode 3	40
4.13	First three vibrational mode shapes of the SAC-9 building.	40
4.14	Load patterns $s_n = m\phi_n$, $n = 1, 2, 3$ normalized to the roof lateral force.	41
4.15	Modal pushover curves obtained with lateral load patterns proportional to the first three mode shapes of SAC-9.	42
4.16	Hinge locations and deformation degree at intermediate steps of the pushover analysis with s_1 load pattern	43
4.17	Displacement time histories of the equivalent SDOF systems excited by 0.7 x El-Centro (a), 1 x El-Centro (b) and 1.5 x El-Centro ground motion (c).	45
4.18	Representation in the ADRS format of the capacity curves of the SDOF systems and the elastic demand spectrum corresponding to different intensities of El Centro ground motion.	47
4.18	Representation in the ADRS format of the capacity curves of the SDOF systems and the elastic demand spectrum corresponding to different intensities of El Centro ground motion (cont.)	48
4.19	Iterative (a) and simplified (b) procedures for the determination of the displacement demand of the first SDOF system.	49
4.20	The effect of higher modes contributions on height-wise variation of floor displacements (a) and storey drift ratios (b) from MPA compared with non linear RHA for 1.5 x El Centro ground motion.	51
4.21	Height-wise variation of floor displacements (c) and storey drift ratios (d) from N2 method and MPA compared with non-linear RHA for 1.5 x El Centro ground motion	51
4.22	(a) 3D representation of the Helix-parking, (b) plan and lateral view. . .	53
4.23	(a) columns profiles and (b) beams profiles.	54
4.24	Lateral load absorption mechanism by the braces.	56

4.25	Representation of the selected ground motions response spectra, the average spectrum and the Eurocode 8 elastic spectrum	57
4.26	3D representation of the mode shapes of the Helix-parking	58
4.27	Modal pushover curves of Helix parking idealised with bilinear relations.	60
4.28	Top displacements in the x-direction (a) and y-direction(b) in correspondence to CM and the edging frames	61
4.29	Elastic demand spectra and capacity curves in the x-direction (a) and y-direction(b).	62
4.30	Torsional effects in terms of normalized top displacements obtained by the extended N2 method, by modal analysis and by pushover analysis.	62
4.31	Height-wise variation of level displacements and level drift ratios from MPA, N2 method and the mean value of non-linear RHA.	63
4.32	Inter-storey drift damage limitation according to EC8 for frame TF2	64
5.1	Acceleration spectra for each of the two components of the ten ground motions selected from the European Strong Database, and their mean acceleration response spectra in bold red	70
5.2	IDA of the contributions of the SAC-9 equivalent SDOF systems to the maximum roof displacement	71
5.3	Functions defining the relations between the the roof displacement and the corresponding maximum inter-storey drift for load patterns proportional to the first mode shape (a), the second mode (b) and the third mode shape (C).	72
5.4	15, 50, and 85% fractile IDA curves for the 9-SAC building from MPA-based approximate procedure.	73
5.5	Sac-9' observed fractions of exceedances and fitted fragility functions obtained using the maximum likelihood approach for Immediate Occupancy (a), Life Service (b) and Collapse Prevention performance levels (c).	75
5.5	SAC-9' observed fractions of exceedances and fitted fragility functions obtained using the maximum likelihood approach for Immediate Occupancy (a), Life Service (b) and Collapse Prevention performance levels (c) (cont.)	76
5.6	Incremental Dynamic Analyses of the building top displacement by combining the contributions of the SDOF systems acting along the x-direction (a), and the y-direction (b).	77
5.7	78
5.8	15, 50, and 85% fractile IDA curves for the Helix-Parking building from MPA-based approximate procedure along the x-direction (a) and the y-direction (b).	79
5.9	Observed fractions of exceedances and fitted fragility functions obtained using the maximum likelihood approach for Immediate Occupancy (a), Life Service (b) and Collapse Prevention performance levels (c)	81

LIST OF FIGURES

5.9	Observed fractions of exceedances and fitted fragility functions obtained using the maximum likelihood approach for Immediate Occupancy (a), Life Service (b) and Collapse Prevention performance levels (c) (cont.) .	82
5.10	Immediate Occupancy, Life Service and Collapse Prevention fragility curves for SAC-9 building from N-RHA (exact) versus MPA-based approximate procedure.	84
5.11	Immediate Occupancy, Life Service and Collapse Prevention fragility curves for Helix-Parking from N-RHA (exact) versus MPA-based approximate procedure.. . . .	85

List of Tables

2.1	Format of the Damage Probability Matrix proposed by Whitman et al. (1973)	8
4.1	Section properties for columns and beams.	33
4.2	Materials mechanical properties	33
4.3	Additional masses on the building floors	34
4.4	Moment-rotation relation parameters and acceptance criteria ranges for the different sections of the frame members computed using FEMA356 recommended equations.	37
4.5	Performance level of steel buildings, adapted from FEMA356	38
4.6	Transition periods and amplification factors for the construction of a simplified smooth elastic response spectrum of El Centro ground motion.	39
4.7	Properties of the inelastic SDOF systems	42
4.8	The peak displacements of the equivalent SDOF systems and the corresponding contributions to the SAC-9 roof displacement under different intensities of El-Centro ground motion.	44
4.9	Intermediate results of the iterative procedure for the determination of the target displacement of the first inelastic system under 1.5 X El Centro ground motion	46
4.10	Section profiles of primary, secondary beams and columns of the ramps connecting the different levels.	52
4.11	Mechanical properties of the materials.	54
4.12	Imposed loads on garages and vehicle traffic areas, from EC1	55
4.13	Parameters of the seven bi-directional ground motions compatible with EC8 selected from the European Strong Motion Database	57
4.14	Properties of the structure significant modes in terms of natural vibration periods and modal mass participation ratios for the first five modes.	59
4.15	Properties of the equivalent inelastic Single Degree of Freedom system	59
5.1	Structural performance level and the associated damage moment frame structures and braced structures form FEMA356.	69
5.2	Characteristic properties of selected records	70

LIST OF TABLES

5.3	SAC-9' observed fractions of exceedances, the Likelihood function values and the Cumulative Distribution function values for each intensity level, for the three performance levels considered.	74
5.4	Helix-Parking's observed fractions of exceedances, the Likelihood function values and the Cumulative Distribution function values for each intensity level, for the three performance levels considered.	80
5.5	Approximate and exact values of fragility curves for both case studies. .	83
A.1	Pushover curves values for the three equivalent SDOFs.	92
A.2	Pushover curves values for the five equivalent SDOFs.	93
A.3	MPA-based IDA for the 295 record.	95
A.4	MPA-based IDA for the 239 record.	96
A.5	MPA-based IDA for the 123 record.	97
A.6	MPA-based IDA for the 336 record.	98
A.7	MPA-based IDA for the 536 record.	99
A.8	MPA-based IDA for the 6264 record.	100
A.9	MPA-based IDA for the 196 record.	101
A.10	MPA-based IDA for the 947 record.	102
A.11	MPA-based IDA for the 595 record.	103
A.12	MPA-based IDA for the 244 record.	104
A.13	Exact IDA for the ten records.	105
A.14	IDA for both components of the record 295.	107
A.15	IDA for both components of the record 239	108
A.16	IDA for both components of the record 123.	109
A.17	IDA for both components of the record 336.	110
A.18	IDA for both components of the record 536	111
A.19	IDA for both components of the record 6264.	112
A.20	IDA for both components of the record 196.	113
A.21	IDA for both components of the record 947.	114
A.22	IDA for both components of the 595 record.	115
A.23	IDA for both components of the 244 record.	116
A.24	Exact IDA for the records considered	117
A.25	Exact IDA for the records considered (cont.)	118

Chapter 1

Introduction

1.1 Background

Belgium lies within an intraplate region of North-western Europe. Comparing to Mediterranean inter-plate zones the seismic hazard in this region is supposed to be low. However, the recent seismic activities showed not only that Belgium is not immune to earthquake but even further that the future occurrence of 6.5 magnitude ground motion is not inconceivable [1]. During the last two decades Belgium has been affected by two damaging earthquakes in 1983 (Liege) and in 1992 (Roermond). The Liege earthquake, which reached an intensity VII on MSK scale resulting in considerable damage to ordinary buildings brought attention of the authorities and experts for the vulnerability of the existing structures and the new structures to be built in the region [2]. After this event, a seismic hazard map was assessed for the whole territory of Belgium. Nevertheless, up to 2011 the seismic risk was accounted only for very important structures such as the nuclear power plants [3]. However, since 2011, application of Eurocode 8 is required [4]. The EC8 defines the common European rules for the design and assessment of civil engineering structures in seismic areas. The EC8 should be applied in conjunction with the national annex which defines the seismic hazard in terms of reference peak ground acceleration. The effective seismic loading is defined in terms of an elastic response spectrum that defines the spectral acceleration in terms of the structural period depending on the importance factor of the structure, structural damping and local soil conditions [5]. In the light of this and considering that the introduction of seismically resistant design in the engineering practice is very recent in Belgium, more studies inherent to seismic vulnerability assessment of the different typologies of existing buildings are needed. This thesis, which the first in the field of seismic vulnerability assessment of structures at KU Leuven University, aligns with this perspective.

1.2 Scope

The seismic risk is defined as the overall expected damage from earthquake in a given time interval. In a given geographical area the importance of seismic risk

depends on the region seismic activity as well as on the structures and infrastructures vulnerability. The seismicity level, refereed also as seismic hazard, is a physical property defined as the probability of occurrence of earthquakes that exceed a prefixed intensity, magnitude or acceleration. Seismic vulnerability, on the other hand, may be defined as the susceptibility of a building to be affected by a given degree of damage due to a certain level of ground shaking. In the recent years there is an increasing research in the development of seismic vulnerability assessment techniques that can be divided in two main categories: empirical and analytical methods [6]. The empirical approach consists essentially in correlating the damage data and intensity of past earthquakes, whereas the analytical methods are based on numerical simulations of the seismic response at different levels of ground motion intensity. For this purpose, the Non-linear Response History Analysis (N-RHA) represents the most complete method that permits an exact simulation of structures performance under ground shaking through a time integration procedure of the equations governing the structure displacement. The use of this method however is limited to research field and to special structure due the high computational cost inherent to the selection and application of a sufficient ground motion records to the numerical model. In this context, a promising method for the analytical vulnerability assessment contemplates the employment of Non-linear Static Procedures (NSPs), instead of non-linear dynamic analysis to assess the structure expected damage.

1.3 Objective

The non-linear static pushover analysis is a simplified method of demand prediction and performance evaluation that found a large use for practical design as an alternative to the nonlinear time history analysis [7]. Nevertheless, it has been shown that, despite its efficiency and applicability, the original method exhibits significant limitations when its applied to irregular structures [7].

In order to overcome these shortcoming many attempts have been proposed to improve the capability of the pushover analysis. The main suggestions include considering high mode order effects, stiffness degradation and input motions. Among these improved methods there is the Extended N2 [8] method elaborated by Fajfar and adopted in the Eurocode and the Practical Modal Pushover Analysis developed by Chopra [9].

By making a preliminary exhaustive review of the seismic vulnerability assessment methods and the current pushover methods, the main ultimate aims of this thesis are : 1) to discuss and apply different pushover methodologies for the evaluation of the case studies' seismic response in terms of maximum displacement and inter-storey drift ratios for different ground motion scenarios, 2) to use the nonlinear static methods described for the derivation of incremental dynamic curves and approximate fragility curves 3) to evaluate the accuracy and reliability of the employed approximate methods by comparison with the exact results obtained with the rigorous Non-linear Response History Analysis.

1.4 Outline of the content

This thesis is organized into six chapters. It covers several aspects ranging from the context behind the selection of the research subject, the state of the art review, the application of different pushover methods and the vulnerability assessment of two case studies.

Chapter 2 is dedicated to the review of the state of the art of seismic vulnerability assessment while in Chapter 3 the different non-linear static pushover analysis procedures are described and presented as a valid tool for seismic assessment.

Structural characteristics of the case studies employed are illustrated in Chapter 4. The study employs two steel buildings with different seismic resistant systems. The first structure, a nine-story building, is seismically designed and belongs to the Moment Resisting Frame (MRF) typology. The second case study is a parking building in steel with prefabricated concrete decks which stability to lateral loads is provided by an adequate number of concentrated V-bracings. After the presentation of the assumed modelling options, the results of the structural analysis of both structures are presented and compared. The accuracy of the employed NSP methods is evaluated by comparing seismic demand in terms of displacements and drift to the results of non-linear response history analysis. Emphasis is given also to the evaluation of the damage limitation requirement according to the EC8, considering a seismic input defined by the EC8.

In Chapter 5 the seismic vulnerability of case studies is assessed analytically by the determination of approximate and exact fragility curves that provide a statistical correlation between the structure capacity and the expected damage due a specified demand range.

In Chapter 6 the findings of this study are summarized and discussed.

Chapter 2

State of the art of seismic vulnerability assessment

2.1 Introduction

The extent of earthquakes effects depends not only on ground motion intensity but also and above all on the intrinsic susceptibility to damage of the urban and infrastructure systems existing on the affected geographical area. The intrinsic vulnerability is as matter of fact the main cause of massive loss of lives and economic assets. Briefly, seismic vulnerability is defined as the probability that a building or group of buildings will suffer a certain level of structural damage as a function of a parameter describing seismic intensity (e.g. macroseismic intensity, Peak Ground Acceleration (PGA)).

For the seismic vulnerability assessment, there are various methods that differ in computational effort and reliability. The choice of the method is conditioned by the availability of the required data and technology as well as on the needed level of detail and accuracy. Mainly, it is possible to distinguish between two different approaches: empirical and analytical. In empirical methods, the evaluation of the expected damage is based on statistical correlation between the observed damage in buildings of the same typology and the intensity of past earthquakes, whilst in the analytical approach, the assessment of the expected performance loss relies on numerical modelling of the building and the selection of adequate seismic inputs.

The deterministic methods are more suitable for the assessment of the expected performance of building stock, being able to produce statistical functions that relate a building typology on a given site to the expected ground motion scenario. The construction of the vulnerability functions relies on the availability of a large set of surveys that comprise the diverse spectrum of performances of a certain structure category to the whole range of potential seismic intensity examined, and several observations of the performance of structures under the same level of intensity. When the functions are constructed and a ground shaking scenario is defined (in terms of intensity), it is then sufficient to rate the individual building (with similar

characteristics compared to the building stock used for their construction) against a predetermined accepted probability of damage in order to assess its vulnerability. Although the different variants of the deterministic approach are formulated as

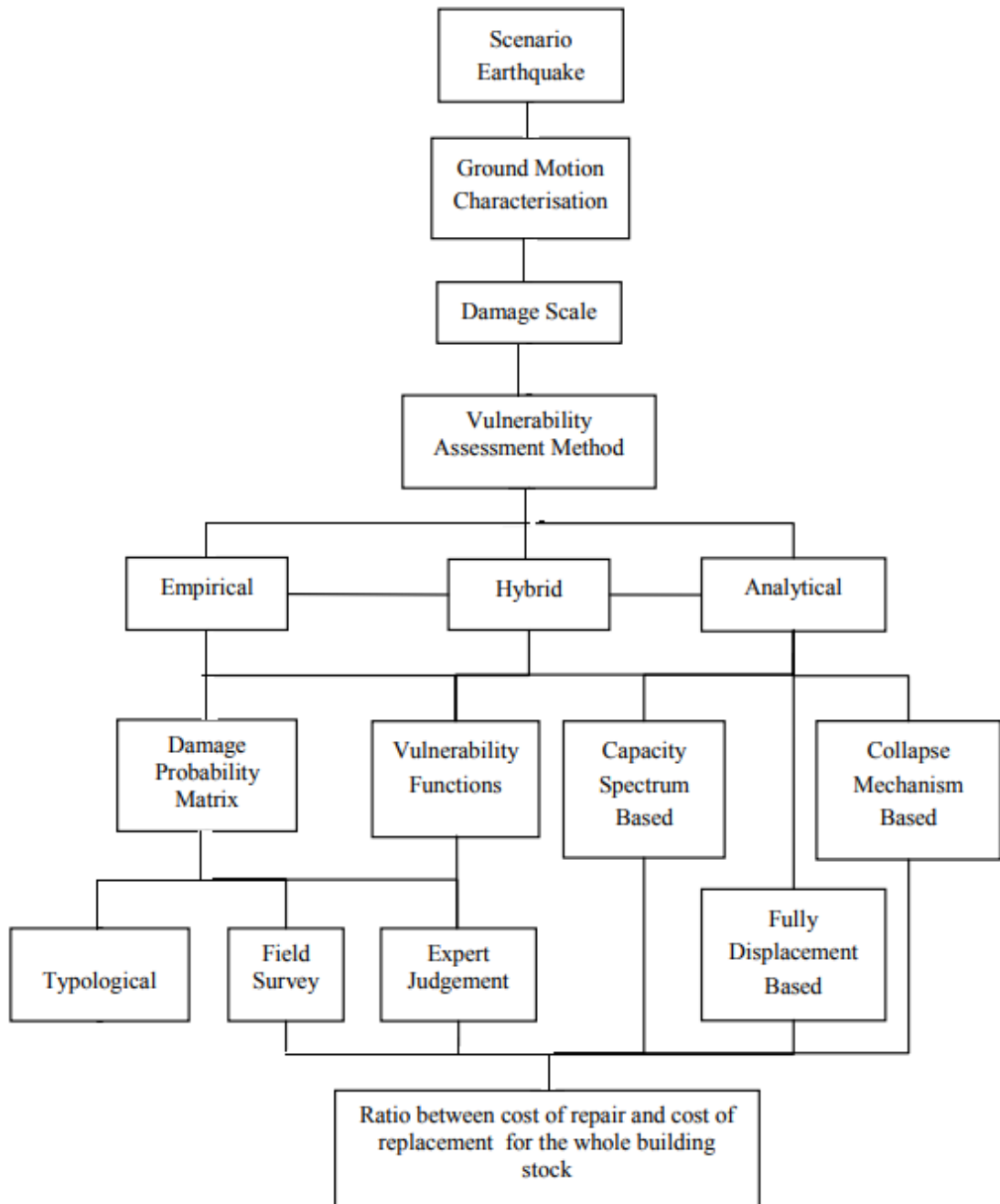


Figure 2.1: The different methodologies for the seismic vulnerability assessment. (Adapted from (Calvi et al. 2006))

empirical methods and thus capable of providing a realistic assessment, there are some shortcomings that limit their application to single buildings. For instance, these methods do not consider the dynamic properties of the buildings, and exclude an explicit modelling of the uncertainties related to data collection. In addition to a potential inaccurate compilation of the post-earthquake surveys, the collected data is often not homogeneous, leading to higher statistical accuracy for low to moderate damage range compared with high damage range [10].

In order to overcome these shortcomings different authors proposed the use of analytical tools in order to characterize seismic behaviour of numerical models representing different building typologies. The accuracy of the analytical methods depends on the availability of the necessary data to characterize materials as well as on the reliability of the numeric model. Although they allow to account for the various sources of uncertainties, they are computationally demanding and rely on a more significant amount of details compared to the empirical methods [6]. The analytical methods are particularly suitable when assessing single buildings or a few buildings of similar category. They are also recommended for the assessment of improved performance after strengthening and retrofit.

As shown in the flow chart 2.3 both analytical and empirical methodologies share two fundamental components: the characterization of the ground shaking and the quantification of the expected damage through a preliminary selection of appropriate parameters. The selected parameters are supposed to correlate the earthquake with the damage to the buildings. Peak ground acceleration (PGA) and macroseismic intensity have been the traditional option, while more recent proposals have correlated the seismic vulnerability of the buildings to ground motions response spectra. For the quantification of the structures capacity loss, in empirical methods the damage is modelled on discrete scale such as the MSK scale, the Modified Mercalli scale and the EMS98 scale, whilst in analytical procedures it is linked to limit-state mechanical properties of the structures, such as inter-storey drift capacity.

Following, different variants of both empirical methods and analytical approaches for the derivation of the vulnerability functions are described with particular emphasis on the specific applications of the analytical methods.

2.2 Empirical methods

The first employment of the empirical methods for the seismic vulnerability assessment of existing buildings dates back to the 1970s [11]. The first version of the empirical methods employed the micro-seismic intensity as the parameter defining the ground motions destructive potential. The macroseismic intensity constituted the only reasonable option, since at that time hazard maps were constructed in terms of these physical quantity. There are two main types of empirical vulnerability quantification that depend on the damage observed after earthquakes :

- Damage Probability Matrices (DPM), which is a discrete representation of the

conditional probability $P[D = j|i]$ of reaching a damage degree j , due to a ground motion of intensity i ;

- Vulnerability functions, which are continuous relations representing the likelihood of exceedance of a certain damage level as a function of the ground motion intensity.

2.2.1 Damage probability matrices

The method, developed by Withman et al. [11], is based on the assumption that buildings belonging to the same building typology have the same probability to suffer a given damage state for a given ground shaking destructive potential. In the matrix format adopted (see table 2.1) the fraction of building is provided as a function of the structural and non-structural damage ratio and the intensity of the ground motion. The quantification of damage is done through the use of damage index ranging from zero to unity, where 0 represents undamaged state while 1 represents collapse state of the building.

Whitman et al. assumed as a damage index the repair cost normalized to the cost of a total reconstruction. Whitman et al. (1973) obtained Damage Probability Matrices for different structural classes on the basis of the damage produced by the 1971 San Fernando earthquake to more than 1600 buildings.

Table 2.1: Format of the Damage Probability Matrix proposed by Whitman et al. (1973)

Damage State	Structural Damage	Non-structural Damage	Damage Ratio (%)	Intensity of Earthquake				
				V	VI	VII	VIII	IX
0	None	None	0-0.05	10.4	-	-	-	-
1	None	Minor	0.05-0.3	16.4	0.5	-	-	-
2	None	Localised	0.3-1.25	40.0	22.5	-	-	-
3	Not noticeable	Widespread	1.25-3.5	20.0	30.0	2.7	-	-
4	Minor	Substantial	3.5-4.5	13.2	47.1	92.3	58.8	14.7
5	Substantial	Extensive	7.5-20	-	0.2	5.0	41.2	83.0
6	Major	Nearly total	20-65	-	-	-	-	2.3
7	Building condemned		100	-	-	-	-	-
8	Collapse		100	-	-	-	-	-

After the 1981 Irpinia earthquake, the method was employed for the first time in Europe by Braga et al. to represent the damage distribution of Italian buildings for different seismic intensities [12]. Braga et al. compiled the DPM based on the Medvedev Sponheuer Karnik (MSK) scale for Italian buildings subdivided into three vulnerability classes (A,B, and C). Considering that the Italian seismic catalogue is based on Mercalli scale (MSC), Di pasquel et al. suggested to adapt the Damage Probability Matrices scale from MSK scale to MSC scale.

Giovinazzi et al. [13] proposed a macroseismic approach that allowed the evaluation of damage probability matrices based on the EMS-98 macroseismic scale. Giovinazzi et al. suggested to use the quantitative terms ("few", "many", "most") to indicate the proportion of buildings that suffer a certain degree of damage for different intensity levels. In addition, Giovinazzi et al. assumed a beta distribution of damage in order to overcome the problem of incompleteness of the DPM due the absence of data for all damage grades for a given level of intensity.

2.2.2 Continuous Vulnerability Curves

The discrete nature of macroseismic scale represented a real challenge for developing relations in a continuous form between the expected damage and the earthquake intensity. Spence et al. [14] proposed as a solution the use of a Parameterless Scale of Intensity (PSI) to obtain vulnerability curves on the basis of the observed damage of structures evaluated on MSK damage scale. Orsini [15] used the same ground-motion parameter to derive vulnerability curves for apartment units in Italy. Through the study of surveys describing the post-earthquake damage of thousands of Italian buildings Sabetta [16] derived continuous vulnerability curves. The buildings were categorised into three structural typologies and six damage levels were defined according to the MSK macroseismic scale. An average damage index, calculated as the weighted mean of the frequencies of each damage level, was evaluated for each urban area where damage occurred and each structural category. Empirical fragility curves with a binomial distribution were derived as a function of PGA, Arias Intensity and effective peak acceleration.

Recent developed continuous empirical vulnerability functions do not adopt PGA neither macroseismic intensity to represent the ground motion but are linked to the spectral ordinates at the first-mode period of vibration of the building [17, 18]. Generally these parameters has been found to obtain vulnerability functions which show enhanced correlation between the ground shaking input and damage.

2.3 Analytical methods

In all the listed empirical methods, the elaboration of damage probability matrices necessitates the characterization of the ground motion and the identification of the different degrees of structural damage. Singhal and Kiremidjian presented for the first time a systematic method for developing ground motion-performance loss relationships that does not require the analysis of post-earthquakes'surveys [19]. Instead, the probability of damage is assessed by evaluating the response of a numerical model of the building subjected to an adequately large set of ground motion records with a wide spectrum of parameter variations. The approach developed was implemented to derive damage probability matrices and fragility curves for reinforced concrete buildings. The buildings were categorised into three classes on the basis of floor numbers and the probabilities of damage were evaluated by the use of nonlinear dynamic analysis. The modified Mercalli Intensity was adopted as the ground-motion

intensity parameter, while for the production of the fragility curves the spectral acceleration was used. The main steps of the proposed method are :

1. Identification and characterization of the structural parameters that condition the dynamic response of the structure;
2. Characterization of the probable ground motions;
3. Evaluation of the structural response considering the uncertainty in the structural response and variability in the ground shaking;
4. Evaluation of the conditional probability for reaching or exceeding a damage state given a ground motion intensity using the Monte Carlo Simulation method;
5. Derivation of the fragility curves by fitting log-normal distribution functions to the discrete points representing the fraction of exceedances for each damage level.

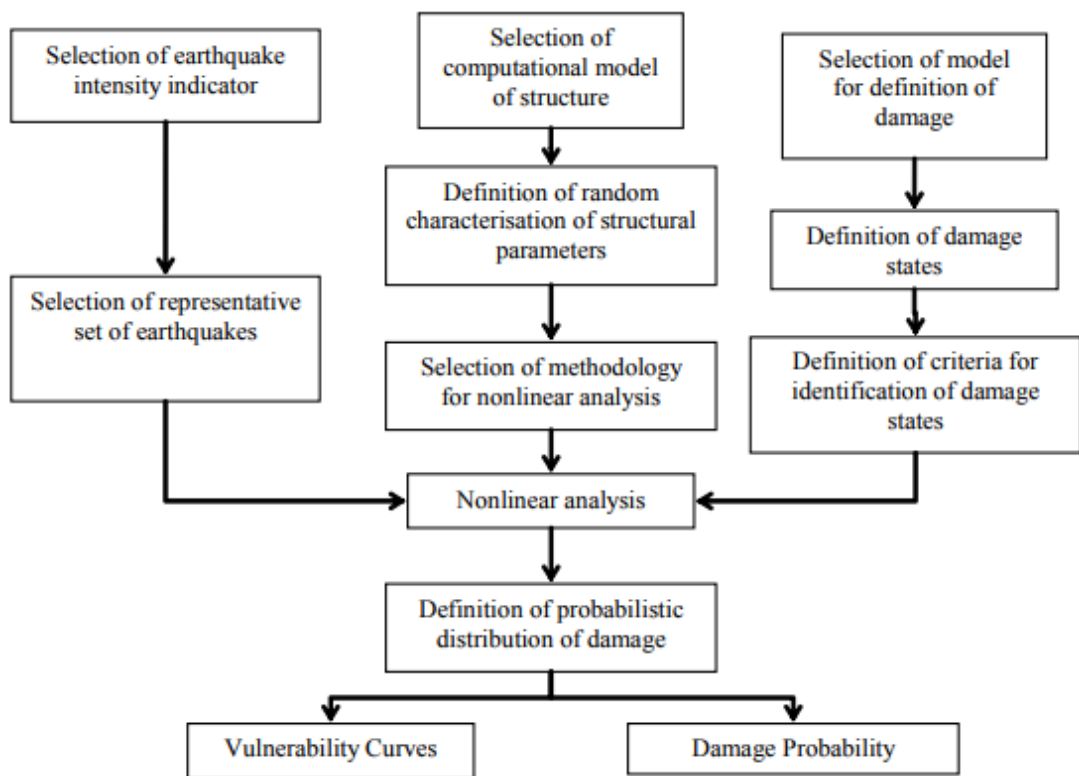


Figure 2.2: The different components of the evaluation of analytical vulnerability functions and DPMs (adapted from Dumova (2004))

In the approach followed by Singhal and Kiremidjia [19] and later by Masi [20] the structural response of the prototype models under ground motions of various

intensity levels was assessed via Non-linear Response History Analysis (N-RHA) with artificial and real accelerograms. The result of each analysis was employed to evaluate the damage index used as an indicator of performance loss. The values of damage index used to define the damage limit states are calibrated using surveys from several damaged buildings after past earthquakes.

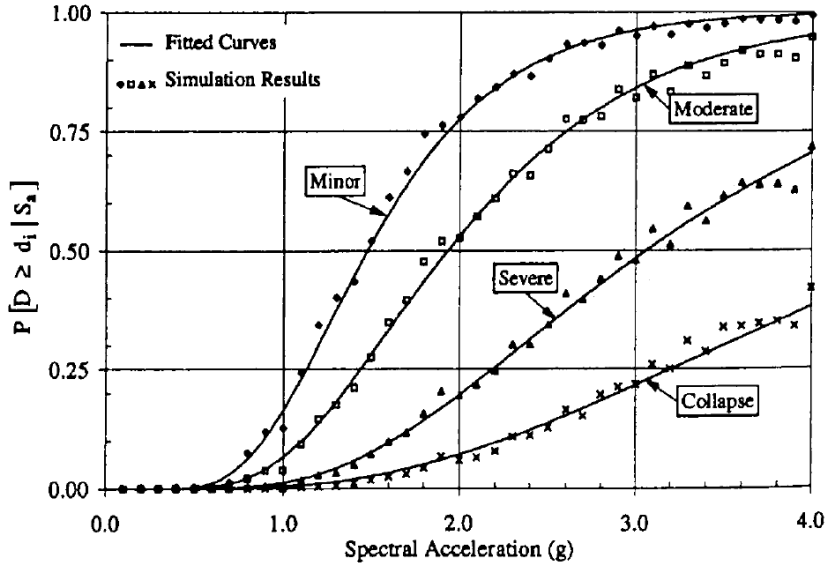


Figure 2.3: Fitted analytical fragility curves for different damage levels

One of the main drawbacks of the traditional analytical methods is the computational effort and time required to perform several full non-linear response history Analysis for different Multi Degree Of Freedom (MDOF) models and for each intensity level of a given ground motion scenario. Thus the functions cannot be easily derived for different urban areas or regions with various construction peculiarities. In order to overcome this limitation, different researches proposed and applied a simplified analytical methodology wherein the vulnerability assessment component is based on the use of Non-linear Static Procedures (NSP) in lieu of N-RHA in the framework of a Displacement-based approach.

2.3.1 Displacement-Based Methods

The first proposal of a fully displacement-based vulnerability assessment was developed by Calvi [21]. The originality of the proposed approach lies in the use of displacements as the main quantification parameter of damage and a spectral representation of the earthquake demand along with the principles of Displacement-Based Design approach. The building which is a MDOF is reduced to an equivalent Single Degree Of Freedom (SDOF), the period of vibration of which is calculated using the empirical formula in Eurocode 8 [22], which directly link the height of a

building to its period. Calvi accounted for different displacement capacities according to the collapse mechanism or displacement pattern at a certain limit state, while accounting for the mechanic and geometric properties of the structures within a building class. As showed in figure 2.5 and 2.6 the column soft storey and beam-sway collapse mechanisms were considered for moment resisting frames whilst for masonry buildings various in-plane collapse modes have been considered (see Figure 16). For each building typology, in order to determine the fraction of building exceeding a limit state or collapsing, the capacity displacement range is plotted against the displacement response spectrum adequately reduced in order to account for the dissipative capacity of the structure as shown in figure 2.7.

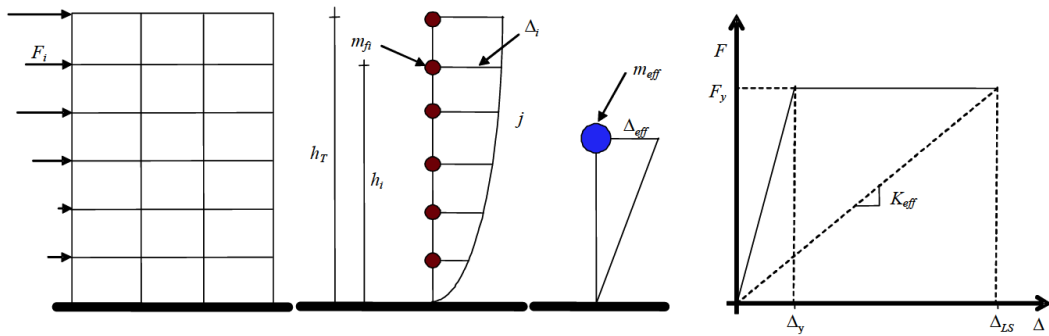


Figure 2.4: Simplified scheme for the transformation from an MDOF system to an equivalent SDOF system.

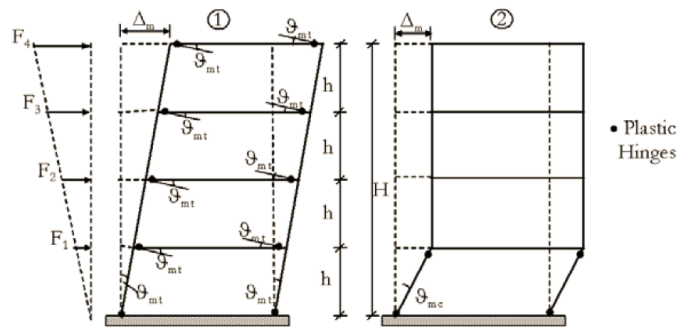


Figure 2.5: Distributed damage/ ductile failure mechanism (left) and soft-storey failure mechanism (right).

A similar method was adopted within the framework of the HAZUS (Hazard US) programme [23], a natural hazard analysis methodology developed by the Federal Emergency Management Agency (FEMA). The vulnerability assessment component of the proposed methodology is based on the Capacity Spectrum Method. The latter approach is one of the simplified nonlinear static procedures developed for buildings (see Chapter 3).

Shinozuka [24] obtained the vulnerability curves of a bridge by two different

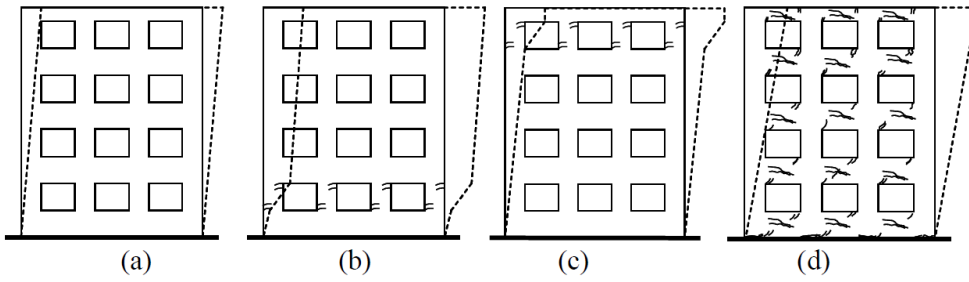


Figure 2.6: In-plane deformed shapes for different masonry limit states

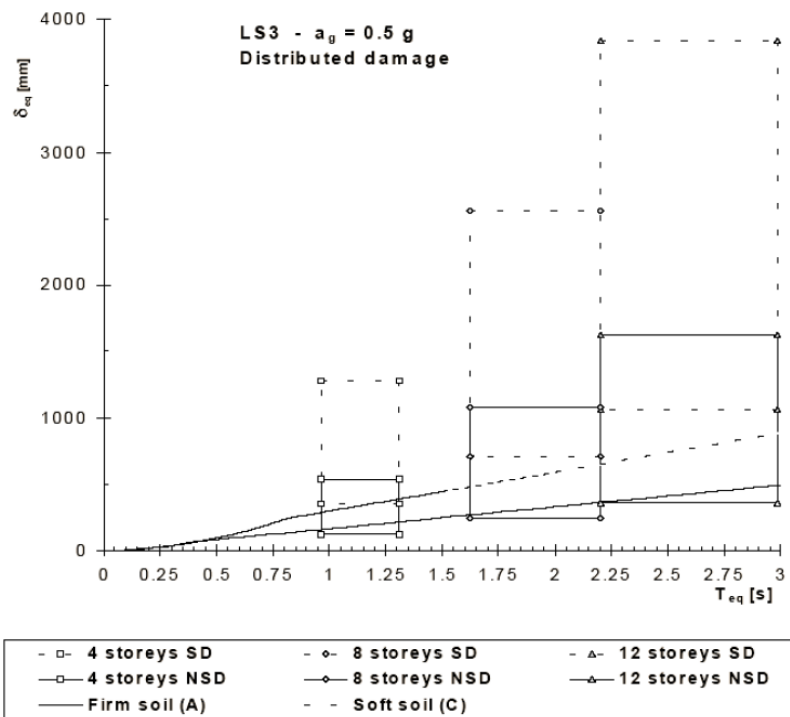


Figure 2.7: Intersection of the reduced demand spectrum and the capacity area for different building typologies

analytical approaches; the first uses the response history analysis and the second utilizes the capacity spectrum method. In the research, ten bridges of the same typology and a large set of ground shaking records were examined to account for the uncertainties related to the structural capacity and ground motion, respectively. The comparison indicated that the accuracy of the approximate fragility curves is satisfactory for the state of low to moderate damage, but not acceptable for the state of high state of damage where non-linear behavior becomes significant.

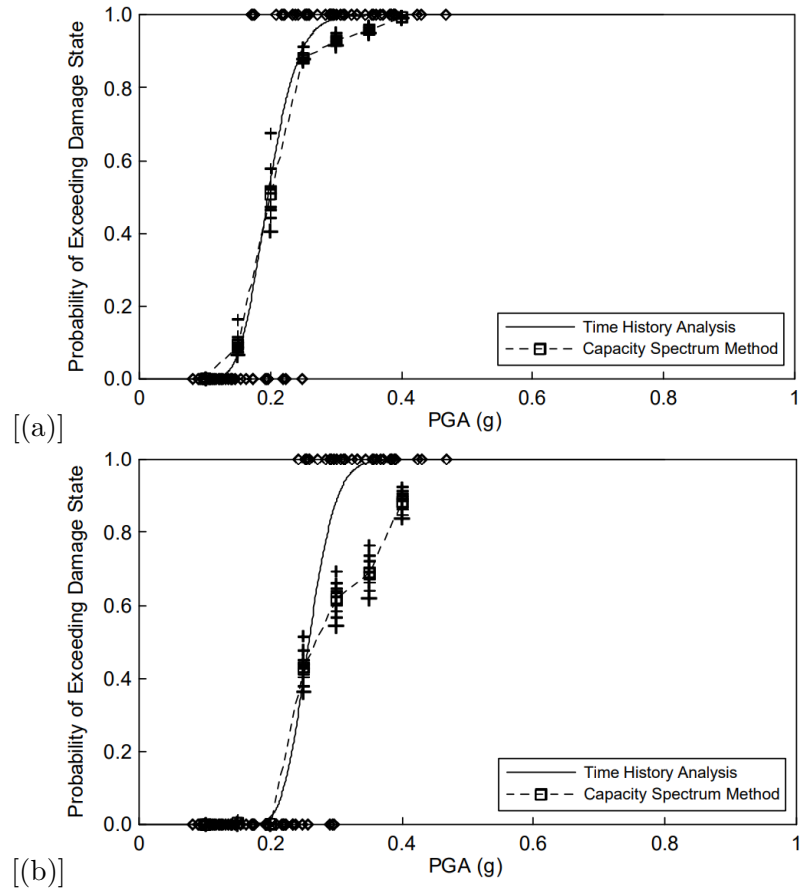


Figure 2.8: Vulnerability curves for a bridge model for State of Minor Damage (a) and for State of Major Damage (b), from Shinozuka,2001

2.3.2 General Remarks on Analytical Methods

The construction of seismic hazard maps in terms of spectral ordinates instead of macroseismic intensity or PGA represents one of the main reasons for the recent development of the analytical tools as a valid alternative to the traditional empirical methods. The replicability of the vulnerability curves' construction constitutes one of the main advantages brought by this new approach since it permits to undertake a accurate sensitivity analyses which give important insight into how much the results are influenced by the models, data, uncertainties and assumptions made.

However, one should bear in mind that many factors might compromise the reliability of the analytical methods as the adequacy of numerical models to accurately predict the response of real buildings; the precision in converting numerical indices of damage into real damage of actual structures; the possibility of accounting for human errors in the design and construction of buildings, which are often the main causes of disastrous failures.

Chapter 3

Non-linear static procedures

3.1 Introduction

Generally, the seismic response of structures is three-dimensional, non-linear and time-dependent. Currently, the Non-linear Response History Analysis (N-RHA) represents the most rigorous and efficient method that takes into consideration all these three aspects, through a time integration procedure of the governing equations of the structure motion excited by several ground motion acceleration records [25]. However, the high computational cost, inherent to the selection of the ground motion sets and the interpretation of the wide range of results, represents a relevant drawback that discourages a wide use of this rigorous method in the professional practice.

Taking into consideration that structural analysis is not intended to predict the exact behaviour of the structure but rather to get information for making design decisions, different approximate approaches have been sought. In the past few years Non-linear Static Procedures (NSPs) have been established as the most adequate alternative for a reliable evaluation of the structural response while retaining the simplicity of use of the linear methods. The basic concept underlying the NSPs consists in the reduction of the structure's response to that of an equivalent inelastic Single Degree of Freedom (SDOF) system, the lateral load bearing capacity of which is obtained through a pushover analysis [25]. As shown schematically in figure 3.1 the pushover analysis provides a characteristic non-linear force-displacement curve by subjecting the structure to a monotonously rising lateral load simulating inertial forces that occur as a result of ground shaking.

There are different variants of the NSPs that differ in the type of the load pattern employed, whether the adaptability of the load to the structure stiffness variation is considered or not and on how the dissipative capacity of the structure is accounted. The most common pushover-based approaches are the Capacity Spectrum Method (CSM) adopted in the American standard FEMA and the N2 method which is included in the Eurocode 8 [7].

These methods are found to provide adequate results for regular buildings, but seem to underestimate the seismic demand for irregular structures that exhibit

torsional behaviour under seismic excitation [7]. Different authors have attempted to overcome this limitation by developing methods capable to account for torsional responses. Chopra and Goel [9] proposed to include the effects of higher modes in order to take the response's torsional component into consideration, whilst Fajfar et al. [26] suggested to extend the N2 method by incorporating the results from the conventional pushover analysis with those from elastic modal analysis. In this chapter, the evolution and the theoretical background of aforementioned NSP methods are described as well as the procedures for their practical implementation.

3.2 Modal Pushover Analysis

The Modal Pushover Analysis has its theoretical roots in structural dynamic analysis. The MPA is based on the assumption that the distribution of forces over the structure, equivalent to the seismic excitation (known as effective earthquake forces), can be expanded as modal inertial distributions even when the structure is expected to deform beyond its elastic range. The contribution of each term of the expansion is obtained separately by performing a pushover analysis using as load pattern the respective inertia force distribution. The structure response quantities are obtained by combining the contributions of the significant modes using an appropriate combination rule. In brief, the method contemplates the reduction of response of the structure, modelled as Multi Degree Of Freedom system (MDOF), to the combination of the responses of Single Degree Of Freedom (SDOF) systems.

3.2.1 MDOF to SDOF transformation

In this section the equations defining the relation between MDOF system and equivalent SDOF system are derived using the principles of dynamic theory [25]. The differential equations, in a matrix form, governing the response of a multi-story building to ground shaking \ddot{u}_g are as follow:

$$m\ddot{u} + c\dot{u} + f_s(u, \text{sign } \dot{u}) = -m\ddot{u}_g \tag{3.1}$$

where m , c and f_s are the mass matrix, the damping matrix and the resisting forces vector, respectively, while ι is the vector of influence, i.e the i th component represents

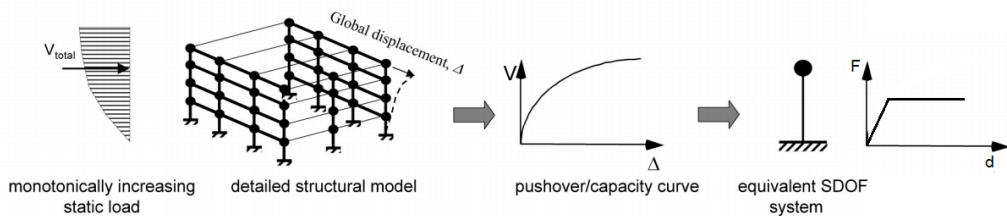


Figure 3.1: Schematic representing the generation of an equivalent SDOF system by pushover analysis from FEMA 440

the acceleration at the i th degree of freedom due to a unit ground acceleration at the base. for simple structural models with degree of freedoms corresponding to the horizontal displacements at storey levels, ι is a unity vector.

\ddot{u}_g is the time history of ground acceleration. These equations are usually solved by performing a transformation of coordinates from normal coordinate u to nodal coordinates through the relation

$$u = \sum_{n=1}^N \phi_n q_n(t) \quad (3.2)$$

which expresses the displacement vector as a linear combination of the natural mode shapes of the structure ϕ , and the modal coordinates $q(t)$. Substituting into equation (3.1), pre-multiplying by ϕ_n^T , and using the mass- and classical damping-orthogonality property of modes gives

$$\ddot{q}_n + 2\zeta_n \omega_n \dot{q}_n + \frac{F_{sn}}{M_n} = -\Gamma_n \ddot{u}_g(t) \quad n = 1, 2, \dots, N \quad (3.3)$$

where Γ_n is the modal transformation factor, an indicator of the modal mass ratio responding to the ground motion, i.e gives a measure of the degree to which the n th mode participates to the global dynamic response.

$$\Gamma_n = \frac{L_n}{M_n} \quad (3.4)$$

with

$$L_n = \phi_n^T m \iota \quad (3.5)$$

$$M_n = \phi_n^T m \phi_n \quad (3.6)$$

The non-linear resisting force defined as

$$F_{sn} = F_{sn}(q, \text{sign } \dot{q}) = \phi_n^T f_s(u, \text{sign } \dot{q}) \quad (3.7)$$

is a function of all modal coordinates $q_n(t)$, which results in the coupling of modal coordinates as the structure is expected to deform beyond its elastic range. The first simplification of the MPA method consists in the assumption that this coupling is weak and hence negligible [25]. As a consequence the normal coordinate depends only on the respective modal coordinate

$$u(t) = \sum_{r=1}^N \phi_r q_r(t) \cong \phi_n q_n(t) \quad (3.8)$$

With this approximation, the solution of n th differential equation in terms of the modal coordinate q_n can be expressed by the equation

$$q_n(t) = \Gamma_n D_n(t) \quad (3.9)$$

where $D_n(t)$ is governed by

$$\ddot{D}_n + 2\zeta_n\omega_n\dot{D}_n + \frac{F_{sn}}{L_n} = -\ddot{u}_g(t) \quad (3.10)$$

and

$$F_{sn} = F_{sn}(D_n, \text{sign } \dot{D}_n) = \phi_n^T f_s(D_n, \text{sign } \dot{D}_n) \quad (3.11)$$

The solution of equation (3.10) provides $D_n(t)$, the response of the n th-mode inelastic SDOF system, a SDOF system that, under small oscillations, has the same dynamic properties of the n th-mode of the corresponding linear MDOF system. The floor displacement of the MDOF structure associated with the n th-'mode' inelastic SDOF system is obtained by substituting $D_n(t)$ into equation (3.1). In other words, the solution for a single mode of the full system is simply Γ times the solution of the inelastic SDOF with the same dynamic properties.

The non-linear relation $F_{sn} - D_n$ between the resisting force and the modal coordinates respectively, required to solve equation (3.10), is determined by pushover analysis. The procedure involves the application of an incremental distribution of lateral forces to the building up to a prefixed target displacement. Assuming that the contribution of each mode to the total response of the structure is decoupled from the other modes, the most rational distribution of forces to employ is given by

$$s_n = \Gamma_n m \phi_n \quad (3.12)$$

where m is the structure diagonal mass matrix and I_0 is the diagonal matrix of polar moment of inertia about a vertical axis through the centre mass. The distribution of forces s_n , in fact, is the only force distribution capable of producing displacements proportional to ϕ_n . The pushover analysis returns the n -th pushover curve, a representation of the base shear (V_{bn}) as a function of the roof displacement (u_{rn}) increment in the appropriate direction. For irregular buildings, the pushover procedure leads to two non-identical pushover curves corresponding to the two horizontal directions. In that case the pushover curve employed is the one in the same direction as the dominant component of the mode shape. The pushover curve is idealized into a bilinear relation. The most common idealization method of the load-deformation curve is commonly named as the equal-energy method figure (3.2). The initial stiffness of the idealized system is obtained in such way that the areas under the actual and the idealized force-deformation curves are equal. The obtained bi-linear relation is then converted to $F_{sn}/L_n - D_n$ relation through the modal transformation factor by rearranging the equation (3.9)

$$\frac{F_{sn}}{L_n} = \frac{V_{bn}}{M_n^*} \quad (3.13)$$

$$D_n = \frac{u_{rn}}{\Gamma_n \phi_{rn}} \quad (3.14)$$

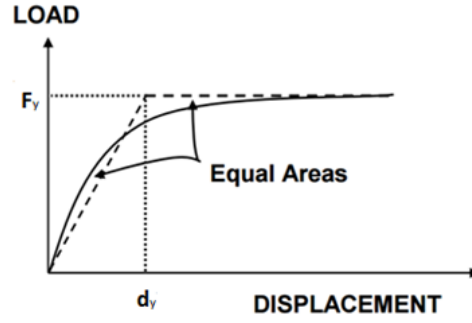


Figure 3.2: Idealization of the pushover curve using the equal energy principle.

where $M_n^* = L_n \Gamma_n$ is the effective modal mass. Considering that the slop of the elastic branch of $F_{sn}/L_n - D_n$ defines the angular frequency of the SDOF system the natural period is given by

$$T_n = 2\pi \left(\frac{L_n D_{ny}}{F_{sny}} \right)^{0.5} \quad (3.15)$$

3.2.2 Step-By-Step Procedure

The practical implementation of Modal Pushover Analysis can be summarized in 5 main steps:

1. Obtain the pushover curve by pushover analysis for reach of the significant modes considered on the basis of a preliminary modal analysis. For the n th mode the load pattern is given by the force distribution

$$s_n = \Gamma_n m \phi_n \quad (3.16)$$

2. Idealize the pushover curve by a bilinear relation by imposing the energetic equivalence between the two curves. Convert the bilinear relation into the $F_{sn}/L_n - D_n$ force displacement relation of the equivalent n th inelastic SDOF using equations

$$\frac{F_{sn}}{L_n} = \frac{V_{bn}}{M_n^*} \quad (3.17)$$

$$D_n = \frac{u_{rn}}{\Gamma_n \phi_{rn}} \quad (3.18)$$

where M_n^* and L_n corresponds to the direction of the selected pushover curve.

3. NON-LINEAR STATIC PROCEDURES

3. Knowing the dynamic parameters (T_n, ξ_n) determine the peak displacement demand D_n of each of SDOF systems through Response History Analysis or inelastic response spectrum of the ground motion considered.
4. Extract the response quantities r_n of interest for each mode from the last step of the corresponding pushover analysis performed up to the roof displacement given by

$$u_{rn} = \Gamma_n D_n \phi_{rn} \quad (3.19)$$

5. Combine mode contributions with well-known modal combination rules to approximately obtain inelastic seismic demand quantities. If the modes are closely spaced (tall buildings) the Complete Quadratic Combination (CQC) yields more accurate results by taking into consideration the coupling caused by modal damping. If the modes period differ by more than 10% they are considered all statistically independent and their combination can be carried by the Square Root of the Square Sum technique (SRSS).

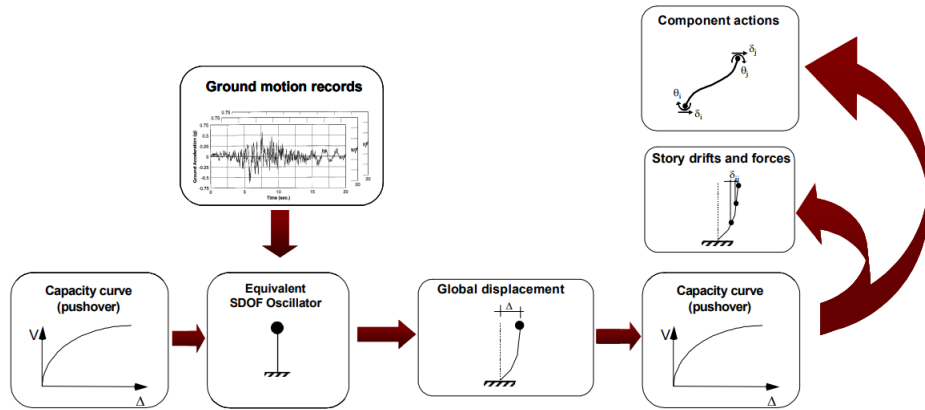


Figure 3.3: Flow chart depicting simplified SDOF nonlinear analysis process.(from (FEMA 440))

The procedure described can be further simplified by estimating the seismic demand directly from the elastic design spectrum in conjunction with empirical equations for the ratio of deformations of inelastic and elastic systems [27]. In this way, it is possible to avoid the complications of selecting and scaling ground motions for non-linear response history analysis required in point 3 of the conventional procedure. Instead of using non-linear RHA for each excitation, the peak displacement D_n of the SDOF system can be estimated by multiplying the median peak deformation of the corresponding linear system, known from the design spectrum, by the inelastic deformation ratio C_{Rn} . There are several empirical equations for C_{Rn} . In this study, the equations proposed by Newmark and Hall [28] are employed.

$$C_R = \begin{cases} \infty & T_n < T_a \\ (R_y^2 + 1)/2R_y & T_b < T_n < T_c \\ 1 & T_n > T_c \end{cases} \quad (3.20)$$

A further insight on the physical meaning of these factors is given in the next section.

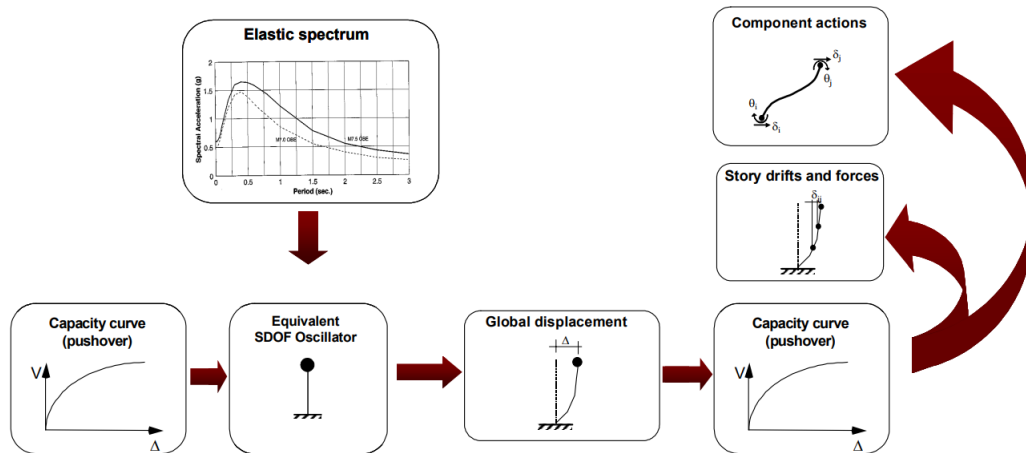


Figure 3.4: Flow chart depicting simplified SDOF non-linear analysis with the seismic demand estimated from elastic response spectrum from FEMA 440.

3.3 N2 Method in CSM format

The capacity spectrum method (CSM) is a non-linear static procedure widely used as an alternative to the rigorous nonlinear time history analysis for its simplicity and good accuracy. Indeed, the method allows a rapid comparison of the structural capacity and the seismic demand by means of an illustrative construction that comprises both capacity and demand curves. The seismic demand imposed on the structure corresponds to the crossing point of the two curves, both represented in Acceleration Displacement Response Spectrum (ADRS) format instead of the traditional spectral acceleration versus period format.

The lateral bearing capacity of the structure, represented by a bilinear force-displacement curve, is determined by a non-linear static pushover analysis. The demand, instead, is obtained by an iterative procedure that depends on both the ground shaking intensity and the dissipative capacity of the structure.

The original version of the CSM, developed by Freeman [29] and later adopted in the USA code ATC-40, entails the use of equivalent linear systems, with equivalent effective damping and period, in order to account for the dissipative capacity of the structure. The intersection between the over-damped elastic spectrum corresponding to the expected level of damage and the capacity curve approximates the seismic demand imposed on the system [29].

The original method however, as demonstrated by different authors, exhibits several shortcomings in the form of non-convergence and underestimation of the real displacement demand. Chopra and Goel, for instance, showed that CSM in ATC-40 underrates by more than 50 % the actual displacements determined by a non-linear history analysis [9]. According to Krawinkler the main flaw of the method relies on the assumption that the hysteric dissipative capacity of the structure can be represented by an equivalent viscous damping [30].

In order to overcome the original method deficiencies Fajfar (Simplified procedure [26]) and Chopra (Iterative procedure [9]) proposed to represent the seismic demand by inelastic demand spectra instead of using equivalent linearisation and damped elastic spectra. The inelastic demand spectra are obtained from their elastic counterparts by using spectral reduction factors.

3.3.1 Capacity Curve

Unlike the Modal Pushover analysis, the N2 method in its original version does not involve accounting of the pushover curves of all the significant modes but only two pushover curves, one for each lateral direction. For each direction, the lateral loads are assumed to be proportional to the displacement shape of the vibrational mode dominant along same direction (in terms of modal mass participation ratio) weighted by the storey masses

$$s = p\Psi = pM\Phi \tag{3.21}$$

where M is the mass matrix and p is a multiplicative factor that controls the magnitude of the lateral load. Similarly, to the MPA, the resulting Base shear-roof

displacement relation $V - u_r$ is then converted to the non-linear force-displacement relation of the inelastic SDOF system $F - D$ by the use of the modal transformation factor

$$F_{sn} = \frac{V_{bn}}{\Gamma_n} \quad (3.22)$$

$$D_n = \frac{u_{rn}}{\Gamma_n} \quad (3.23)$$

These relations are different from those used in the framework of the MPA method. This is because, while in the latter methods mode shapes' vectors are orthormalised with respect to the mass matrix, in the CSM method they are usually normalised to the top displacement.

3.3.2 Seismic Demand

Most structures are designed to undergo deformations beyond their limit of linearly elastic behaviour allowing an acceptable damage to take place in the event of intense ground shaking. The dissipative capacity of the structure associated with the damage is accounted for in force-based earthquake resistant design, through the use of strength reduction factors as shown in figure (3.5). Specifically, the design base shear coefficient is computed from the inelastic demand spectrum obtained by scaling its elastic counterpart by the reduction factor

$$S_a = \frac{S_{ae}}{R_\mu} \quad (3.24)$$

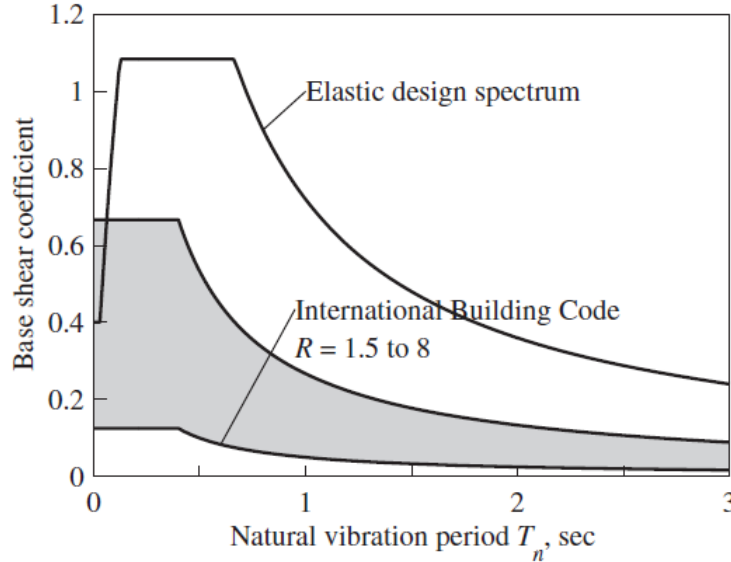


Figure 3.5: Comparison of base shear coefficients from elastic design spectrum and *International Building Code*. From (Chopra 1998)

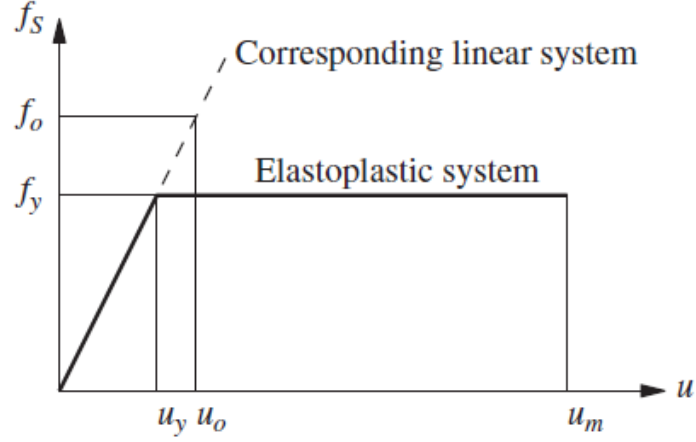


Figure 3.6: Elasto-plastic system and its corresponding linear system. From (Chopra 1998)

The magnitude of these reductions depends on various factors such as the structure's stiffness and ductility as well as on the soil conditions at the structure site. Considering an elastic perfectly plastic SDOF and the corresponding elastic system as shown in figure (3.6), the strength reduction factor is defined as the ratio of the elastic strength demand to the inelastic strength demand

$$R_y = \frac{f_o}{f_y} = \frac{u_o}{u_y} \quad (3.25)$$

where f_y may be interpreted as the minimum lateral yielding strength required to avoid yielding in the system under a given ground motion and f_o as the lateral yielding strength necessary to avoid that the value of inelastic deformation experienced by the system exceeds a predefined limit value under the same ground motion. The maximum tolerable displacement ductility demand is defined by the ductility factor

$$\mu = \frac{u_m}{u_y} \quad (3.26)$$

where u_m is the peak displacement of the elasto-plastic system due to the ground motion. Substituting into equation (3.25) gives

$$R_\mu = \frac{\mu u_o}{u_m} \quad (3.27)$$

The values of R_μ are determined empirically on the basis of the observed performance of different structural systems in previous strong earthquakes. In this study, the relations proposed by Vidic et al. [31] are used.

$$\begin{aligned} R_\mu &= (\mu - 1) \frac{T}{T_c} + 1, & T &\leq T_0 \\ R_\mu &= \mu, & T &\geq T_0 \\ T &= 0.65\mu^{0.3}T_c \end{aligned} \quad (3.28)$$

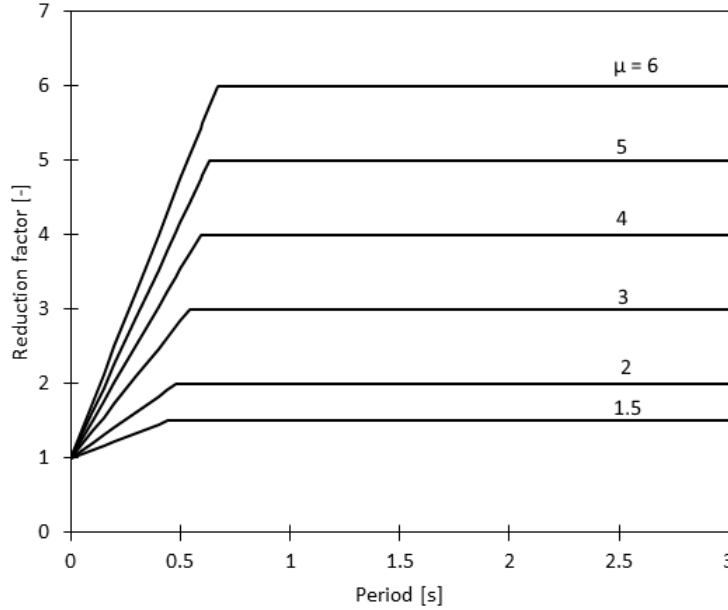


Figure 3.7: Ductility-dependent reduction factor R_μ spectrum

where T_c is the characteristic period of the ground motion spectrum defined as the transition period between the constant acceleration region and the constant velocity region of the spectrum. The expressions in (3.15) correspond to a bilinear spectrum of the reduction factor as shown in figure 3.7. In the short-period region R_μ increases proportionally to the period from a unitary value to the ductility factor value. In the medium and long-period the elastic and inelastic system have approximately the same maximum displacement and therefore, from equation (3.26), the reduction factor assumes a constant value equal to the ductility factor [31].

3.3.3 SDOF displacement demand

The iterative procedure

As to perform CSM, capacity and demand curves are preliminarily plotted in an Acceleration Displacement Response Spectrum (ADRS) format. Differently from the traditional acceleration versus period spectrum shown in figure (3.8), in ADRS format the abscissa shows spectral displacement whereas the period is represented by radial lines starting from the origin as shown in figure 3.9. The capacity spectrum is obtained from the force displacement curve by dividing the forces by the equivalent mass m^* of the SDOF system defined as

$$m^* = \sum m_i \phi_i \quad (3.29)$$

The demand spectra in ADRS format are obtained starting from elastic response spectrum using the following relations

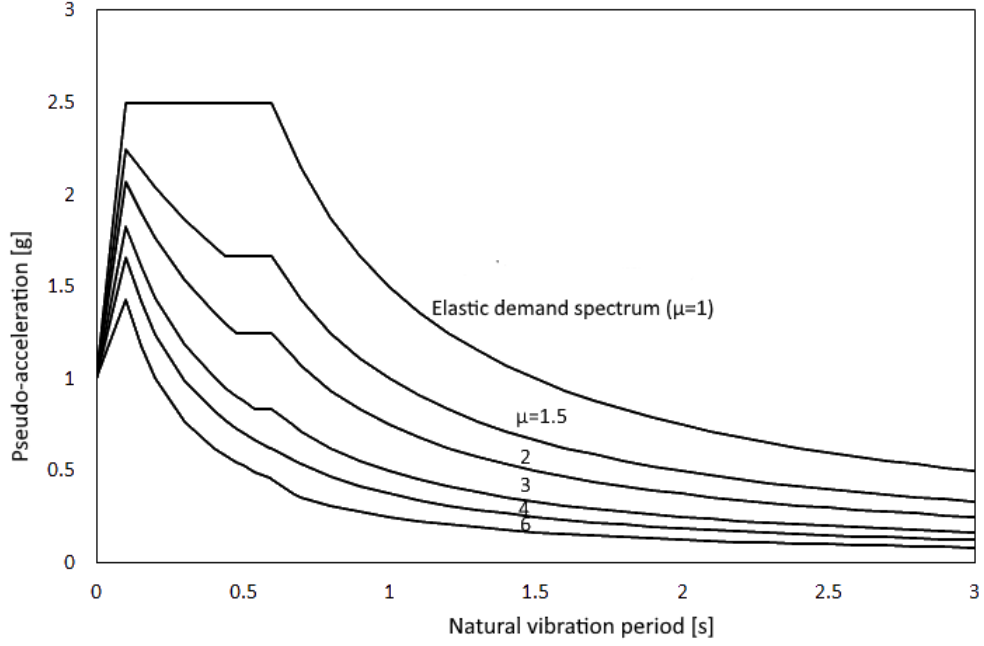


Figure 3.8: Demand spectra for constant ductilities

$$S_{de} = \frac{T^2}{4\pi^2} S_{ae} \quad (3.30)$$

$$S_{dp} = \mu \frac{T^2}{4\pi^2} S_{ap} \quad (3.31)$$

where S_{ae} and S_{de} are values in the elastic spectrum of pseudo-acceleration and displacement, respectively, while S_{ap} and S_{dp} are the values of the inelastic spectrum. The capacity spectrum and the elastic demand spectrum are drawn first in the ADRS format, while the inelastic demand spectrum is determined by an iterative procedure as it depends on the ground motion as well as on the structure ductility. The seismic demand imposed on the SDOF system corresponds to the intersection of the capacity spectrum and the inelastic demand spectrum. The iterative procedure consists of the following steps (see figure 3.10):

1. Assume an arbitrary initial ductility factor μ_i and plot the corresponding inelastic demand spectrum using the reduction factor formulae
2. Assume the displacement demand as the abscissa of the intersection of the yielding branch of the capacity diagram and the assumed demand curve.
3. Compute the ductility value μ_j associated with the intersecting demand curve as the ratio between d_j and d_y .

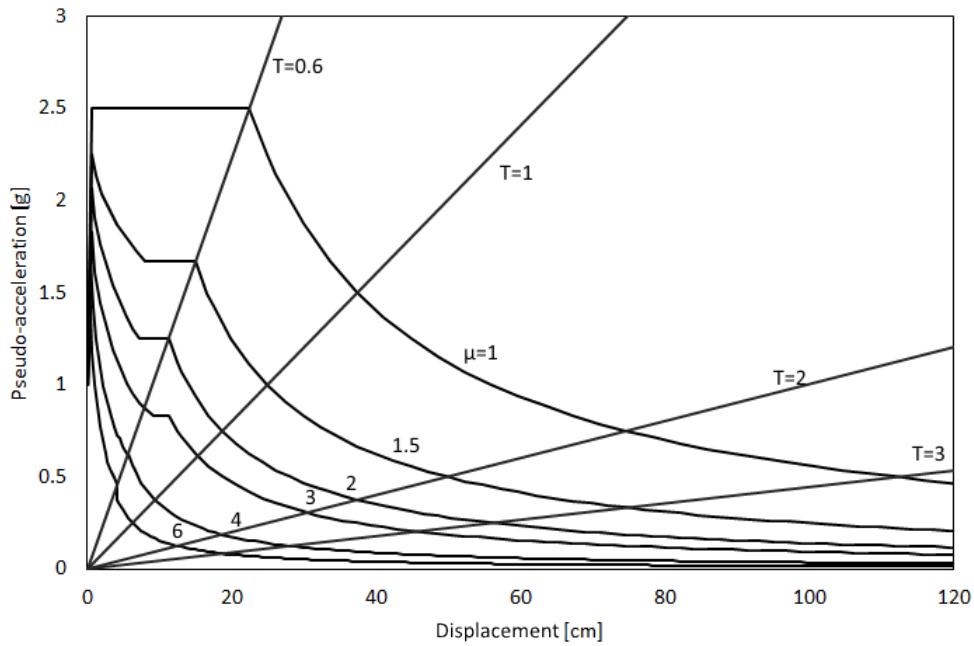


Figure 3.9: Demand spectra for constant ductilities in ADRS format

4. Compare the ductility factor determined obtained in step 3 with the one assumed in step 1. If $\mu_j > \mu_i$ assume a lower ductility factor and repeat step from 1 to 3 until convergence.

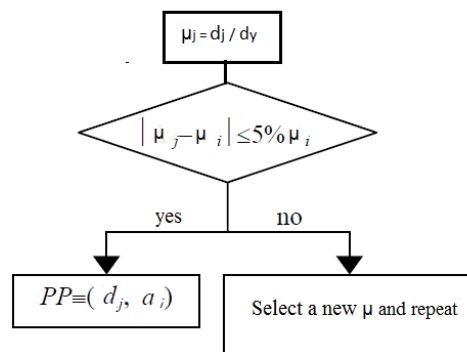
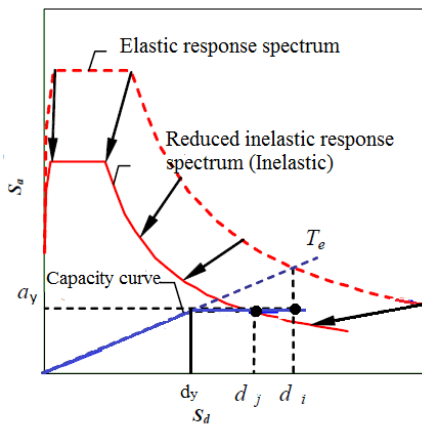


Figure 3.10: Illustration of the main steps of the iterative procedure.

The Simplified Procedure

Fajfar proposed a more direct approach to determine the seismic demand called N2 method [26] in an attempt to simplify the procedure for practical design. The N2 method is similar to the CSM proposed by Chopra and Goel except it does not require iterative procedure for medium- and long-period structures, for which the equal displacement rule applies.

The procedure consists in plotting in ADRS format the capacity spectrum, the elastic demand spectrum and the radial line corresponding to the elastic period of the idealized bilinear system. If the system elastic period is larger than T_o the inelastic displacement demand is equal to the elastic displacement corresponding to the crossing point of the period radial line and the elastic demand spectrum. The ductility demand is equal to the reduction factor and is determined as the ratio between the elastic acceleration S_{ae} and the yield acceleration representing the acceleration demand of the inelastic system. If, instead, the elastic period T^* is smaller than T_o and the target ductility is low, iteration is required unless the T_o is assumed conservatively equal to T_c . The reduction factor is obtained as the ratio between S_{ae} and S_{ay} while the ductility demand is calculated from the rearranged equation (3.15)

$$\mu = (R_\mu - 1) \frac{T_0}{T^*} + 1 \quad (3.32)$$

The displacement demand is determined as

$$D^* = S_d = \mu D_y^* \quad (3.33)$$

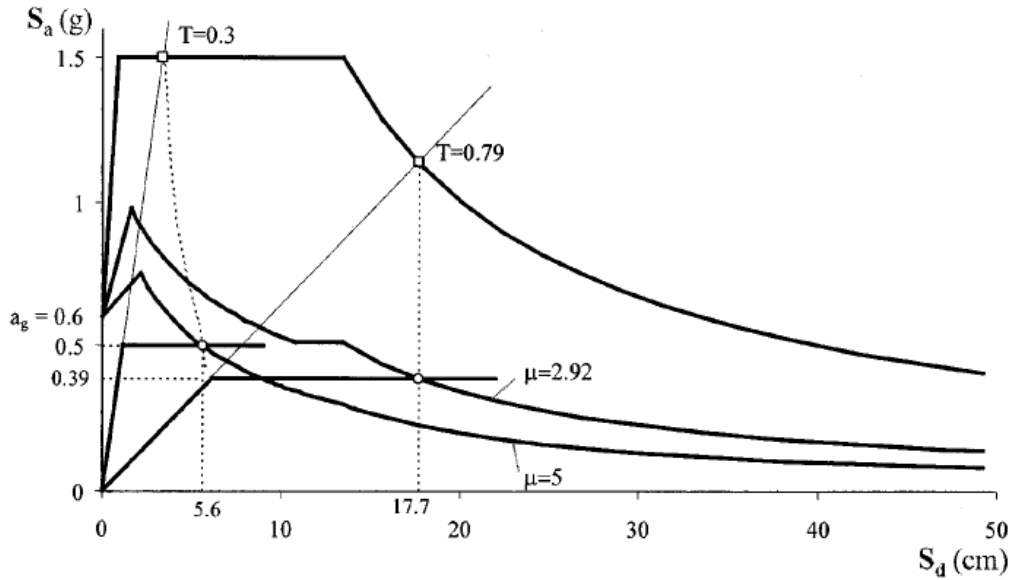


Figure 3.11: Demand and capacity spectra for two illustrative examples from Fajfar 1999

In both cases, the inelastic demand, in terms of accelerations and displacements, corresponds to the intersection point of the capacity spectrum and the demand spectrum that corresponds to the ductility demand as shown in figure 3.11.

3.3.4 MDOF system seismic demand

The displacement demand imposed on the SDOF system is transformed into the peak roof displacement of the structure through the use of the transformation factor. The local seismic response of the structure is obtained by a pushover analysis carried out up to the roof peak displacement. The results of the pushover analysis should be integrated with the torsional effects. The amplification of demand due torsion is determined by a response spectrum analysis using as input the same response spectrum employed in the pushover analysis. In particular, the amplification factors to be applied to the relevant results of pushover analyses are defined as the ratio between the roof displacements obtained by elastic modal analysis and by pushover analysis.

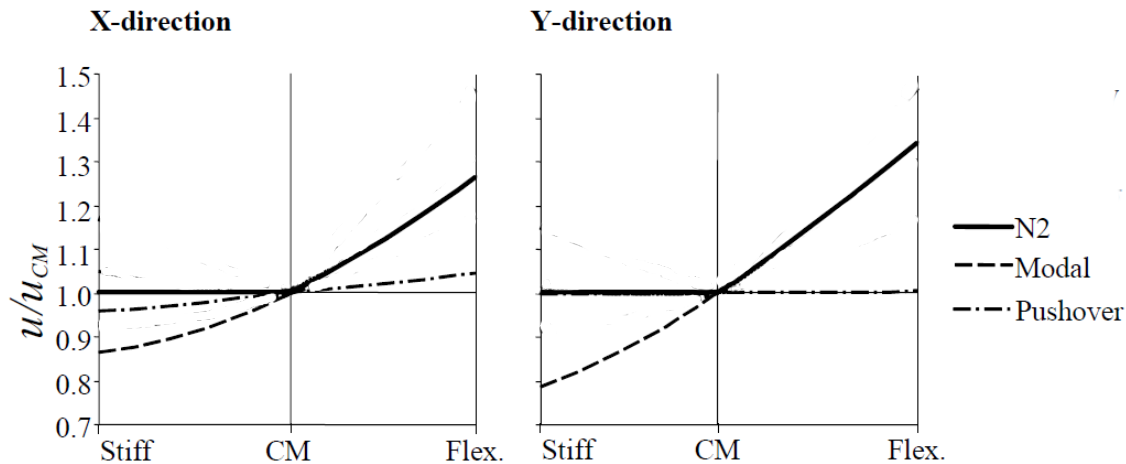


Figure 3.12: Torsional effects in terms of normalized top displacements obtained by N2 method as the envelop of the results obtained by modal analysis and pushover analysis, from Fajfar 2005.

3.4 Conclusion

The different NSPs, presented in this chapter were developed as a valid simplified alternative to the exact N-RHA. The common factor shared by those methods lies in the good degree of accuracy with a reduced computational cost. This is achieved differently on the basis of the employed assumptions and simplifications. The Modal Pushover Analysis method stands out for the fact that is based on the well-known structure dynamic theory. By including higher modes effects the structure response is reduced to that of single degree of freedom systems. However, the method does

3. NON-LINEAR STATIC PROCEDURES

not renounce totally to the inherent complexity of nonlinear dynamic analysis since it requires N-RHA for single SDOFs. In addition, the method neglects both the coupling between modes during the response as well as the change in vibration shapes and stiffness. The CSM and N2 method on the other hand offer a rapid solution for design purposes through a visual and intuitive comparison of the capacity of the structure (in the form of a pushover curve) with the design seismic demand on the building (in the form of over-damped elastic response spectrum in the CSM or inelastic response spectrum for the N2 method). These methods rely also on the principle of equivalent SDOF but differently from the MPA method they do not require selection and scaling of ground motions since the demand is represented in the form of response spectrum. Whereas on one hand this simplification reduces notably the required computational cost, on the other hand the static representation of the demand ignores the frequency content of the ground shaking.

Chapter 4

Case studies

Two case studies with different lateral resistant systems are presented and analysed with the use of Non-linear Static Procedures. For each building the geometric properties are presented and the modelling options assumed during the performed studies and the dynamic properties of the buildings are described. Following the results of the seismic assessment of both case studies are presented and discussed. The reliability of the Non-linear Static methods is evaluated by comparing the computed seismic demand, in terms of displacements and inter-storey drift, to the results of non-linear response history analysis.

For the parking structure, a particular relevance is given also to the evaluation of the damage limitation requirement according to the EC8.

4.1 SAC-9 Building

The 9-storey structure, shown in figure 4.1, was designed by the American consultant firm Brandow & Johnston Associates in the context of a joint research project (SAC) that involved three non-profit organizations: Structural Engineers Association of California (SEAOC), the Applied Technology Council (ATC), and California Universities for Research in Earthquake Engineering (CUREE). The structure was designed to serve as standard office buildings located over stiff soil, with a limit drift capacity of $h/400$, where h is the storey height.

The nine-story building (SAC-9) has a plan dimension of 45.73 m x 45.73 m and a height of 37.19 m above the ground level. The building has five bays of 9.15 m in both east-west and north-south directions. The building has a basement level and the concrete foundation walls surround the soil restraining the structure at the ground level from horizontal displacement.

The horizontal force resisting system of the building consists of perimeter steel moment resisting frames (SMRF). Each of the four perimeter frames is a rectilinear skeleton of beams and columns, with the beams rigidly supported on the columns. The resulting rigid behaviour leads to the rise of high values of bending moment and shear force at the extreme sections of frame members. The bending rigidity and

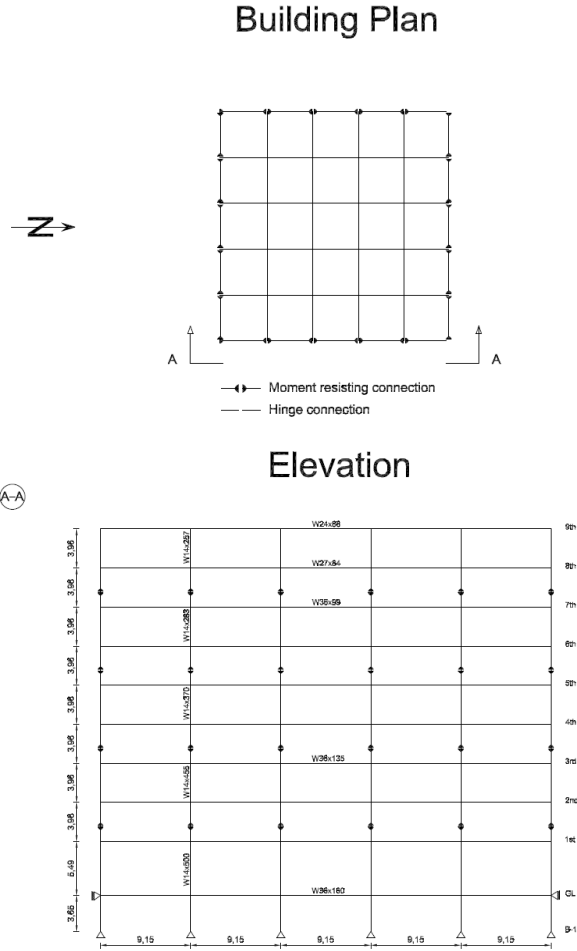


Figure 4.1: Los Angeles 9-storey SAC building adapted from Chopra et al 2002.

strength of the perimeter frame members is, therefore, the primary source of lateral stiffness and strength for the entire building.

The interior frames, designed to carry only gravitational loads, have simple (shear) connections. The moment resisting frames are realized by five different beam profiles and five column profiles with decreasing cross section from the bottom- up. For the columns, the splices are located on the first, third, fifth, and seventh levels at 1.83 m above the centre-line of the beam to column. The characteristics of all sections are presented in table 4.1.

Beams are made of A36 steel, while the columns were designed with A 570 Gr. 50 steel. The properties of the materials are summarised in table 4.2. The expected values are the product of a code-prescribed factor and the nominal minimum values. This factor is around 1.1 for A570 Gr. 50 steel and 1.5 for A36 steel class, as with the FEMA 356 Table 5-3 [32].

Beams are rigidly connected to the columns by welded connections with cover

Table 4.1: Section properties for columns and beams.

Section	A [$\times 10^{-2} m^2$]	ky [-]	kz [-]	Ixx [m^4]	Iyy [m^4]	Izz [$\times 10^{-4} m^4$]
W14x257	4.88	0.255	Inf	0	0	14.2
W14x283	5.37	0.259	Inf	0	0	16
W14x370	7.03	0.272	Inf	0	0	22.6
W14x455	8.65	0.286	Inf	0	0	29.9
W14x500	9.48	0.292	Inf	0	0	34.2
W24x68	1.3	0.49	Inf	0	0	7.62
W27x84	1.6	0.495	Inf	0	0	11.9
W30x99	1.88	0.53	Inf	0	0	16.6
W36x135	2.56	0.537	Inf	0	0	32.5
W36x160	3.03	0.498	Inf	0	0	40.6

Table 4.2: Materials mechanical properties

Steel class	Density ρ [Kg/m^3]	Young modulus E [MPa]	Nominal yield stress F_y [MPa]	Nominal tensile stress F_u [MPa]	Expected yield stress F_{ye} [MPa]	Expected tensile stress F_{ue} [MPa]
A36	7697	200,000	248	400	372	440
A570	7697	200,000	345	423	393	455

plates on both the beam flanges to make sure that formation of plastic hinge takes place away from the face of the column. The panel zone is strengthened by doubler plates as shown in figure 4.2. The cover plates and the doubler plates are designed with the same steel grade as the beams and columns respectively.

For seismic analysis, the additional masses of the structure from various components such as floor slabs, ceiling, flooring, mechanical, electrical, partitions, roofing and a penthouse located on the roof, are considered. A summary of these masses is presented in table 4.3.

4.2 Modeling of SAC-9 building

The finite element analysis program Sap2000 v19. was employed to perform all analyses. Sap2000 can predict the static and dynamic behaviour of plane and space frames undergoing large displacements, accounting for both geometric and mechanical non-linearities.

For seismic analysis only the moment resisting (MR) frame along the north-south direction is modelled considering the building symmetry and regularity in elevation. A basic centreline model is used i.e. the frame members extend from centreline to centreline. Consequently, the internal actions are computed at the connection centreline rather than at the faces of beams and columns, which results

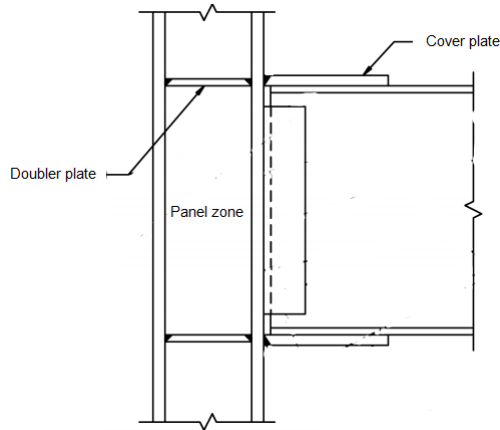


Figure 4.2: Typical column-beam welded connection with panel zone strengthened with doublers.

Table 4.3: Additional masses on the building floors

Floor	mass/length
GL	10427
1	10919
2	10689
3	10708
4	10735
5	10746
6	10746
7	10746
8	10746
9	11643

in a conservative estimate of bending moment and shear values. For simplicity, the dimensions and distortions of panel zones are not considered. This modelling approximation is also motivated by the fact that the use of centreline dimensions compensates for the disregard of panel zone shear deformations [33].

The bi-dimensional model represents only the perimeter frame and ignores the interior bays. However, although the interior frames do not contribute in carrying the lateral loads, their contribution to the $P - \Delta$ effects cannot be neglected. The gravity loads carried by those frames lead to the rise of significant additional overturning moments on the deformed configuration of the perimeter frames. In the model, these effects are accounted by considering an additional ghost column attached to the MR frame by rigid links as shown in figure 4.4. The dummy column is loaded at each floor by the gravity loads carried by all the gravity frames and the MR frames orthogonal to the north-south MR frame. The column slices are hinged both ends. In this way, the column can follow the deflected shape of the frame without carrying any

bending moment induced by lateral loads. A simple schematization of this modelling simplification is shown in figure 4.3. The total moment acting on the cantilever beam with the vertical load acting on it is

$$M = Hh + P\Delta \quad (4.1)$$

If the vertical load is applied on the dummy column rigidly connected to the cantilever beam, the vertical equilibrium yields

$$P\Delta = RhR = \frac{P\Delta}{h} \quad (4.2)$$

Hence the total bending moment at the bottom of the cantilever beam is

$$M = Hh + Rh = Hh + P\Delta \quad (4.3)$$

which is equal to the expression found for the initial scheme. Therefore, the schemes are structurally equivalent.

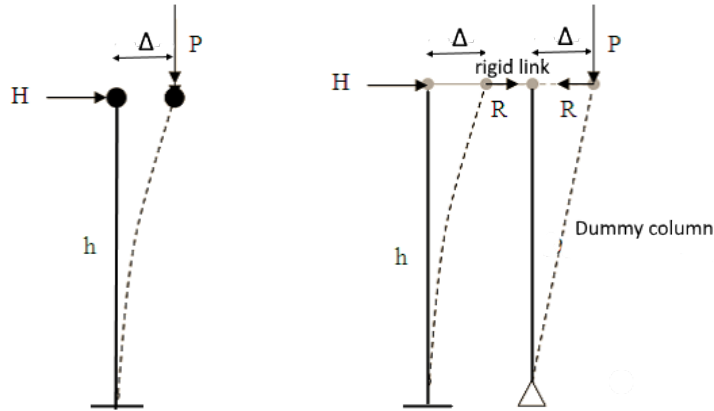


Figure 4.3: Principles of the use of a dummy column to include P- Δ effects.

4.2.1 Concentrated plasticity model

For the non-linear static and dynamic analyses, the post yielding behaviour is simulated by assigning concentrated plastic hinges to the beams and columns. The elastic behaviour occurs over member length, then deformation beyond the elastic limit occurs entirely within hinges, which are modelled in discrete locations as shown in figure 4.5.

For beams, the behaviour of the plastic region is generally described by a moment-rotation relation. The plastic rotation angles depend on the member geometry as well as on the material's mechanical properties. In the case of columns, the plastic behaviour depends also on the level of axial forces. The plastic moment, i.e the

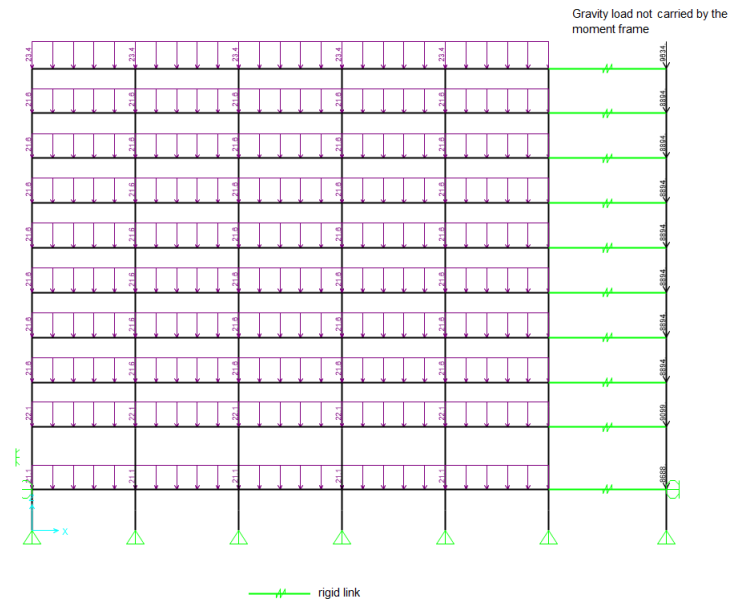


Figure 4.4: Modelling interior (gravity) columns to include P-Delta effects.

maximum moment of resistance of a fully yielded cross-section, is given as $F_{ye}Z$, where Z is the plastic section modulus. Under a monotonic loading the yielding is followed by a constant strain hardening and then a post peak residual strength range.

In this study, the parameters that define the backbone relation for the structural elements are computed using the equations in FEMA 356 Table 5-3, that provides also acceptance criteria in terms of allowable rotations taking into consideration the

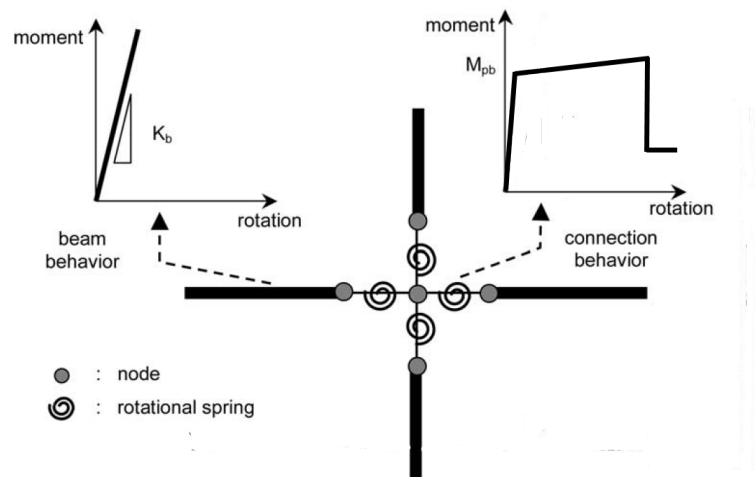


Figure 4.5: Model with concentrated non linear zones at extremes of frame members

Table 4.4: Moment-rotation relation parameters and acceptance criteria ranges for the different sections of the frame members computed using FEMA356 recommended equations.

Section	M_y [kNm]	θ [rad]	a [-]	b [-]	c [-]	IO [-]	LS [-]	CP [-]
W24x68	1015	0.0102	8	10	0.52	0.85	7.8	9.6
W27x84	1399	0.009	7.7	9.7	0.49	0.8	7.4	9.1
W30x99	1789	0.008	7.6	9.6	0.49	0.8	7.4	9.1
W36x135	2919	0.0068	8.3	10.4	0.55	0.9	8.1	9.9
W36x160	3579	0.0067	9	11	0.6	1	9	11
W14x257	2755	0.0064	9	11	0.6	1	9	11
W14x283	3066	0.0063	9	11	0.6	1	9	11
W14x370	4164	0.0061	9	11	0.6	1	9	11
W14x455	5295	0.0085	9	11	0.6	1	9	11
W14x500	5939	0.0053	9	11	0.6	1	9	11

required performance level. The equations recommended by FEMA are based on the analysis of the results of over 300 tests on beams and columns sub-assemblies.

The non-linear parameters and the acceptance criteria ranges computed for the SAC-9 building's beams and columns sections are presented in table 4.4. A brief description of damage entity corresponding to the different acceptance criteria is presented in table 4.5.

The values of the parameters refer to the generic moment-rotation relation in figure 4.7 where θ is the elasto-plastic rotation of the element, θ_y is the rotation corresponding to the material yielding, Δ is the total elasto-plastic displacement, and Δ_y is the displacement corresponding to the material yielding as shown in figure 4.6.

The plastic force-deformation or moment-rotation curve defines the non-linear behaviour under monotonic loading. Under load reversal or cyclic loading, the behaviour will deviate from the initial monotonic backbone curve due the hysteresis i.e. the process of energy dissipation through deformation. In this study, for simplicity, the back-bone curves are used in combination with an isotropic hysteresis model.

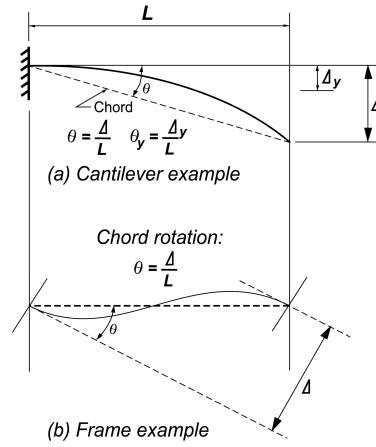


Figure 4.6: Description of chord rotation, adapted from FEMA356.

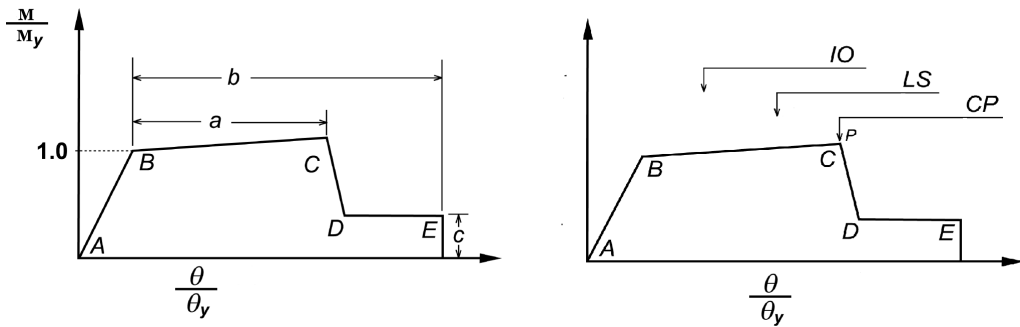


Figure 4.7: Generalized element moment-rotation relations for modelling and acceptance criteria, adapted from FEMA356.

Table 4.5: Performance level of steel buildings, adapted from FEMA356

Level	Description
Immediate Occupancy	"Restricted damage, no lasting drift, structure maintains initial stiffness and strength, lift can be resumed to use, Fire protection serviceable" .
Life Safety	"Medium damage, some lasting drift, some remaining stiffness and strength in all floors, damage to partition, structure may be out of range of economical rehabilitation"
Collapse Prevention	"Serious damage, large drift, little remaining strength and stiffness but loading bearing column and wall function, structure is near failure"

Table 4.6: Transition periods and amplification factors for the construction of a simplified smooth elastic response spectrum of El Centro ground motion.

Transition periods [s]				Amplification factors [-]		
T_a	T_b	T_c	T_d	a_A	a_v	a_d
0.03	0.13	0.41	2.95	3.66	2.05	1.63

4.2.2 Seismic input

Considering the building's location, the frame was analysed with El Centro earthquake ground motion (May 18 1940, Imperial Valley, California). For the non-linear time history analysis, the North-South component of the ground motion (PGA= 0.32 g) was considered. The record taken from the PEER's database, is shown in figure 4.8. In order to obtain comparable results, for the N2 a simplified smooth response spectrum of El-Centro ground motion is considered, figure (4.9). The simplified spectrum was constructed according to Newmark and Hall procedure [25] using the amplification factors in table 4.6. In addition, in order to assess the influence of ground motion intensity on the accuracy of the used methods, the ground motion and the respective spectrum are scaled up by the factors 0.75, 1 and 1.5.

The N-RHA was performed using Hilber-Hughes-Taylor numerical method ($\gamma = 0.5$; $\beta = 0.25$) with a time step of 0.01s. A viscous damping of $\xi = 0.02$ was assumed and the geometric non-linearities $P-\Delta$ were accounted.

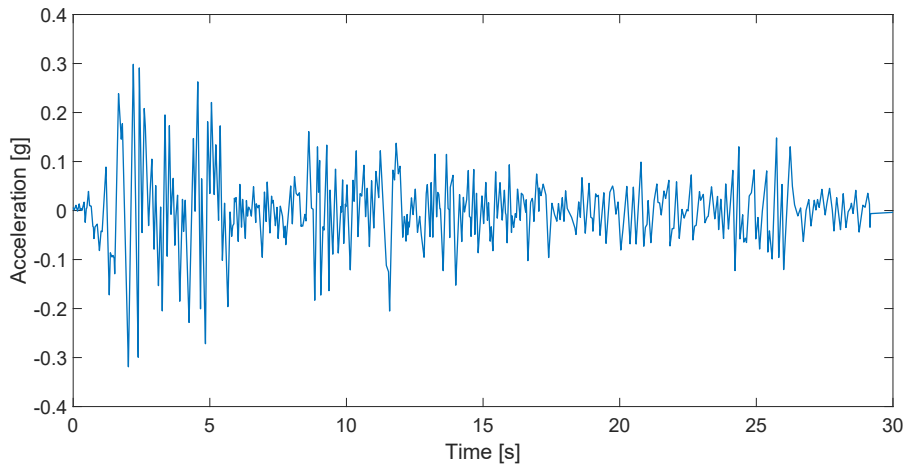


Figure 4.8: North-South component of El Centro ground motion from PEER's database.

4.2.3 Modal Pushover Analysis

A preliminary modal analysis was performed to select the significant modes in terms of modal mass participation ratio i.e. the portion of the total seismic mass that is

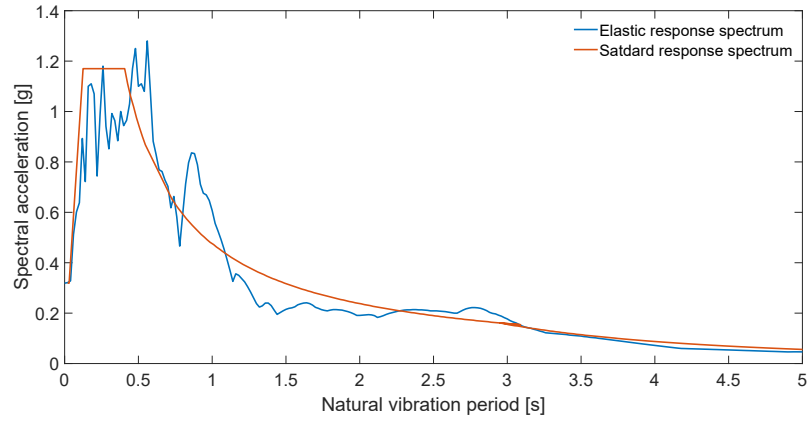


Figure 4.9: Elastic response spectrum of El-Centro ground motion.

activated by each mode. Figure 4.12 shows that the first three vibrational mode shapes are typical of regular tall buildings: the fundamental mode is a translational mode, with a period of 2.27s and maximum displacement at the roof; the second mode is a parabolic shape mode with a period of 0.89s and a maximum displacement also at the roof; and the third mode has a period of 0.49 seconds and forms an "S" shape.

The modal mass participation ratios are 0.77, 0.10, and 0.04, respectively. Hence, the dynamic response of the building is highly dominated by its fundamental mode.

For the pushover analyses the lateral load patterns were taken proportional to the first three modes as shown in figure 4.15. The pushover analyses were performed in displacement control up to near collapse in order to observe the building's maximum lateral strength in terms of base shear. Displacement control was used to measure the building's roof displacement that results from the applied loads, and to adjust the magnitude of the loading in attempt to reach the prefixed target

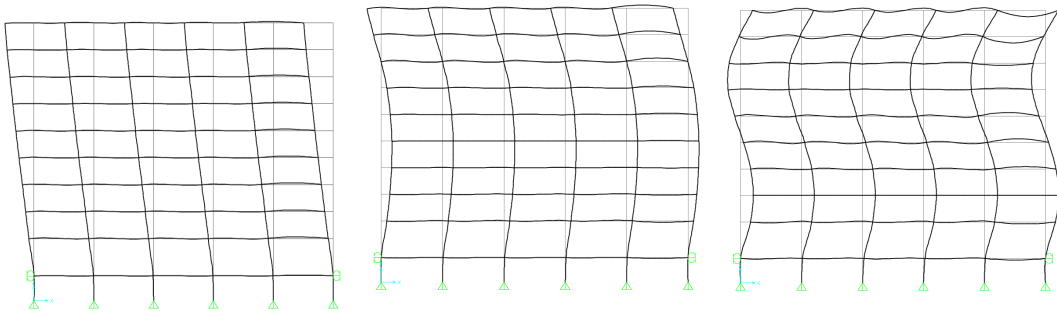


Figure 4.10: Mode 1

Figure 4.11: Mode 2

Figure 4.12: Mode 3

Figure 4.13: First three vibrational mode shapes of the SAC-9 building.

displacement. The resulting pushover curves, shown in figure 4.15, represent the normalized base shear force and the associated top lateral displacement at each increment.

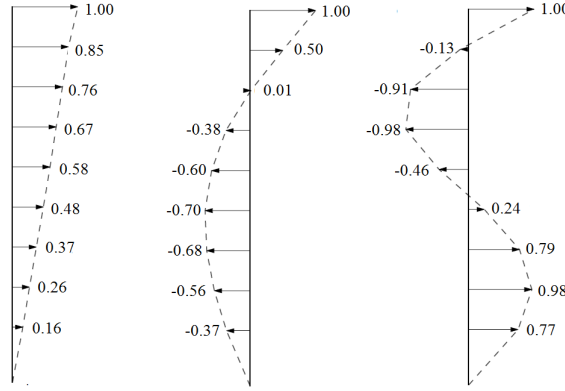


Figure 4.14: Load patterns $s_n = m\phi_n$, $n = 1, 2, 3$ normalized to the roof lateral force.

From the pushover curve in figure 4.15, and figure 5.2, that illustrate the intermediate steps of the pushover analysis for the first mode, it can be seen that the response of the structure is elastic up to a base shear-value of around 15% of the total weight of the structure. The non-linear behaviour takes place with the yielding of beams of the first and the third floor above the ground level. The post yield behaviour exhibits only a short strength plateau followed by a rapid decrease in lateral load resistance due the $P - \Delta$ effects.

In addition, the sequence of hinge formation illustrated in figure 5.2 shows clearly that the MR frame was designed according to the strong column-weak beam approach in order to maximize the energy dissipation before reaching the collapse condition. In fact, the plastic hinges form initially at the beam ends and successively only at the bottom columns above the ground level.

The pushover curves were idealised with bi-linear curves assuming a zero post-yielding stiffness, which in turn were converted into the force-deformation relation of the equivalent SDOF systems using the relations (2) and (3.3.1). The properties of the respective SDOF systems, presented in table 4.7, were computed such that the bi-linear SDOF system dissipates the same amount of energy as the MDOF system as previously shown in figure 3.2.

Knowing the stiffness and yield strength of the single degree of freedom systems, the displacement time histories were determined by solving the governing equations (3.10). For this purpose, the constant average acceleration variant of Newmark method [25] was used with a time stepping $\Delta t = 0.01s$.

The resulting displacement histories due different intensities of the El-Centro ground motion are shown in figure (4.17).

4. CASE STUDIES

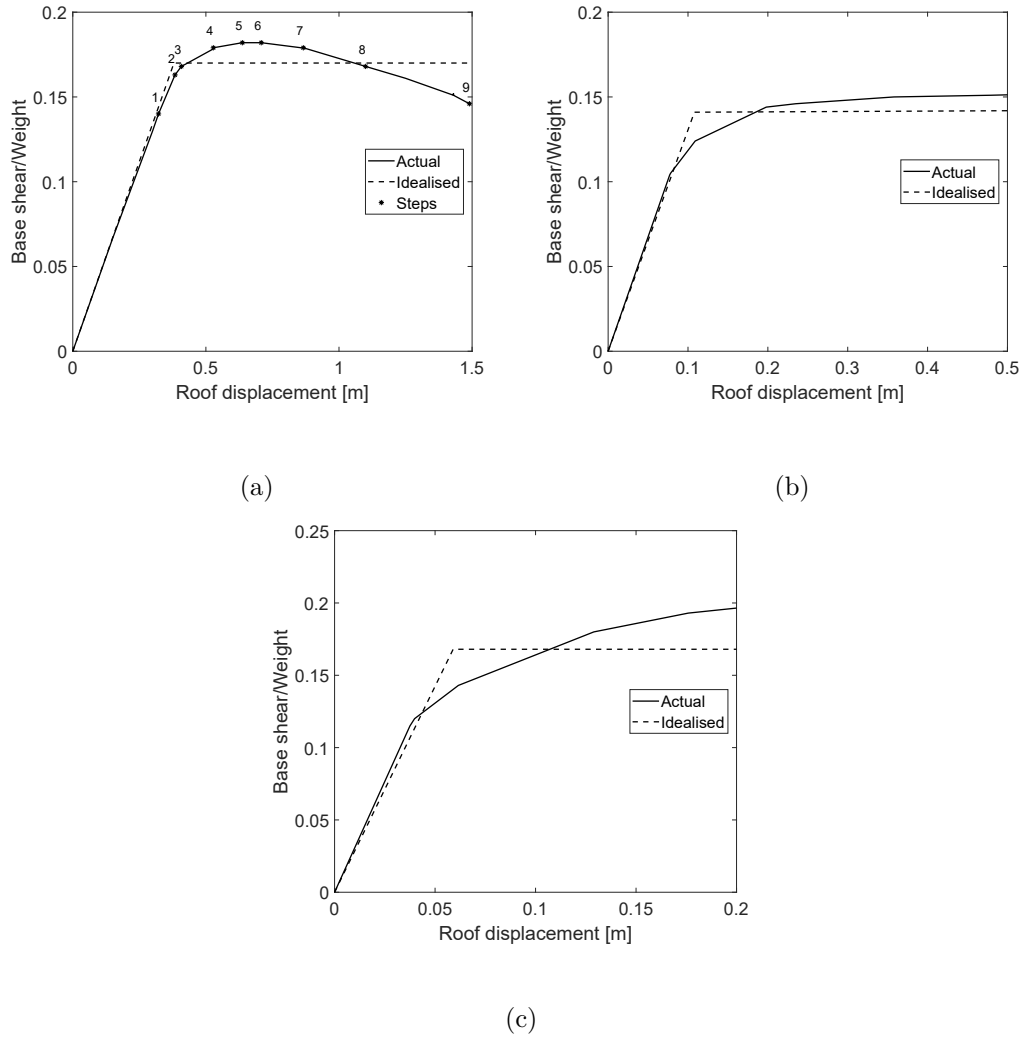


Figure 4.15: Modal pushover curves obtained with lateral load patterns proportional to the first three mode shapes of SAC-9.

Table 4.7: Properties of the inelastic SDOF systems

SDOF system	T_n [s]	D_{ny} [m]	F_{sny}/L_n [m/s ²]	Γ_n [-]	M_n^* [kN/m/s ²]	L_n [kN/m/s ²]
"Mode" 1	2.268	0.27	2.07	1.37	37000	27063
"Mode" 2	0.844	0.22	12.16	-0.51	4988	-9209
"Mode" 3	0.473	0.24	42.8	0.24	1700	6964

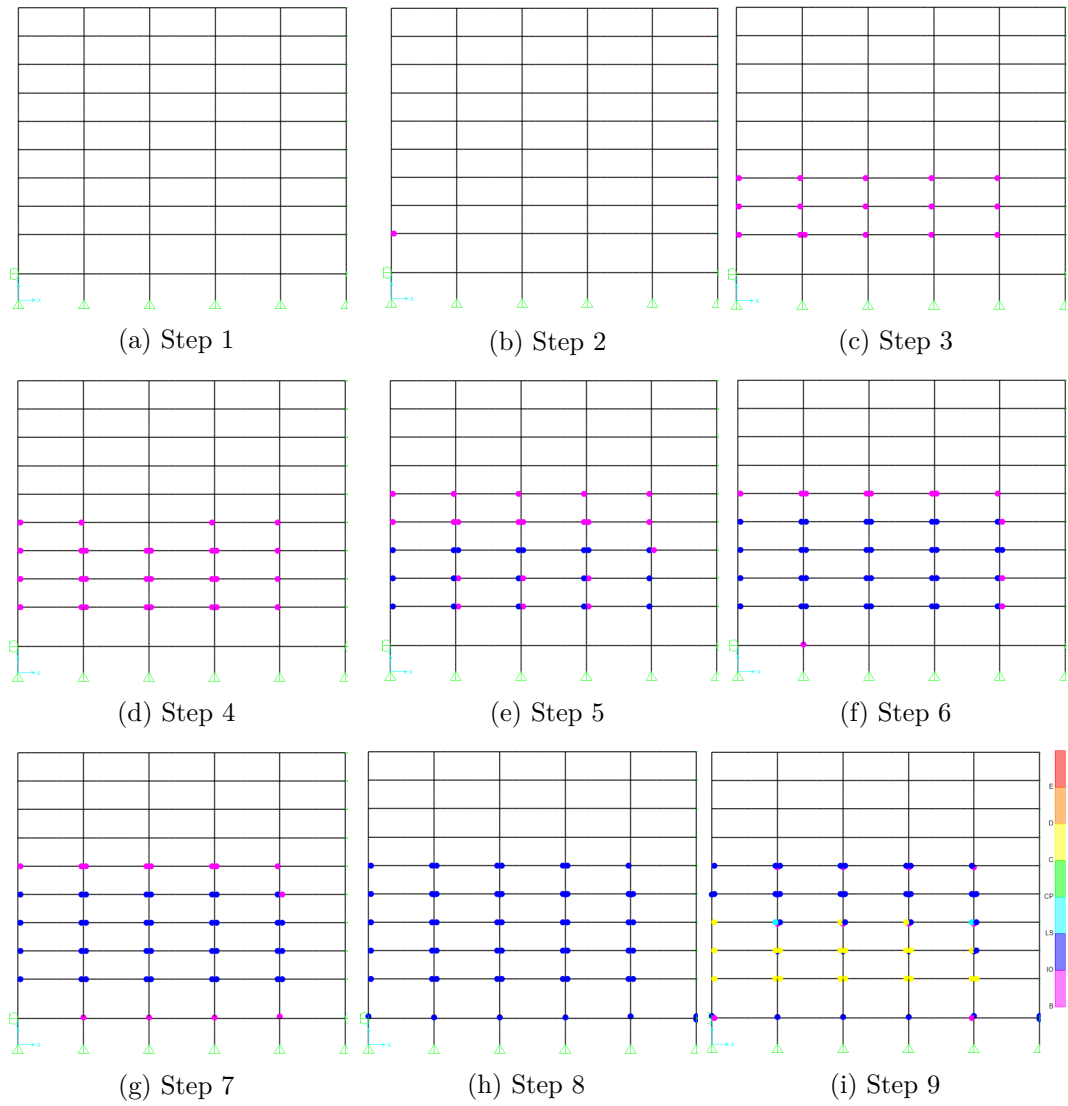


Figure 4.16: Hinge locations and deformation degree at intermediate steps of the pushover analysis with s_1 load pattern

4. CASE STUDIES

From the displacement time histories, the peak values of the SDOF systems were selected and converted to the correspondent roof displacement values of the building using the transformation factors in table 4.7. The global response of the structure is obtained by combining the contributions of the three modes. For the combination the SRSS rule was used since the building's first three vibrational modes differ by more than 10%. A summary of the intermediate and final results is presented in table 4.8.

Table 4.8: The peak displacements of the equivalent SDOF systems and the corresponding contributions to the SAC-9 roof displacement under different intensities of El-Centro ground motion.

	0.7 x El Centro		1 x El Centro		1.5 x El Centro	
	D_{max} [m]	u_r [m]	D_{max} [m]	u_r [m]	D_{max} [m]	u_r [m]
"Mode" 1	0.18	0.25	0.27	0.32	0.35	0.48
"Mode" 2	-0.1	0.05	-0.14	0.07	-0.21	0.11
"Mode" 3	0.05	0.01	0.07	0.02	0.09	0.02
SRSS	-	0.25	-	0.32	-	0.49

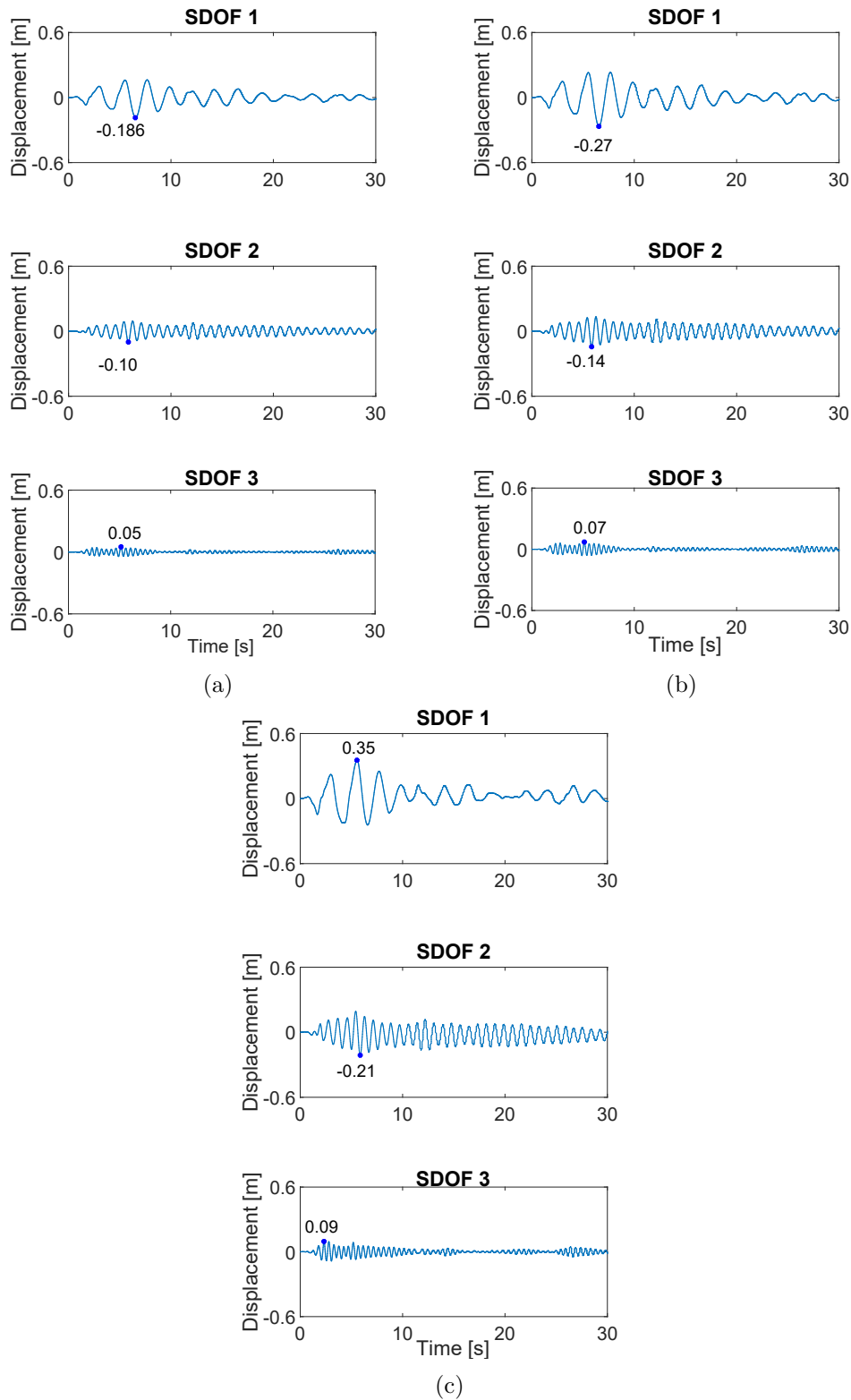


Figure 4.17: Displacement time histories of the equivalent SDOF systems excited by 0.7 x El-Centro (a), 1 x El-Centro (b) and 1.5 x El-Centro ground motion (c).

4.2.4 N2 Method

For each of the three equivalent SDOF systems the capacity curve was derived from the force-displacement relation by dividing the force values by the modal mass. The resulting relations were then converted into the Acceleration Displacement Response Spectrum (ADRS) format by the use of the equations (3.31). The demand spectrum, instead, is assumed as the elastic response spectrum of El-Centro ground motion.

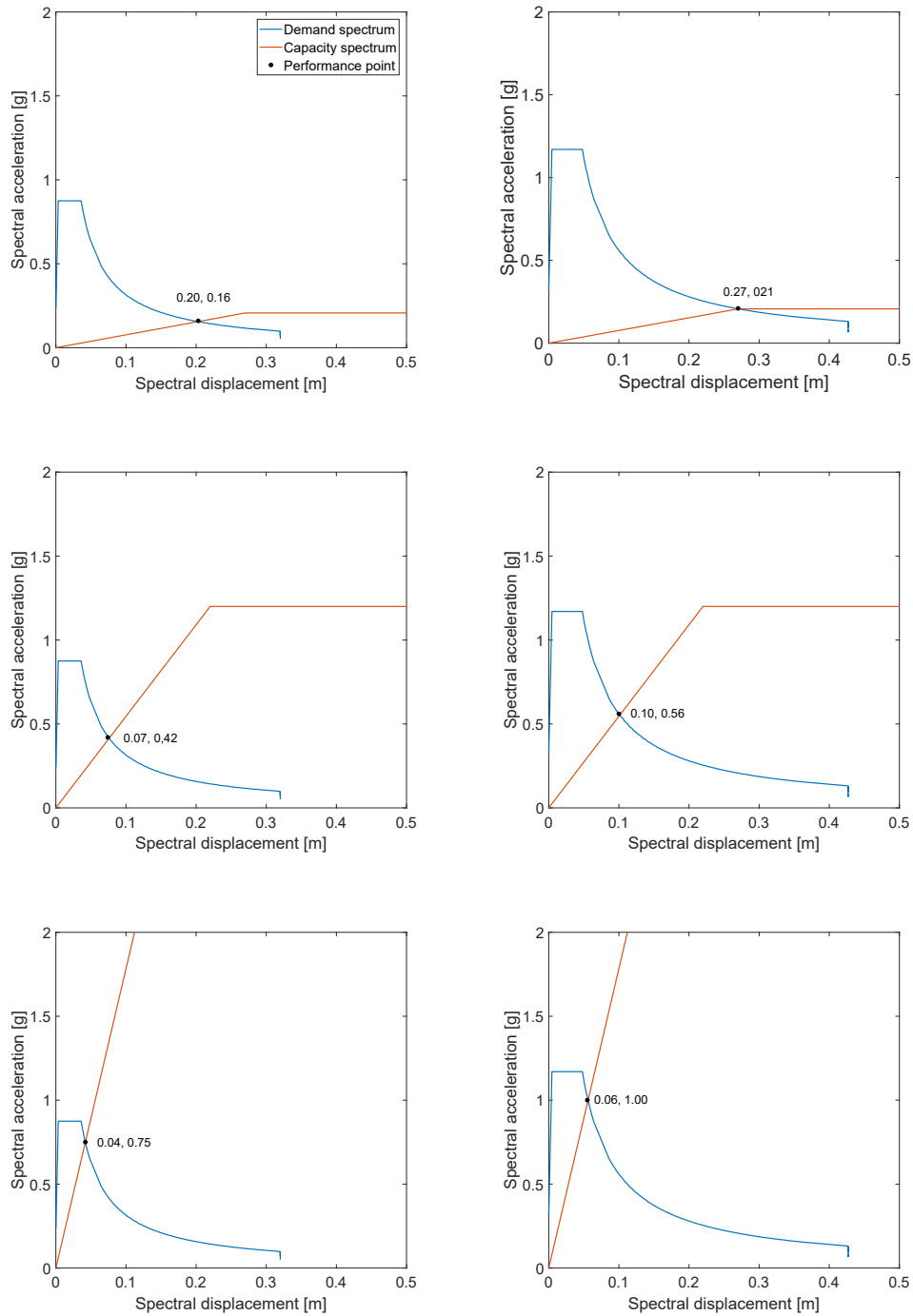
From graphs in figure 4.18 it is clear that all the three SDOF systems respond elastically to ground motion intensity lower or equal to 1 x El Centro. Hence, the seismic demand is simply given by the intersection of the elastic demand spectrum and the line corresponding to the elastic period of the equivalent SDOF system.

Under 1.5 x El Centro only the first SDOF system is excited beyond its elastic range and the seismic demand was computed using both the iterative and simplified procedure, as shown in figure 4.19. For the iterative procedure a ductility factor of 1.1 was initially assumed. The iteration converged to $\mu = 1.5$. The intermediate and final results are summarised in table 4.9 .

Equivalent results are obtained with the simplified procedure. Assuming an unlimited elastic behaviour of the SDOF system, seismic demand is represented by the intersection of the elastic demand spectrum and the line corresponding to the elastic period $T = 2.268$ s of the SDOF system as shown in figure (4.19). The corresponding values $S_{ae} = 0.207$ g and $S_{de} = 0.4$ m are obtained. The reduction factor R_μ amounts to $R_\mu = S_{ae}/S_{ay} = (0.31$ g)/(0.207 g) = 1.5. Since the period of the system $T = 2.268$ s is larger than the characteristic period of the spectrum $T_c = 0.58$ s, the equal displacement rule applies: $\mu = R_\mu = 1.5$, $S_d = S_{de} = 0.4$ m. The seismic demand of the equivalent SDOF system is graphically represented by the intersection of the capacity curve and the demand spectrum for $\mu = 1.5$ as it is clear from figure 4.19 b.

Table 4.9: Intermediate results of the iterative procedure for the determination of the target displacement of the first inelastic system under 1.5 X El Centro ground motion

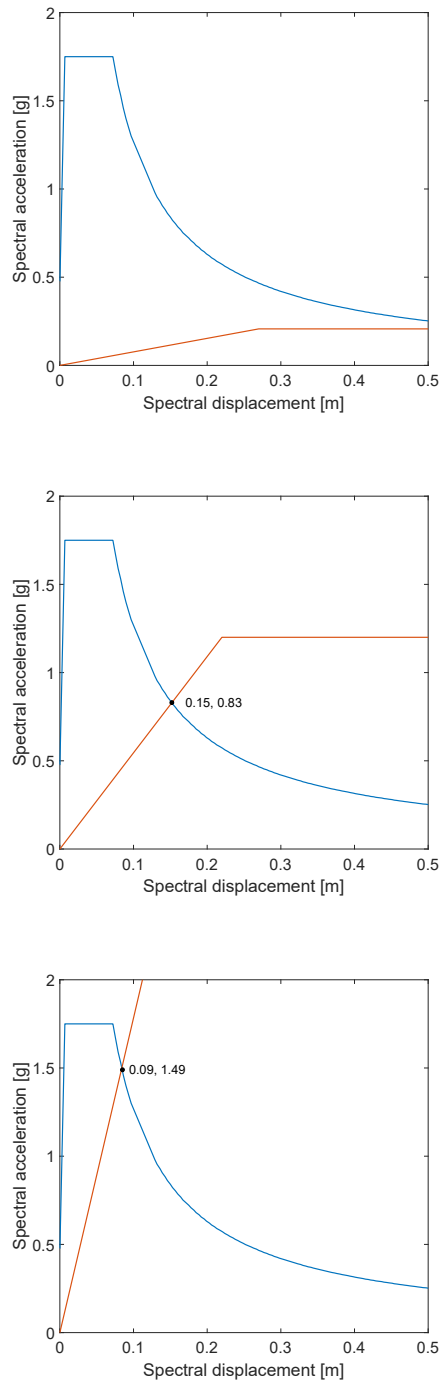
Iteration	μ [-]	S_d [m]	S_a [g]	S_d/S_y [-]	Error [%]
1	1.1	0.55	0.207	2.0	82
2	1.2	0.51	0.207	1.9	58
3	1.3	0.47	0.207	1.7	31
4	1.4	0.435	0.207	1.6	14
5	1.5	0.4	0.207	1.5	0



(a) Capacity spectrum of the three "modes" versus elastic demand spectrum corresponding to 0.75 x El Centro.

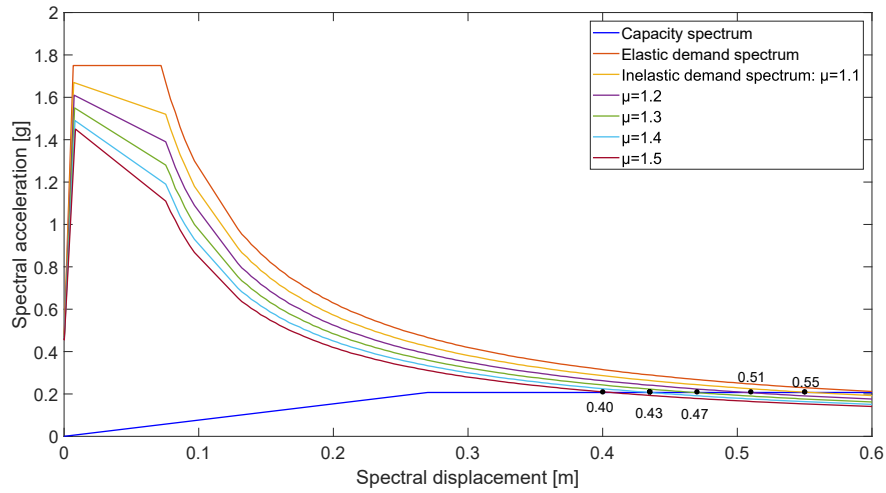
(b) Capacity spectrum of the three "modes" versus elastic demand spectrum corresponding to 1 x El Centro.

Figure 4.18: Representation in the ADRS format of the capacity curves of the SDOF systems and the elastic demand spectrum corresponding to different intensities of El Centro ground motion.

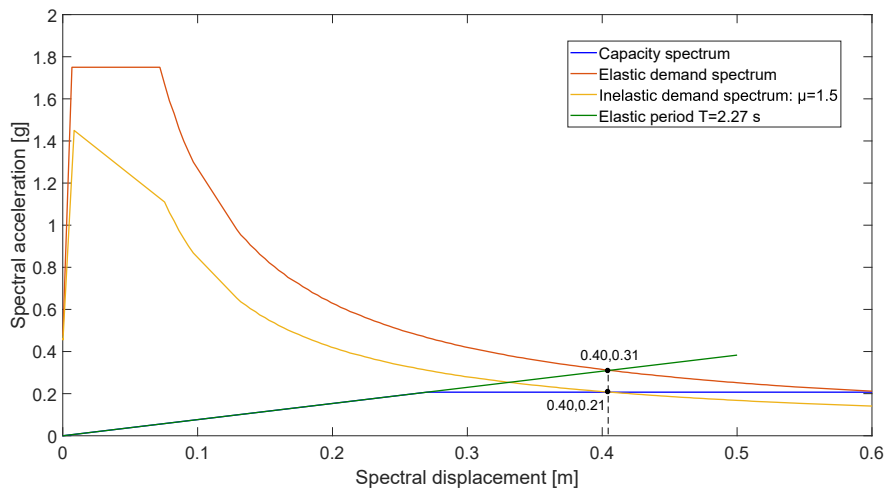


(c) Capacity spectrum of the three "modes" versus elastic demand spectrum corresponding to 1.5 x El Centro.

Figure 4.18: Representation in the ADRS format of the capacity curves of the SDOF systems and the elastic demand spectrum corresponding to different intensities of El Centro ground motion (cont.)



(a)



(b)

Figure 4.19: Iterative (a) and simplified (b) procedures for the determination of the displacement demand of the first SDOF system.

4.2.5 Results Discussion

Figure 4.20 compares floor displacements, inter-storey drifts ratios (as % of floor height) over the height of the 9-storey building, corresponding to an intensity of 1.5 x El-Centro ground motion computed by the MPA method and the exact N-RHA. In order to highlight the influence of higher modes the peak values of floor displacement and drift ratios are plot including one, two, and three modes. It is clear that the higher mode contributions have little influence on the one-mode estimate of the roof displacement. Hence, the first mode is sufficient to predict the building global response in terms of peak displacement. However, if the local response of the buildings elements in terms of inter-storey drift is considered, the first mode alone seems inadequate and hence it is necessary to account for the significant response contributions of the second and third mode in order to achieve a considerable improvement.

The MPA, including three modes, gives an accurate estimation of the displacements of the lower floors while it overestimates the upper floor displacements by up to 18%. The drifts are underestimated by up to 4 per cent in the lower storeys, overestimated by up to 25 per cent in the middle storeys, and up to 10 for the upper floors.

The inadequacy of the first mode alone in estimating inter-storey drifts is mainly attributable to the fact that first mode shape is transnational while the second and third modes include the simultaneous displacement of the floors in opposite directions.

Figures 4.21a and 4.21a plot the approximate values from MPA and N2 and the exact values from non-linear RHA for the roof displacement and inter-storey drift ratios, respectively. By comparing the results of the N2 method and the MPA method considering for both the contributes of all the three modes it is clear that the N2 method estimations higher values overestimates the real responses of the structure. The conservatism of N2 method's results arises mainly from the use of an approximate smooth response spectrum instead of the real response spectrum for comparative purposes.

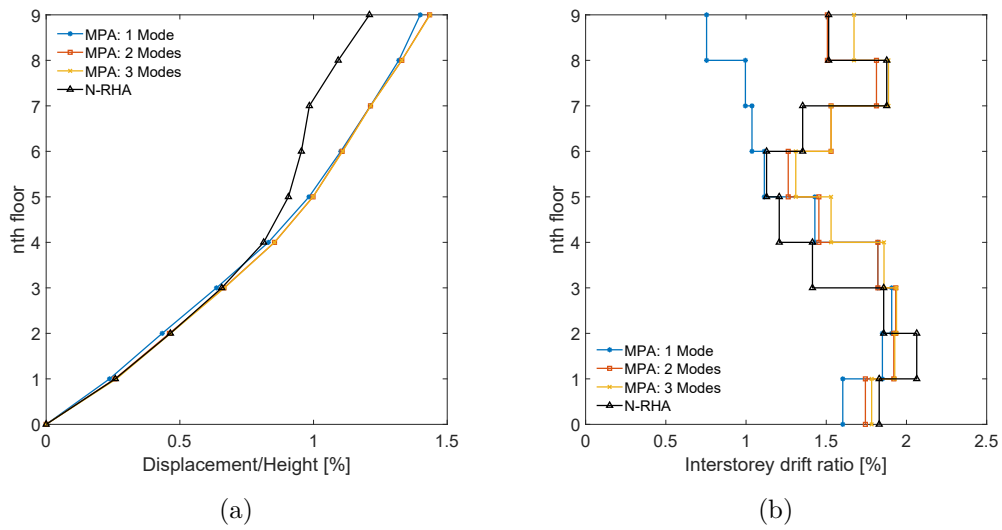


Figure 4.20: The effect of higher modes contributions on height-wise variation of floor displacements (a) and storey drift ratios (b) from MPA compared with non linear RHA for 1.5 x El Centro ground motion.

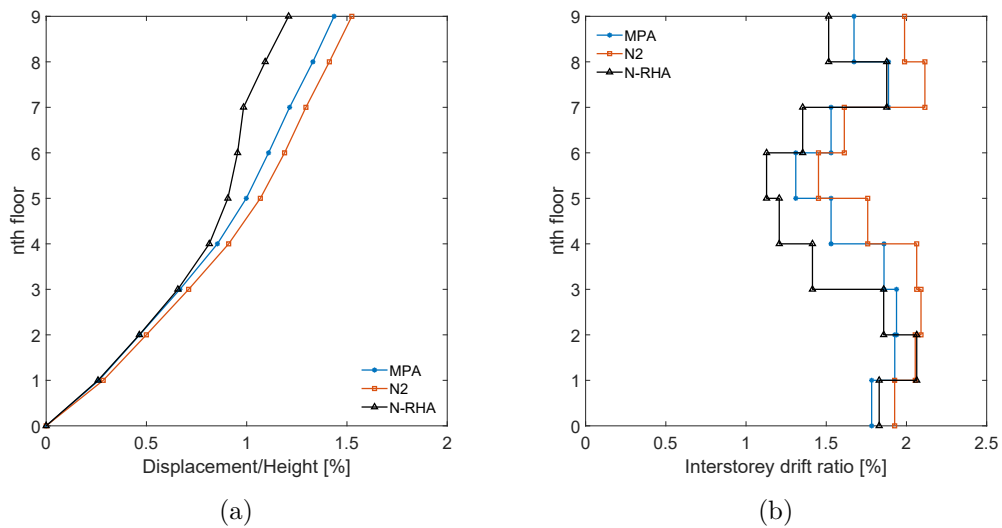


Figure 4.21: Height-wise variation of floor displacements (c) and storey drift ratios (d) from N2 method and MPA compared with non-linear RHA for 1.5 x El Centro ground motion

4.3 Helix parking

4.3.1 Overview

This is a nine-level parking garage structure located in Hasselt, Belgium. The building has a rectangular plant with dimensions 28.20x48.00m and consists of two-bay single threaded helix. The parking aisles slope along their length of 5.4 % and they are connected by flat cross-ramps.

The gravity load resistant system is made by concrete decks supported on steel wide flange secondary beams which in turn are supported on the main longitudinal beams. The main beams are connected directly to the columns with simple shear connections. The pedestrian access to the parking is via a stair-elevator tower.

The structure has no facade and the stability to lateral loads is provided by an adequate number of inverted- V-bracings. The planimetric collocation of the four vertical sets of bracings is shown in figure 4.23b. The decks are made of prefabricated composite slabs with a thickness of 80 mm for the top three ramps of each bay and 103 mm for the bottom ramps, whereas the stair core has a wall thickness of 200mm. The steel skeleton is made by of twelve different beam sections decreasing cross section from the bottom- up. A summary of the different profiles and their collocation is presented in table 4.10. Beams are made of S355 steel, while the columns were designed with S235 steel. The decks concrete is a C30/37. The properties of the materials are summarised in table 4.11.

4.3.2 Loads

In addition to the self weight of the beams and the prefabricated slabs, and a permanent load of 0.89 kN/m², due to floor finishing and partitions, the following imposed live load are considered: 5 kN/m² for the levels 1 to 3, and 2.5 kN/m² for the levels 4 to 9. These values are determined according to the EC1 provisions based

Table 4.10: Section profiles of primary, secondary beams and columns of the ramps connecting the different levels.

Ramp	Longitudinal beam	Transversal beam	Column
0-1	IPE360	IPE360	HE240B
1-2	IPE550	IPE600	HE240B
2-3	IP360	IPE360	H240A
3-4	IP300	IPE550	HE240B
4-5	IPE330	IPE360	HE240A
5-6	IP300	IPE550	HE240A
6-7	IPE330	IPE360	HE240A
7-8	IP300	IPE550	HE240A
8-9	IPE330	IPE360	HE240A

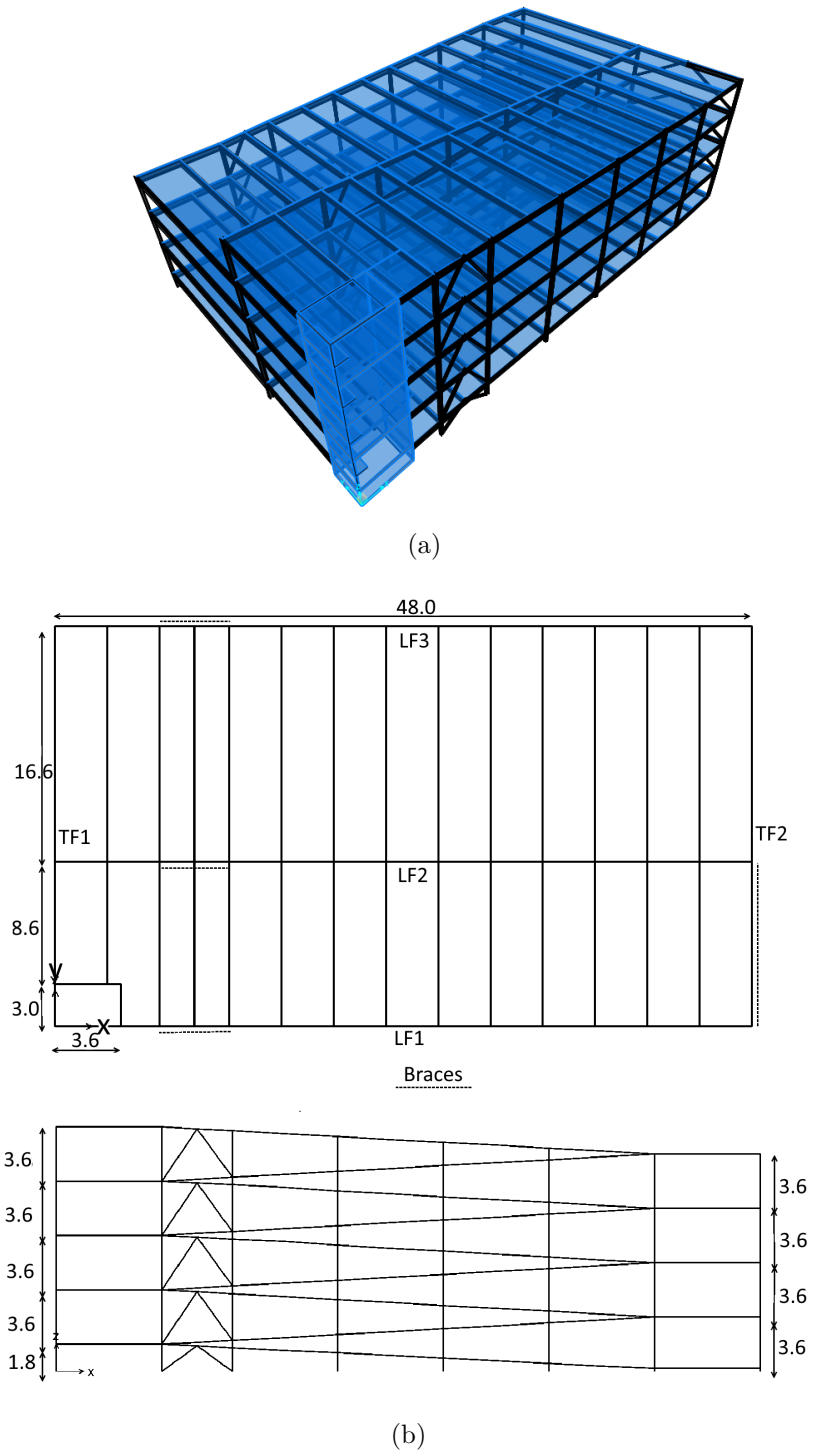


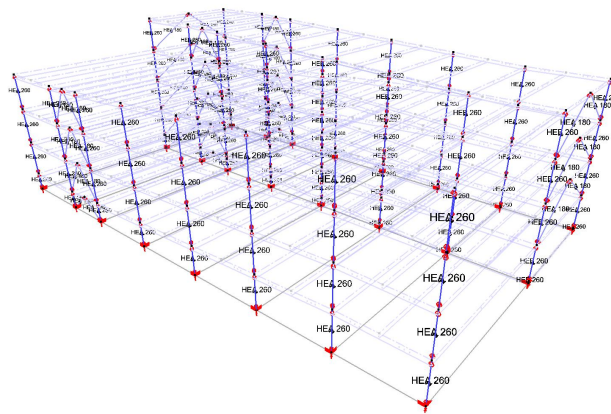
Figure 4.22: (a) 3D representation of the Helix-parking, (b) plan and lateral view.

4. CASE STUDIES

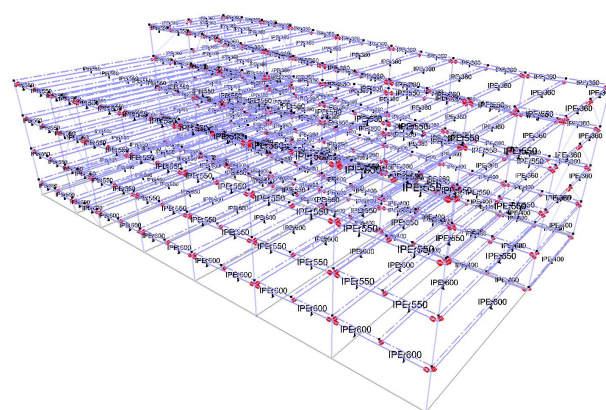
Table 4.11: Mechanical properties of the materials.

Material	Density [Kg/m^3]	Young modulus [MPa]	Nominal yield stress F_y [MPa]	Nominal tensile stress F_u [MPa]	Expected yield stress F_{ye} [MPa]	Expected tensile stress F_{ue} [MPa]	Concrete compressive strength F_{ck} [MPa]
S235	7697	200,000	235	360	258	396	-
S355	7697	200,000	355	510	390	561	-
C30/37	2548	33650	-	-	-	-	30

on the structure typology as shown in table 4.12. In particular the first three levels are considered to be category G while the upper levels belong to the F category. Following EC8, in the seismic design combination, dead loads are considered with their nominal values, while live loads with 30% of their nominal value.



(a)



(b)

Figure 4.23: (a) columns profiles and (b) beams profiles.

Table 4.12: Imposed loads on garages and vehicle traffic areas, from EC1

Categories of traffic areas	q_k [kN/m ²]	Q_k [kN]
Category F Gross vehicle weight: ≤ 30 kN	q_k	Q_k
Category G 30 kN < gross vehicle weight ≤ 160 kN	5,0	Q_k
NOTE 1 For category F, q_k may be selected within the range 1,5 to <u>2,5</u> kN/m ² and Q_k may be selected within the range 10 to <u>20</u> kN.		
NOTE 2 For category G, Q_k may be selected within the range 40 to <u>90</u> kN.		
NOTE 3 Where a range of values are given in Notes 1 & 2, the value may be set by the National annex. The recommended values are underlined.		

4.3.3 Structural behaviour

The structural system is made up of non-moment resisting frames with limited number of bays equipped with braces throughout the height of the structure. Bracing sets are included in both plan directions (two in each direction) in order to limit the twisting arising from non-symmetrical stiffness in plan. A single level bracing is made by two diagonal members (braces) that extends from the extremes of a beam and joints at mid-span of the upper beam, forming a shape of an inverted V. This particular shape of bracings has the effect of limiting the overall lateral drift of the structure as well as the shear force and bending moment demands on beams and columns. In particular the earthquake-induced lateral forces are absorbed as axial compressive and tensile force in the braces as shown in figure 4.24. Therefore under severe ground motions the diagonal members buckle in compression and yield in tension. The compression buckling strength is minor than the tensile yield capacity, and for consecutive loading cycles, the buckling strength is further decreased due to the antecedent inelastic excursion. Therefore, bracing sets are designed such that the lateral resistance in tension and compression is comparable in both directions.

4.3.4 Modelling of the Helix-Parking

The parking was modelled with space frame model assuming the centreline dimensions. Material inelasticity was considered through the use of lumped plasticity elements. The assignment of concentrated plasticity regions was reserved only to the dissipative zones of the structure under cyclic loads (e.g. moment connections), namely the bottom columns and the bracing bars. For the columns, the concentrated plasticity is associated with coupled axial and biaxial-bending behaviour. The 3D interaction (yield) surface that describes the coupling was computed using the equation (4.4) from the American standard ASCE, and assuming an elastic-perfectly plastic axial load-displacement relationship.

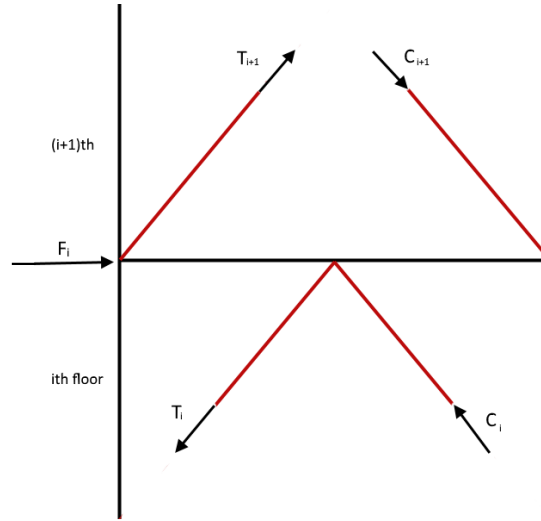


Figure 4.24: Lateral load absorption mechanism by the braces.

$$M_{CE} = 1.18ZF_{ye} \left(1 - \frac{P}{P_{ye}} \right) \leq ZF_{ye} \quad (4.4)$$

where

M_{CE} = expected flexural strength;

Z = plastic modulus section;

F_{ye} = expected yield strength of the material;

P = axial force in the member;

P_{ye} = expected axial yield force of the member = $A_g F_{ye}$.

A single plastic is assigned to the middle of the braces in order to capture the buckling of the braces in compression or a potential yielding in tension. The parameters of the axial force-displacement relation that describes the behaviour of the plastic region, were computed using FEMA-356 Table 5-5 [32].

The decks were modelled using thick shell elements in order to have an accurate load transfer from slabs to secondary and main beams. A thick shell behaviour was assumed also for the stair core.

4.3.5 Seismic Assessment Features

For the Modal Pushover Analysis as well as for the N2 method the Eurocode8 [22] design response spectrum was considered with the Belgian National Annex features- Type 2, Soil C PGA=0.06 g. For non-linear time history analysis, seven real bi-directional ground motion records were considered. The records, were selected from the European Strong Motion Database such that their average spectrum is compatible with EC8 design spectrum using Rexel software [34]. The compatibility condition ensures that the average elastic spectrum does not underestimate the code

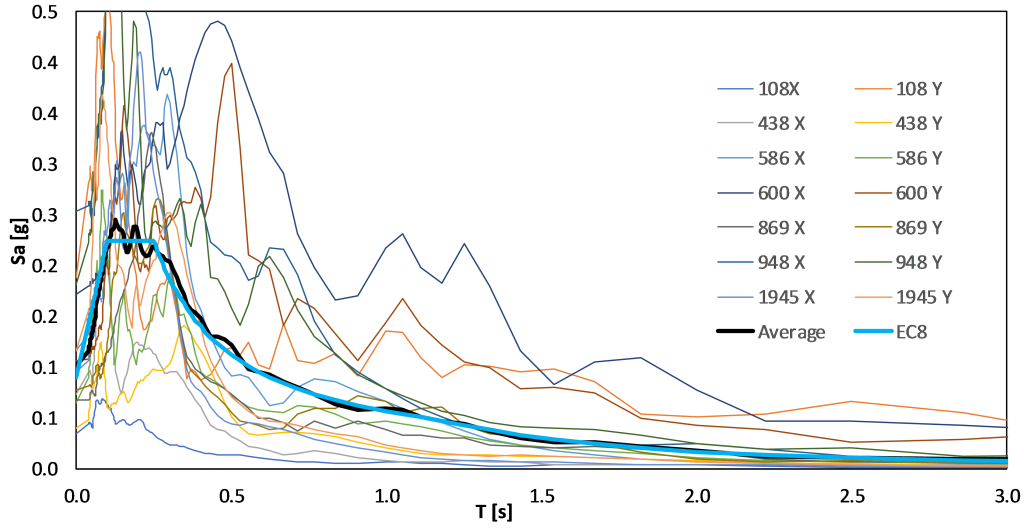


Figure 4.25: Representation of the selected ground motions response spectra, the average spectrum and the Eurocode 8 elastic spectrum

spectrum, with a 10% tolerance in the periods range from 0.1 to 2 s, as shown in figure 4.25. The ground motions' parameters in terms of magnitude and peak values are presented in table 4.13. Each bi-directional record was applied twice, changing the direction of the components and resulting in 14 time-history analyses.

Modal Pushover Analysis

The modal pushover analysis, based on the mode-superposition principle, requires the inclusion of the contributions of a sufficient number of modes of vibration in order to get accurate results. This is particularly the case for irregular structures, as the building analysed here, where torsional component of higher modes is far from negligible. Upon these considerations, a number of modes are considered such that their total mass participation ratio is at least 85 % in both horizontal directions. In order

Table 4.13: Parameters of the seven bi-directional ground motions compatible with EC8 selected from the European Strong Motion Database

Waveform ID	Earthquake Name	Mw	PGA_X [m/s^2]	PGA_Y [m/s^2]	PGV_X [m/s]	PGV_Y [m/s]
869	Umbria Marche (aftershock)	5.1	0.6623	0.7568	0.0428	0.0324
586	Umbria	4.5	1.1352	0.6408	0.0596	0.0387
1945	Pyrgos	4.9	0.9425	1.1366	0.0407	0.0477
438	Kyllini	4.8	0.7137	0.3862	0.0175	0.029
108	Friuli	4.1	0.3402	0.1882	0.0099	0.0101
948	Sicilia-Orientale	5.6	2.4827	1.7867	0.0959	0.1058
600	Umbria Marche	6	1.6852	1.0406	0.1449	0.1176

to include the minimum number of modes to reach this limit the Load-Dependent Ritz vector (LDRV) method was used instead of the classical eigen-vector analysis. The LDRV method, in fact, by taking into consideration the spatial distribution of the dynamic loading neglects the modes that do not excite any mass degree of freedom.

As shown in fig 4.26 mode 1, mode 2 and mode 4 are predominantly acting in the y-direction, whereas mode 3 and Mode 5 in the x-direction. From the participation mass ratio, it is clear also that the lateral and torsional motions are strongly coupled in the first three modes resulting in a stiff torsional behaviour.

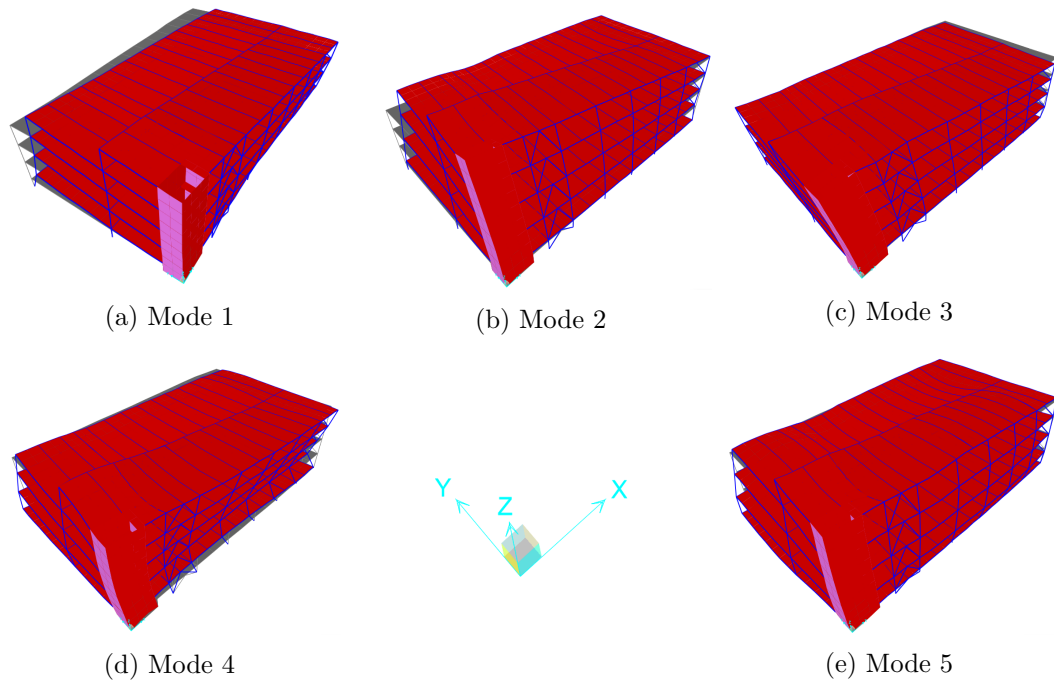


Figure 4.26: 3D representation of the mode shapes of the Helix-parking

Pushover analyses were performed with load patterns proportional to the mode shape for each the 5 modes. Gravitational loads computed according to EC8 seismic combination, were assigned first and the lateral pushover loads were applied under displacement control to capture the softening due to the local buckling of the braces. The monitored displacement, at the centre mass of the top two ramps, was used as a control parameter to plot the pushover curves. Additionally, for each mode the loads were applied independently in the positive/negative sense along the mode dominant direction up to near collapse. Here, are reported only the pushover curves that yielded higher target displacements. Pushover curves obtained are presented in figure 4.27 with horizontal and vertical axes respectively normalized with respect the height of control point (assumed as the centre mass of top two ramps) and the weight of the structure.

Table 4.14: Properties of the structure significant modes in terms of natural vibration periods and modal mass participation ratios for the first five modes.

Mode	Period [s]	UX [%]	UY [%]	Rz [%]
1	1.01	4.5	41.8	38.6
2	0.49	18.6	26.4	15.4
3	0.40	37	2.5	15.4
4	0.25	7.6	8.6	3.3
5	0.18	18.5	6.1	1.6
Tot		86.2	85.4	74.3

The target displacement of each of the 5 inelastic SDOF systems was computed by multiplying the median peak deformation of the corresponding linear system, known from the design spectrum, by the inelastic deformation ratio C_{Rn} presented in Table 4.15. According to the empirical formulation of the ratio C_{Rn} proposed by Newmark and Hall the inelastic deformation ratio is unitary for all the considered inelastic SDOF systems.

By combining modal contributions using SRSS technique it was possible to compute the global response of the structure under the seismic demand represented by the Eurocode 8 response spectrum. Figure 4.28 shows the displacements in the x and y-directions in correspondence of control point, and at the top of the edging frames along the transversal and longitudinal direction. It is clear that the displacement in the x-direction are negligible comparing to the displacements in the y-direction as it is expected considering the difference of stiffness involved in each direction.

Table 4.15: Properties of the equivalent inelastic Single Degree of Freedom system

Properties	Mode 1	Mode 2	Mode 3	Mode 4	Mode 5
Direction	Y	Y	X	Y	X
$\Gamma_n \phi_{rn}$	0.64	0.65	0.78	0.25	0.1
$M_n^* [kN/m/s^2]$	1458	649.76	1289.96	298.92	643
$F_{sny}/L_n [m/s^2]$	0.82	3.54	4.62	7.72	20.69
$D_{ny} [m]$	0.031	0.045	0.038	0.0125	0.002
$T_n [s]$	1.2	0.7	0.57	0.42	0.1
α	0.19	0.14	0.37	0.09	0.002
C_R	1	1	1	1	1

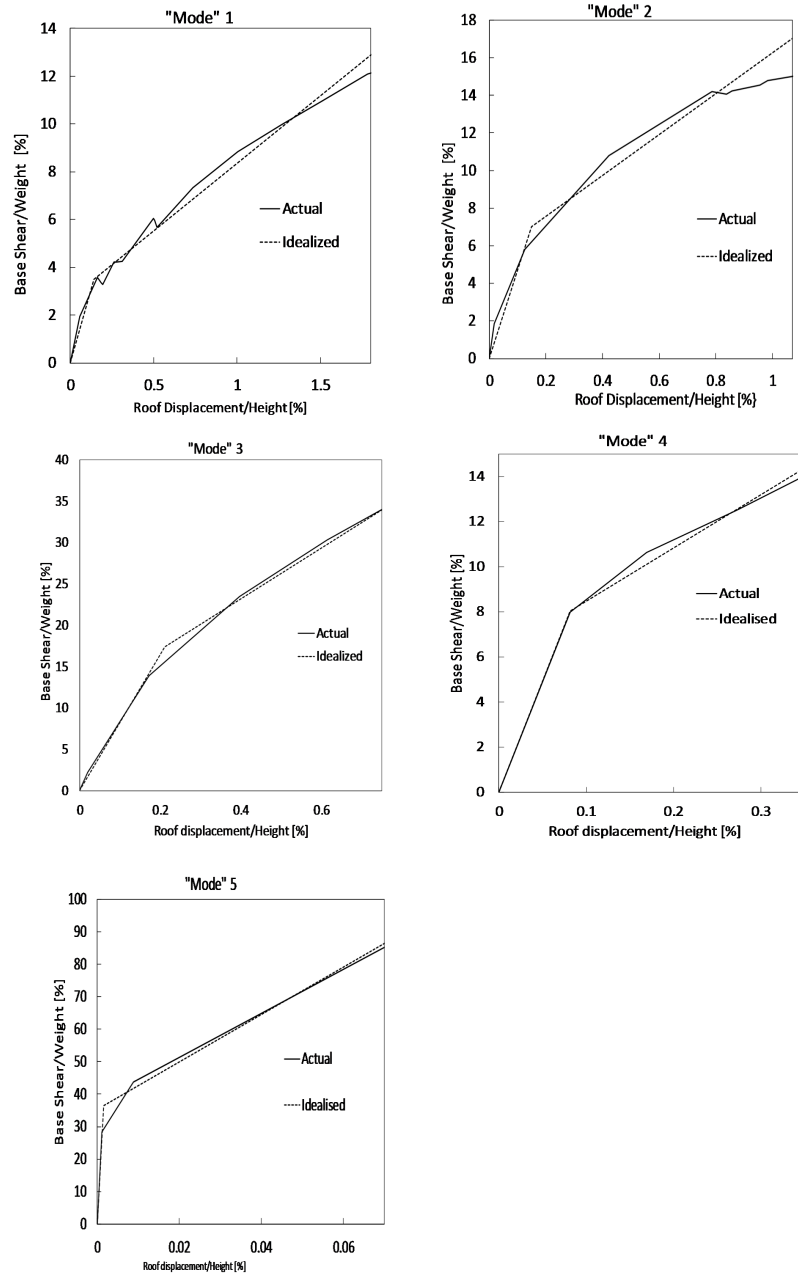


Figure 4.27: Modal pushover curves of Helix parking idealised with bilinear relations.

Extended N2 Method

Pushover analyses were performed in two horizontal directions with lateral loads based on the fundamental mode shapes in the relevant direction, i.e. the load pattern proportional to the first mode shape was used in Y-direction, and lateral loads

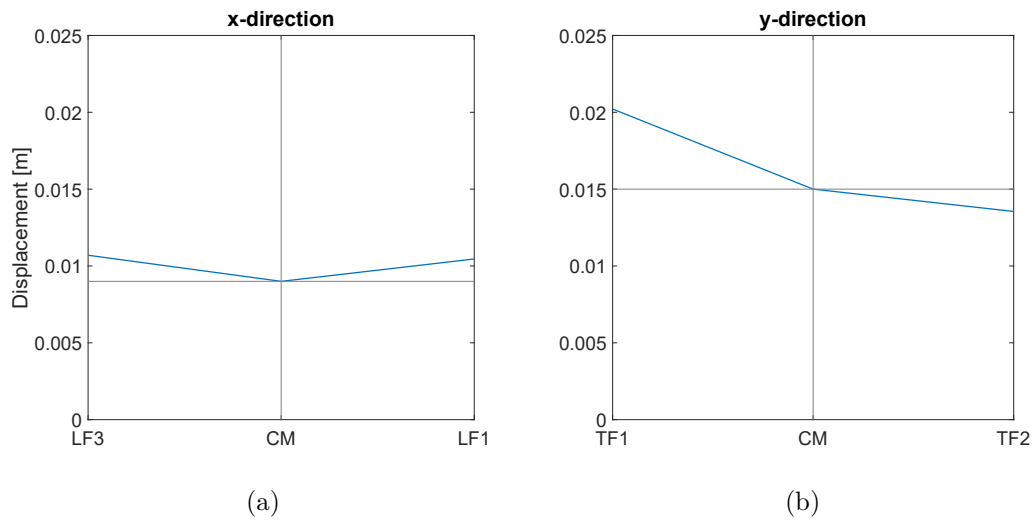


Figure 4.28: Top displacements in the x-direction (a) and y-direction(b) in correspondence to CM and the edging frames

proportional to the third mode shape were used in x-direction.

Each of the resulting pushover curves is plotted in the ADRS format with the response spectrum and the performance point of corresponding SDOF systems is given by the intersection of the two curves as shown in figure. For the equivalent SDOF system the displacement demands, fully in the elastic range, amount to less than 0.01 m and 0.02 m in x- and y- direction, respectively, while the corresponding top displacements of the MDOF system in CM amount to 0.013 m and 0.007 m. These values should be integrated with the contributions of the torsional behaviour.

Torsional effects in terms of normalized roof displacements determined by the extension of the N2 method are presented in graph 4.30.

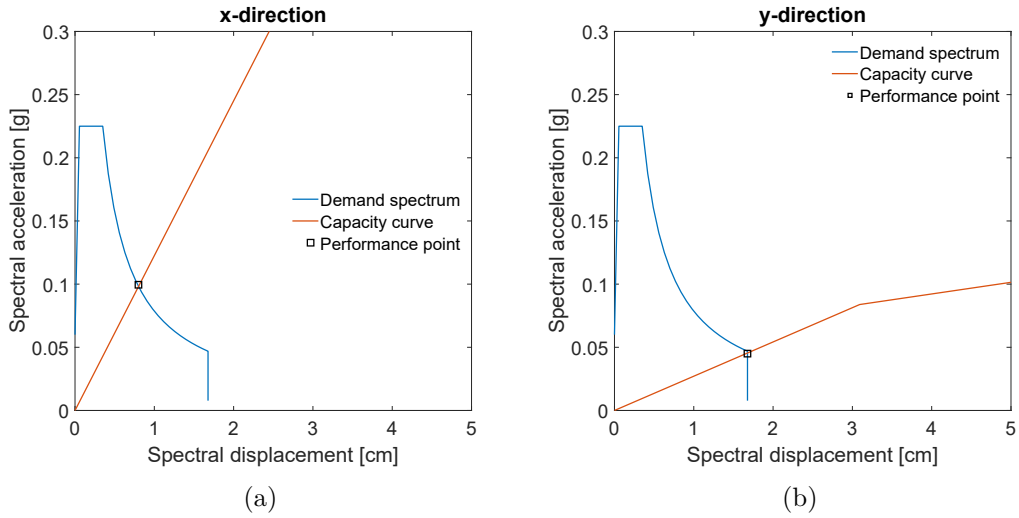


Figure 4.29: Elastic demand spectra and capacity curves in the x-direction (a) and y-direction(b).

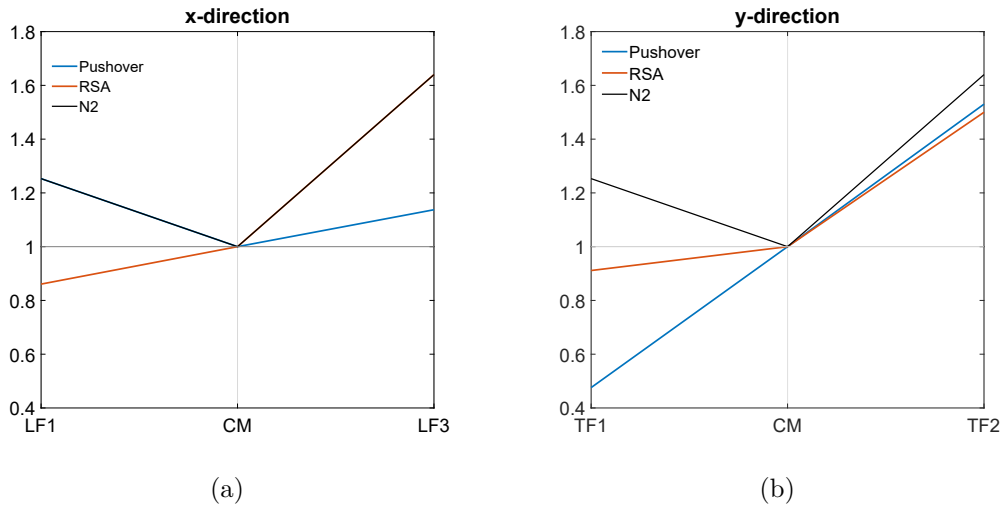


Figure 4.30: Torsional effects in terms of normalized top displacements obtained by the extended N2 method, by modal analysis and by pushover analysis.

4.3.6 Results discussion

The results obtained with the MPA and the extended N2 method are compared here with the mean values of the non-linear response history analyses of the seven records. The comparison is limited to the floor displacements and inter-storey drift of the transversal frame TF2 (see fig 4.23) as it endures the maximum displacements. The results in terms of lateral displacement profiles and inter-storey drifts are shown in figure 4.31. From the plots it is clear the inter-storey drifts are much higher on the first level than in the upper levels. This is clear sign of a soft-story mechanism on the first

level along the Y direction. The extended N2 and the MPA slightly overestimate this mechanism. This phenomenon may be explained by the different restraint conditions: the bottom columns are rigidly connected to the foundation while the connections between the upper columns and beams are simple shear connections leading to a local mechanism.

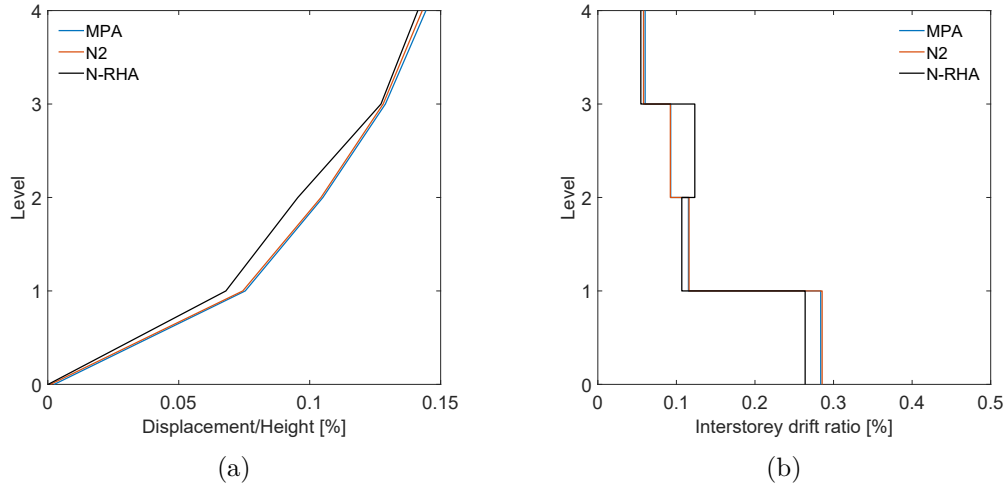


Figure 4.31: Height-wise variation of level displacements and level drift ratios from MPA, N2 method and the mean value of non-linear RHA.

4.3.7 Displacement-based control of damage

In this section, the damage limitation requirement according to the Eurocode 8 is evaluated. A displacement-based verification is done in reference of inter-storey drift. Since the building under analysis have no facade but it is attached to the adjacent building, the inter-storey drift limit is assumed as the minimum defined by the Eurocode:

$$d_r \nu \leq 0.005 h \quad (4.5)$$

where

d_r is the inter-storey drift;

h is the storey height;

ν is the reduction factor, which depends on the return period of the seismic demand. Hence, the value of ν is related to the importance class of the building. Since the case study under analysis belong to an Importance Class II, the value assumed is ν is 0.5.

The elements analysed within this damage limitation verification were columns of the

TF2 frame that exhibited the maximum displacement. From graph (4.32), it is clear that the frame considered building does not exceed the damage limitation criterion.

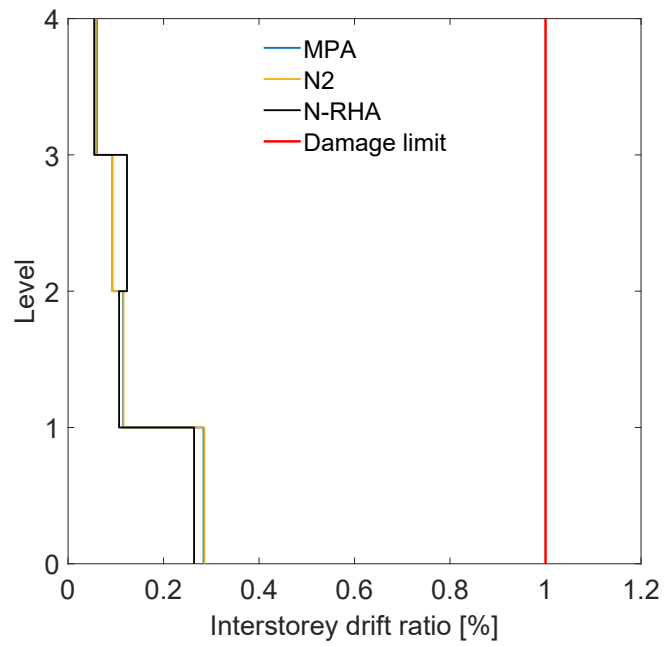


Figure 4.32: Inter-storey drift damage limitation according to EC8 for frame TF2

Chapter 5

Fragility curves

5.1 Introduction

The most commonly used analytical tools to assess seismic vulnerability are fragility curves which provide a statistical correlation between the structure capacity and the expected damage due a specified demand range. Such damage estimations are crucial for disaster planning and formulating risk reduction policies. In this chapter fragility curves will be derived for the case studies by employing a simplified procedure that relies the use of on the non linear static approach. The accuracy of the proposed methodology will be assessed by comparing the fragility curves obtained with incremental non-linear analyses of the case studies.

5.2 Fragility Curves

A fragility function specifies the probability of collapse, or the exceedance of another limit state of interest, of a structure as a function of some ground motion intensity measure, IM. This parameter is often quantified by peak ground parameters (acceleration, velocity or displacement) or spectral acceleration (S_a) corresponding to the fundamental period and a specified damping.

The analytical procedure includes two main steps: 1) determination of the structure performance at different ground motion scenarios, 2) the definition of a criterion to determine whether or not the ground motion caused the collapse or the exceedance of a certain limit state. The first can be achieved by an incremental dynamic analysis (IDA) where a suite of ground motions are repeatedly scaled in order to find the intensity level at which each ground motion causes collapse. However, running non-linear dynamic analyses for a large number of ground motion sets can be extremely demanding and time consuming. Thus, alternative methods have thus been sought and different authors proposed and implemented procedures for construction of fragility curves on the basis of non-linear static method. M. Shinozuka et al. [35] found that CSM-fragility curves are in good agreement with those obtained with non-linear dynamic analysis for structures oscillating predominantly in a single (fundamental) mode. For irregular structures the contributions of higher modes shall

be included for more realistic representation of the expected response.

In this chapter, a Modal Pushover Analysis-based vulnerability assessment is presented and employed to determine the fragility curves of both structures described in the previous chapter.

This simplified procedure relies on the assumption that the structure response at different ground motion intensity levels can be approximated by the weighted response of the equivalent SDOF systems. The method can be summarized in a sequence of steps:

1. Determination of the equivalent SDOF systems, in terms of natural periods and force-displacement relations;
2. Definition of performance levels on the basis of the value assumed by a specific response parameter (e.g. peak interstory drift);
3. Selection of different sets of ground motions with increasing intensity level which is quantified by a ground motion intensity measure, IM. The parameter IM is often assumed as the spectral acceleration corresponding to a specified frequency and damping, though any physical quantification of ground shaking intensity can be employed with this procedure.
4. Computation of peak displacement of the equivalent SDOF systems through time history analysis for each intensity level and ground motion;
5. Conversion of the SDOF peak responses to the structure displacement using modal transformation factors. The MDOF global response is computed by combining the contributes from the considered modes using SRSS technique for each intensity level and ground motion;
6. The maximum displacement of the structure is converted to response parameter that define the performance levels (i.e. drift ratio) through relation evaluated with the respective pushover analysis;
7. The peak drift is then compared to the performance limit values, and the probability of performance level exceedance at a given intensity level $IM=x$, can be estimated as the fraction of records for which the exceedance occurs a level lower than x . A log-normal function is used to fit this data, to provide a continuous estimate of the probability of collapse as a function of the intensity level. The equation for this function is

$$P(PL|IM = x) = \Phi\left(\frac{\ln x - \mu}{\beta}\right) \quad (5.1)$$

where $P(PL|IM = x)$ is the probability of performance level exceedance, at given ground motion with $IM=x$, Φ is the standard cumulative distribution function (CDF) and μ, β are the mean and standard deviation of $\ln x$. These parameters can be estimated from the results of the incremental dynamic analysis. There are two common statistical approaches for estimating these

parameters from the observed data. The method of moments finds parameters such that the resulting distribution has the same moments (e.g., mean and standard deviation) of the observed data. A more general approach is the Maximum Likelihood Method through which the parameters are found such that the resulting distribution corresponds to the highest probability of having produced the observed data. This method, adopted here, has the advantage of being suitable also when the analysis may not be carried out up to IM amplitudes where all ground motions cause collapse.

The likelihood function is defined as the product of the binomial probabilities at each IM level

$$Likelihood = \prod_{j=1}^m \binom{n_j}{z_j} p_j^{z_j} (1 - p_j)^{n_j - z_j} \quad (5.2)$$

where m is the number of IM levels, n is the number of ground motions, z the number of observed performance level exceedances and p_j is the probability of performance level exceedance with $IM = x_j$, The distribution parameters are determined by substituting p and maximizing the likelihood function obtained

$$\{\mu, \beta\} = \max_{\mu, \beta} \prod_{j=1}^m \binom{n_j}{z_j} \Phi\left(\frac{\ln x - \mu}{\beta}\right)^{z_j} \left(1 - \Phi\left(\frac{\ln x - \mu}{\beta}\right)\right)^{n_j - z_j} \quad (5.3)$$

Numerically the same results are obtained by maximizing the logarithm of the likelihood function

$$\{\hat{\theta}, \hat{\beta}\} = \arg_{\theta, \beta} \max \sum_{j=1}^m \left\{ \ln \binom{n_j}{z_j} + z_j \ln \Phi\left(\frac{\ln(x_j/\theta)}{\beta}\right) + \ln \left(1 - \Phi\left(\frac{\ln(x_j/\theta)}{\beta}\right)\right) \right\} \quad (5.4)$$

The values on the right hand side of this expression are obtained from the results of the incremental analyses, while the optimization to determine the maximum value is easily performed using many computational software programs. Here, the optimization has been carried in Microsoft Excel using the Goal Seek function.

Typical ground motion IMs are the peaks of the acceleration, velocity and displacement signals (PGA, PGV, and PGD) respectively. This is also because the seismic hazard is often represented in terms of probability of exceedence of these quantities.

Linear spectral ordinates, specially accelerations at the fundamental period of the structure $S(T_1)$, are also often used as IMs for probabilistic assessment of structures. This is mainly because $S(T_1)$ is the response of a single degree of freedom system (SDOF) and therefore it should be, in principle, more correlated with the structural global performance in respect to peaks of ground motion.

Furthermore using $S(T_1)$ as a proxy for earthquakes potential damage is way more efficient for the selection of appropriate ground motion records. In fact when real records are concerned, the current state of best practice is based on the determination of magnitudes and distances most contributing to determine the $S(T_1)$ value corresponding to a specified probability (disaggregation procedure). Choosing $S(T_1)$ as the IM significantly simplifies this procedure as all this concern about the chosen records may be avoided, and ground motions can be at least in principle randomly selected and then modified to have the $S(T_1)$ value of interest just by linear amplification scaling [36].

The IDA requires that a single record is scaled up or down, e.g. all the acceleration values are multiplied by a single scaling factor, SF, to increasing values of the ground shaking's severity. The scale factor values are determined simply by equation (5.5)

$$SF = \frac{IM_T}{IM_U} \quad (5.5)$$

where IM_T is the target intensity level, and IM_U is the intensity value of the unscaled record.

The linear scaling is a common operation in practice and in research. However many studies have raised the concern about the validity of the results obtained from accelerograms that have been amplified or reduced in intensity. The main question is whether the median of results obtained from records that have been scaled to some level of intensity measure IM provide an accurate estimate of the median of results of a set of unscaled ground motions with the same level of IM. In general the answer depends on the structure, the sets of records as well as on the IM and the damage measure. However, it was observed that for steel frames with intermediate period, inter-storey drift as damage measure and $Sa(T_1)$ as IM, the median results matches [37, 38].

5.2.1 Performance Levels

A fundamental step in the development of each of the fragility curve requires the definition of the performance levels or limit states. There are different approaches that correlate the damage limits with the global behaviour (peak roof drift) and/or element local response (plastic hinge rotation). However, it is generally agreeable that, for steel frames the drift ratio (peak interstorey drift/storey height) provides a reliable estimate of the expected damage and a well confirmed compromise between global and local response measures. For this reason, in this study, the inter-storey drift is considered in the determination of the fragility curves. Three limit states are defined, starting from the qualitative description of the different levels specified for the braced structures in FEMA273, and taking into consideration the intermediate steps of the pushover analysis where the structure was loaded laterally up to near collapse. These are termed, Immediate occupancy, Life safety and collapse prevention, limit states, respectively. Table 5.1 sums up the specific damage expected of the two

building topologies analysed and the corresponding drift ratio for each performance level.

Table 5.1: Structural performance level and the associated damage moment frame structures and braced structures form FEMA356.

Elements	Type	Structural Performance Levels		
		Collapse Prevention	Life Safety	Immediate Occupancy
Steel Moment Frames	Primary	Extensive distortion of beams and column panels. Many fractures at moment connections, but shear connections remain intact.	Hinges form. Local buckling of some beam elements. Severe joint distortion; isolated moment connection fractures, but shear connections remain intact. A few elements may experience partial fracture.	Minor local yielding at a few places. No fractures. Minor buckling or observable permanent distortion of members.
	Secondary	Same as primary.	Extensive distortion of beams and column panels. Many fractures at moment connections, but shear connections remain intact.	Same as primary.
	Drift	5% transient or permanent	2.5% transient; 1% permanent	0.7% transient; negligible permanent
Braced Steel Frames	Primary	Extensive yielding and buckling of braces. Many braces and their connections may fail.	Many braces yield or buckle but do not totally fail. Many connections may fail.	Minor yielding or buckling of braces.
	Secondary	Same as primary.	Same as primary.	Same as primary.
	Drift	2% transient or permanent	1.5% transient; 0.5% permanent	0.5% transient; negligible permanent

5.2.2 Seismic input

Ten bi-directional ground motions are here selected from the European Strong Motion database with a magnitude value lower than 7 and higher than 5 [39]. All 10 ground motions are relevant to stiff soil conditions and are a combination of intense and far, intense and close, moderate and close and intermediate records, in order to include a typical interval of magnitudes and distances in the European region as shown in table 5.2. In figure 5.1 the 10 horizontal acceleration spectra are plotted, with respective mean spectra. As it is practically not doable to select real records that cover the whole range of the inelastic structural response of interest the selected records are scaled to the 2% damped spectral acceleration at the fundamental frequency of the analysed structures using equation (5.5).

Table 5.2: Characteristic properties of selected records

Waveform ID	Earthquake	Date	Epicentral Distance [km]	Magnitude Mw	PGA [m/s ²]
239	Dursunbey	18/07/1979	6	5.3	2.131
295	Campano Lucano	23/11/1980	16	6.9	1.725
123	Friuli	11/09/1976	15	5.5	1.286
336	Preveza	10/03/1981	28	5.4	1.402
536	Erzincan	13/03/1992	65	6.6	0.286
6264	South Iceland	17/06/2000	52	6.5	0.692
196	Montenegro	15/04/1979	25	6.9	4.453
947	Potenza	05/05/1990	28	5.8	0.944
595	Umbria Marche	26/09/1997	25	5.7	0.38
244	Valnerina	19/09/1979	39	5.8	0.386

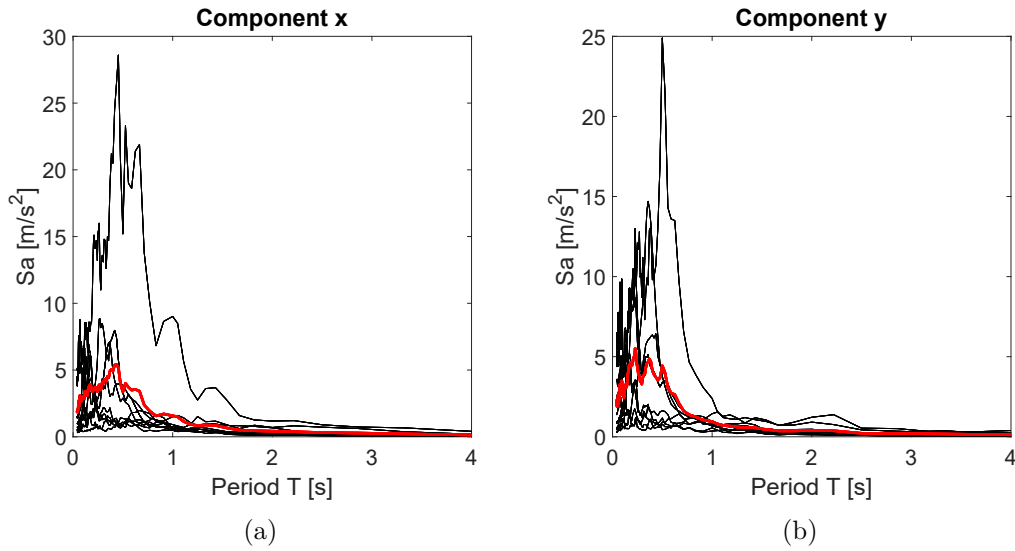


Figure 5.1: Acceleration spectra for each of the two components of the ten ground motions selected from the European Strong Database, and their mean acceleration response spectra in bold red

5.3 Results Discussion

5.3.1 SAC-Building

Figure 5.2a, 5.2b and 5.2c show IDA of the roof displacement considering separately the contribution of the three equivalent SDOF systems for each of the selected ten ground motions. It is clear that there is a significant record to record discrepancy at moderate and higher values of the spectral acceleration. As expected this variability is accentuated when high levels of non linearity are concerned.

What is also immediately noticeable is the non-monotonic trend of some IDA curves, which bend back at some point before resuming the upward trend. This means

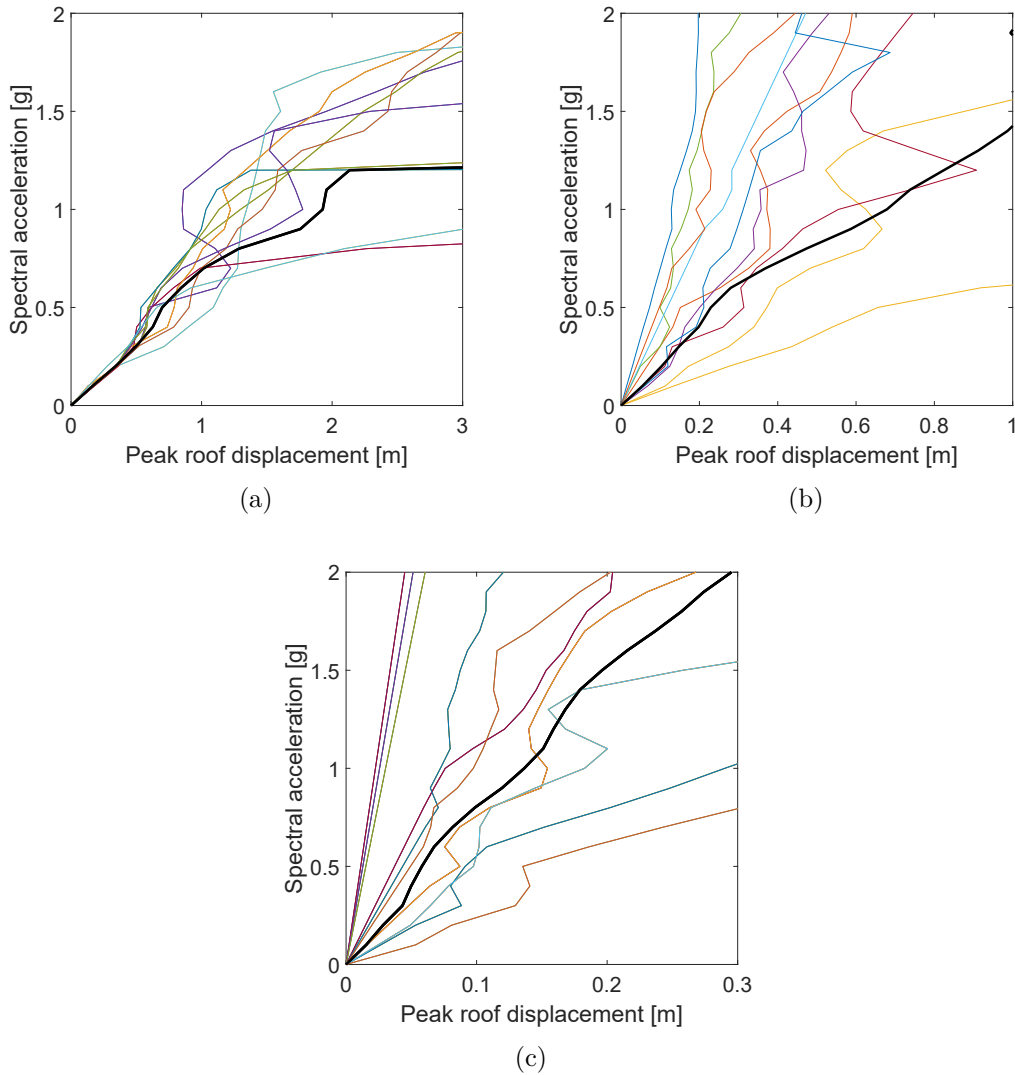


Figure 5.2: IDA of the contributions of the SAC-9 equivalent SDOF systems to the maximum roof displacement

the analysed systems exhibit at higher intensities, the same or even smaller responses to those showed at smaller seismic intensities. This counter-intuitive phenomenon has already been observed by other researches within both a deterministic [40] and probabilistic context [41]. Corell and Vamvatsikos discussed this anomaly as being a likely property (twisting behaviour) of an Incremental Dynamic Analysis (IDA) curve. The main explanation advanced to justify this unusual trend is related to the scaling of the earthquake accelerograms. Scaling up of record may force early, usually weak waves to become strong enough to initiate yielding and yet change the structural response to the forthcoming stronger cycles. The earlier yielding make the system less responsive in later cycles that had previously caused higher response

values.

The graphs 5.3 show the functions, determined by pushover analysis, relating the roof displacement and the maximum inter-storey drift expected at the first floor for each of three equivalent SDOF systems. Through these relations the single values of the roof displacement are converted into the corresponding maximum inter-storey drift values. The overall drift values are obtained by combining the three single contributions for each intensity level and ground motion by means of the SRSS rule. From these data, the 15, 50, and 85% fractile values of the demand given the ground motion intensity are computed to obtain these fractile IDA curves in figure 5.4.

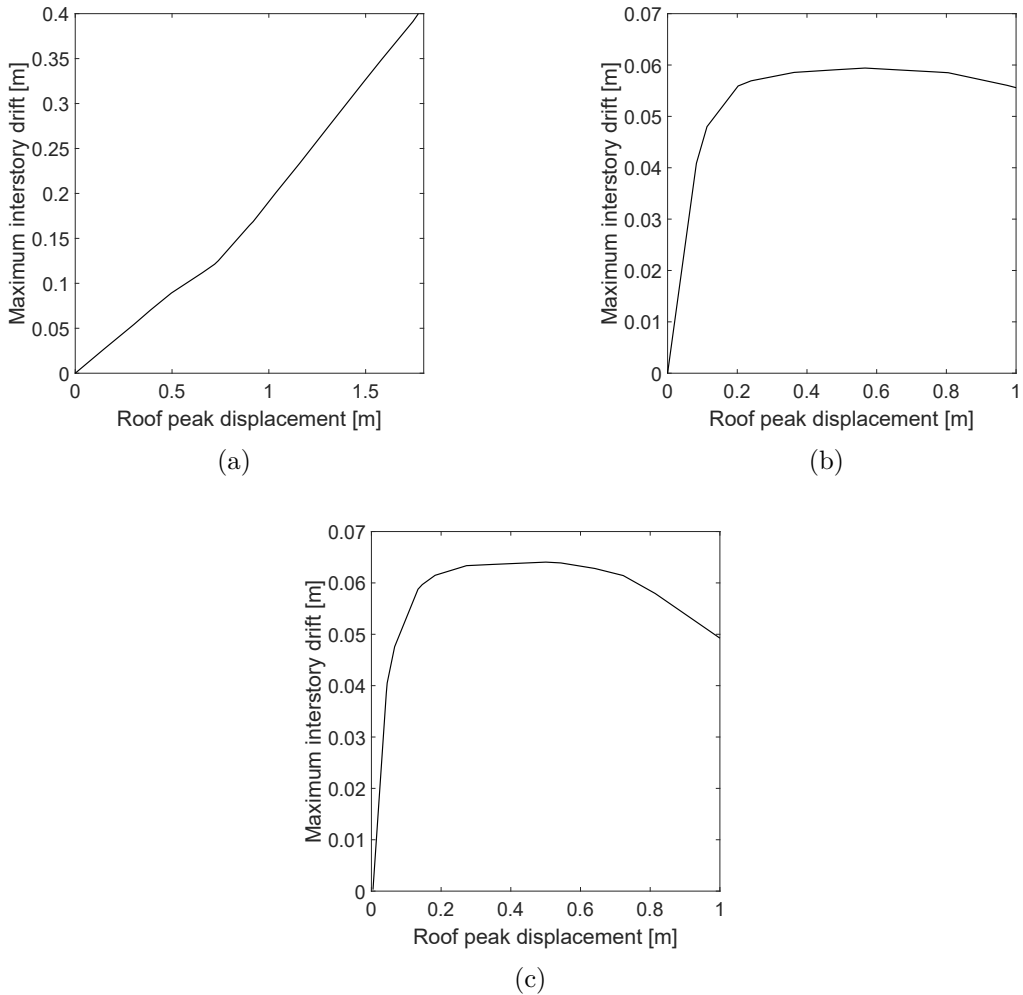


Figure 5.3: Functions defining the relations between the the roof displacement and the corresponding maximum inter-storey drift for load patterns proportional to the first mode shape (a), the second mode (b) and the third mode shape (C).

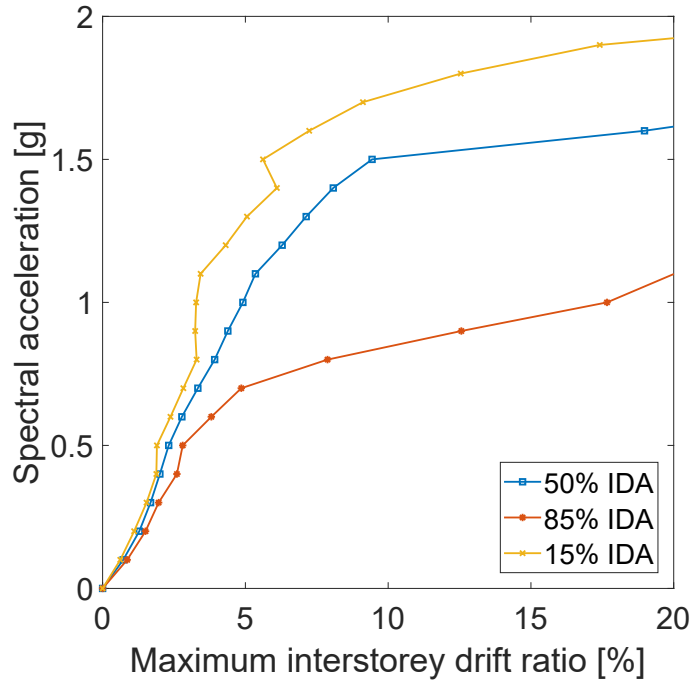
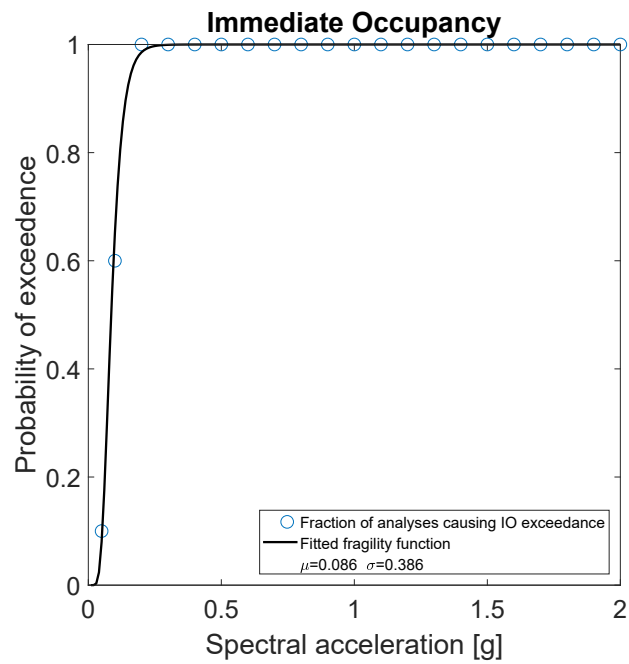


Figure 5.4: 15, 50, and 85% fractile IDA curves for the 9-SAC building from MPA-based approximate procedure.

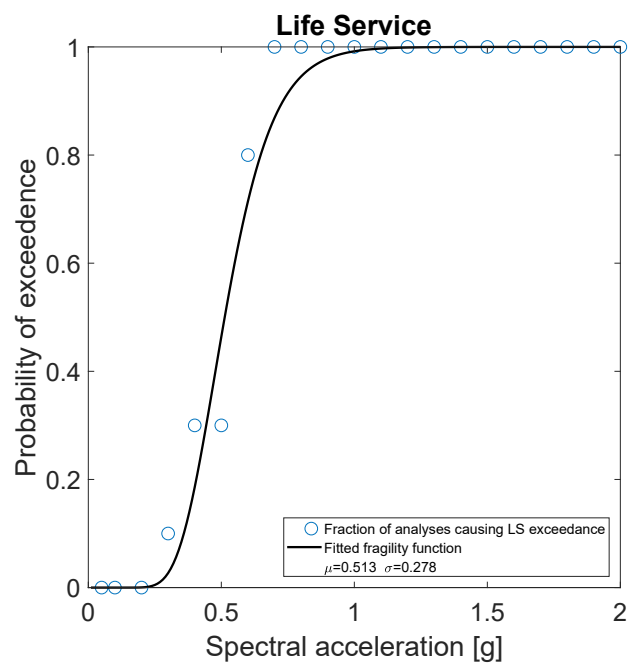
For the fragility assessment the drift values are compared with respect to the three FEMA-defined performance levels for Steel Moment Frames (MRF) element type presented in table 5.1. The number of ground motions exceeding the drift limit are presented in table 5.3 for Immediate Occupancy, Life Service and Collapse Prevention performance limit, respectively. Knowing the exceedance fraction the parameters of each of the fragility curve are computed with the Maximum Likelihood Method.

Table 5.3: SAC-9' observed fractions of exceedances, the Likelihood function values and the Cumulative Distribution function values for each intensity level, for the three performance levels considered.

Sa	Immediate Occupancy			Life Service			Collapse Prevention		
	Fraction of exceedances	Likelihood	CDF	Fraction of exceedances	Likelihood	CDF	Fraction of exceedances	Likelihood	CDF
0.1	0.60	0.238	0.65	0.00	1.000	0.00	0.00	1.000	0.00
0.2	0.90	0.128	0.99	0.00	0.996	0.00	0.00	1.000	0.00
0.3	1.00	0.994	1.00	0.10	0.265	0.04	0.00	1.000	0.00
0.4	1.00	1.000	1.00	0.30	0.250	0.25	0.00	0.999	0.00
0.5	1.00	1.000	1.00	0.30	0.059	0.57	0.00	0.971	0.00
0.6	1.00	1.000	1.00	0.80	0.301	0.81	0.00	0.765	0.03
0.7	1.00	1.000	1.00	1.00	0.485	0.93	0.20	0.207	0.11
0.8	1.00	1.000	1.00	1.00	0.791	0.98	0.30	0.256	0.26
0.9	1.00	1.000	1.00	1.00	0.930	0.99	0.40	0.237	0.45
1	1.00	1.000	1.00	1.00	0.978	1.00	0.60	0.243	0.64
1.1	1.00	1.000	1.00	1.00	0.994	1.00	0.70	0.222	0.78
1.2	1.00	1.000	1.00	1.00	0.998	1.00	0.90	0.379	0.88
1.3	1.00	1.000	1.00	1.00	0.999	1.00	0.90	0.351	0.94
1.4	1.00	1.000	1.00	1.00	1.000	1.00	1.00	0.727	0.97
1.5	1.00	1.000	1.00	1.00	1.000	1.00	1.00	0.860	0.99
1.6	1.00	1.000	1.00	1.00	1.000	1.00	1.00	0.933	0.99
1.7	1.00	1.000	1.00	1.00	1.000	1.00	1.00	0.969	1.00
1.8	1.00	1.000	1.00	1.00	1.000	1.00	1.00	0.986	1.00
1.9	1.00	1.000	1.00	1.00	1.000	1.00	1.00	0.994	1.00
2	1.00	1.000	1.00	1.00	1.000	1.00	1.00	0.997	1.00



(a)



(b)

Figure 5.5: SAc-9' observed fractions of exceedances and fitted fragility functions obtained using the maximum likelihood approach for Immediate Occupancy (a), Life Service (b) and Collapse Prevention performance levels (c).

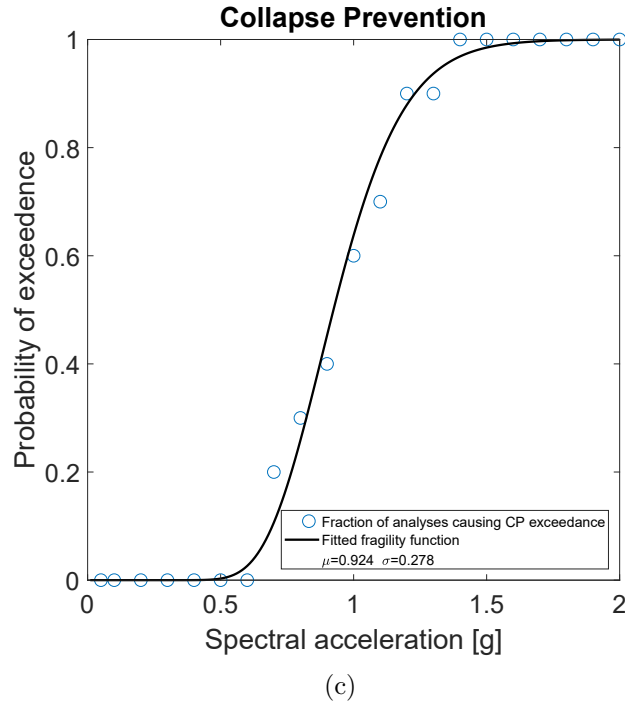


Figure 5.5: SAC-9' observed fractions of exceedances and fitted fragility functions obtained using the maximum likelihood approach for Immediate Occupancy (a), Life Service (b) and Collapse Prevention performance levels (c) (cont.)

5.3.2 Helix Parking

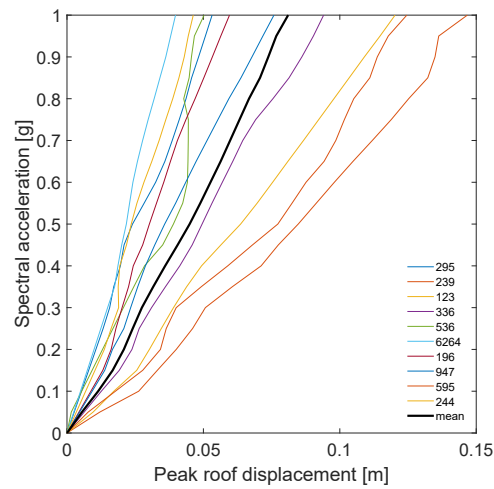
Comparing to the SAC-9 building the Helix parking has more complex dynamics due to irregularities in both plan and elevation. This results in a significant torsional behaviour and hence non-negligible responses in higher modes. For the MPA-based IDA the bidirectional response of the structure is computed by considering five equivalent SDOF systems corresponding to the first five natural modes.

Each component of a bi-directional record was applied to both the SDOFs, acting along x-direction and the SDOFs acting along y-direction, in order to determine the worst direction of the record's components.

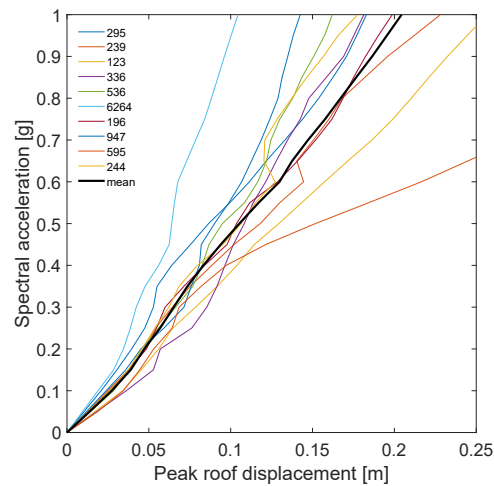
Figure 5.6a and 5.6b plot IDA of the parking top displacement by combining the contributions of the SDOF systems acting along the x-direction, and the y-direction, respectively for each of the ten ground motions considered. For the combination of the effects of the two seismic components the provisions of the EC8 were adopted. As already observed the building is stiffer along x-direction (transversally) than y (longitudinally). In addition, the IDA curves in both directions seem to exhibit a distinct elastic linear region and after yielding they start to weave around their initial elastic slope with an overall hardening trend. The twisting trends is made by successive segments where the local slope decreases with higher Sa and others

where it increases. A similar but more accentuated behaviour has been observed for the SAC-9 building. It is clear also that there is a significant record to record variance at moderate and higher values of the spectral acceleration. As expected this variability is more significant at high levels of intensity where non-linear behaviour plays a crucial role.

The graphs 5.7 show the functions, determined by pushover analysis, linking the roof displacement and the maximum inter-storey drift expected at the first ramp for



(a)



(b)

Figure 5.6: Incremental Dynamic Analyses of the building top displacement by combining the contributions of the SDOF systems acting along the x-direction (a), and the y-direction (b).

5. FRAGILITY CURVES

each of the orthogonal directions x and y . As it is clear from those graphs for each component of the roof displacement both components of the drifts were accounted. Through these relations the single values of the roof displacement were converted into the corresponding maximum inter-storey drift values. The overall drift values are obtained by combining the single contributions acting along the same direction for each intensity level and ground motion by means of the SRSS rule. From these data, the 16, 50, and 84% fractile values of the demand given the ground motion intensity are computed to obtain these fractile IDA curves in figure 5.8.

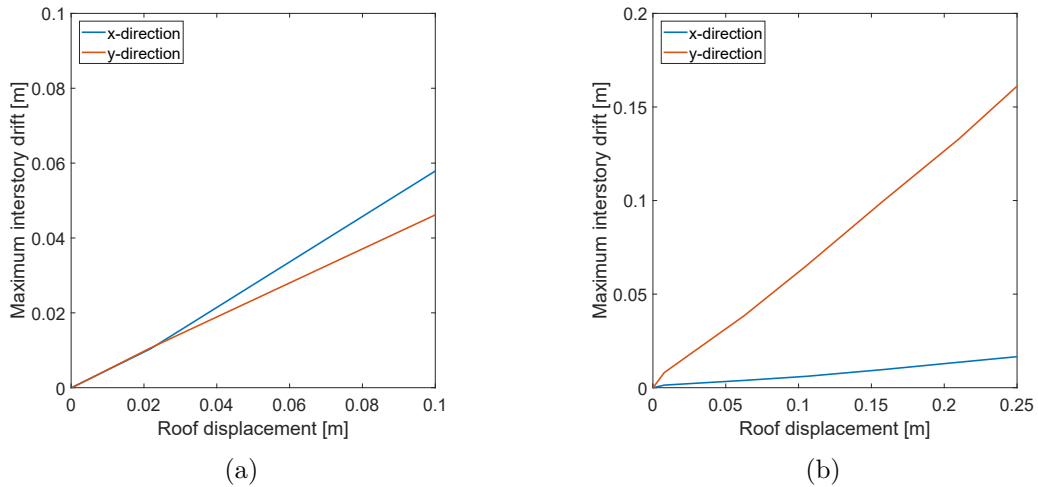


Figure 5.7

Once the 50% fractile IDA curve is known, the fragility curves for the limit states in question were developed. The median drift values were compared with respect to the three FEMA-defined performance levels for Steel Braced Frames presented in table 5.1. The number of ground motions exceeding the drift limit are presented in table 5.4 for Immediate Occupancy, Life Service and Collapse Prevention limit state, respectively.

Knowing the exceedance fraction the parameters of each of the parameters of the log-normal fitting fragility functions were derived with the Maximum Likelihood Method. Figure 5.9c depict the limit state fragility curves for Immediate Occupancy, Life Service and Collapse Prevention limit state, respectively, together with a discrete representation of the fraction of ground motions exceeding the corresponding drift limit.

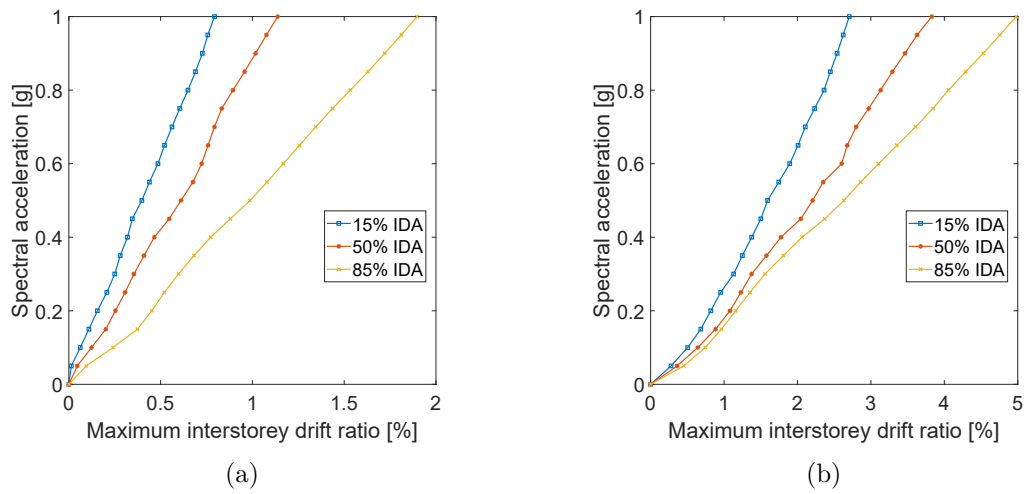
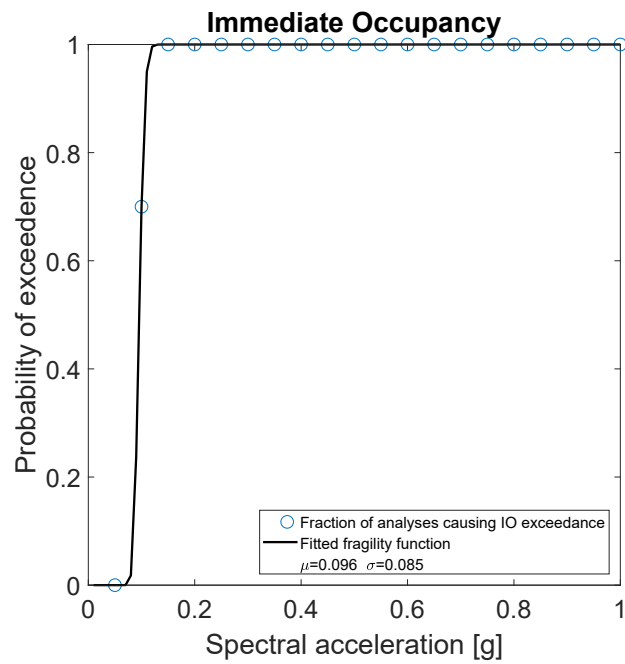


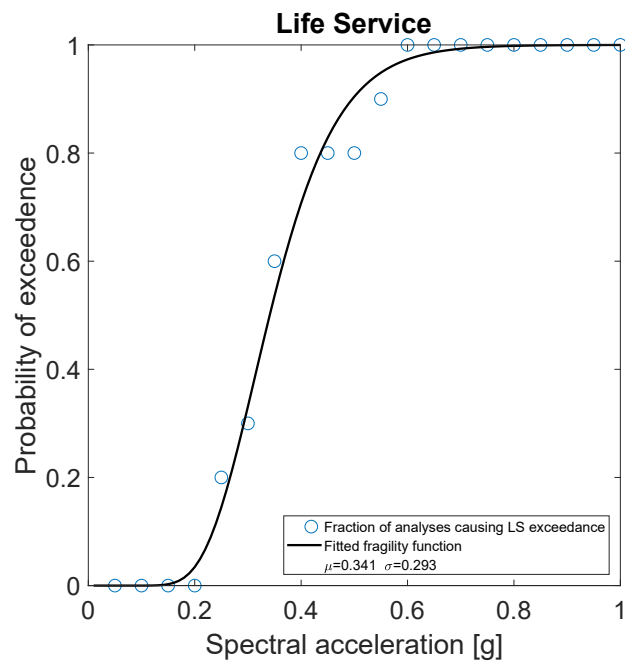
Figure 5.8: 15, 50, and 85% fractile IDA curves for the Helix-Parking building from MPA-based approximate procedure along the x-direction (a) and the y-direction (b).

Table 5.4: Helix-Parking's observed fractions of exceedances, the Likelihood function values and the Cumulative Distribution function values for each intensity level, for the three performance levels considered.

Sa	Immediate Occupancy			Life Service			Collapse Prevention		
	Fraction of exceedances	Likelihood	CDF	Fraction of exceedances	Likelihood	CDF	Fraction of exceedances	Likelihood	CDF
0.1	0.00	1.000	0.00	0.00	1.000	0.00	0.00	1.000	0.00
0.2	0.80	0.302	0.80	0.00	1.000	0.00	0.00	1.000	0.00
0.3	1.00	1.000	1.00	0.00	0.989	0.00	0.00	1.000	0.00
0.4	1.00	1.000	1.00	0.00	0.765	0.03	0.00	0.981	0.00
0.5	1.00	1.000	1.00	0.20	0.267	0.14	0.00	0.825	0.02
0.6	1.00	1.000	1.00	0.30	0.247	0.36	0.10	0.377	0.08
0.7	1.00	1.000	1.00	0.70	0.208	0.59	0.20	0.302	0.20
0.8	1.00	1.000	1.00	0.80	0.296	0.77	0.40	0.241	0.36
0.9	1.00	1.000	1.00	0.80	0.220	0.89	0.60	0.223	0.52
1	1.00	1.000	1.00	0.90	0.324	0.95	0.70	0.261	0.67
1.1	1.00	1.000	1.00	1.00	0.789	0.98	0.70	0.220	0.78
1.2	1.00	1.000	1.00	1.00	0.904	0.99	0.80	0.257	0.86
1.3	1.00	1.000	1.00	1.00	0.959	1.00	0.80	0.153	0.92
1.4	1.00	1.000	1.00	1.00	0.983	1.00	1.00	0.609	0.95
1.5	1.00	1.000	1.00	1.00	0.993	1.00	1.00	0.753	0.97
1.6	1.00	1.000	1.00	1.00	0.997	1.00	1.00	0.851	0.98
1.7	1.00	1.000	1.00	1.00	0.999	1.00	1.00	0.913	0.99
1.8	1.00	1.000	1.00	1.00	1.000	1.00	1.00	0.951	0.99
1.9	1.00	1.000	1.00	1.00	1.000	1.00	1.00	0.972	1.00
2	1.00	1.000	1.00	1.00	1.000	1.00	1.00	0.984	1.00



(a)



(b)

Figure 5.9: Observed fractions of exceedances and fitted fragility functions obtained using the maximum likelihood approach for Immediate Occupancy (a), Life Service (b) and Collapse Prevention performance levels (c)

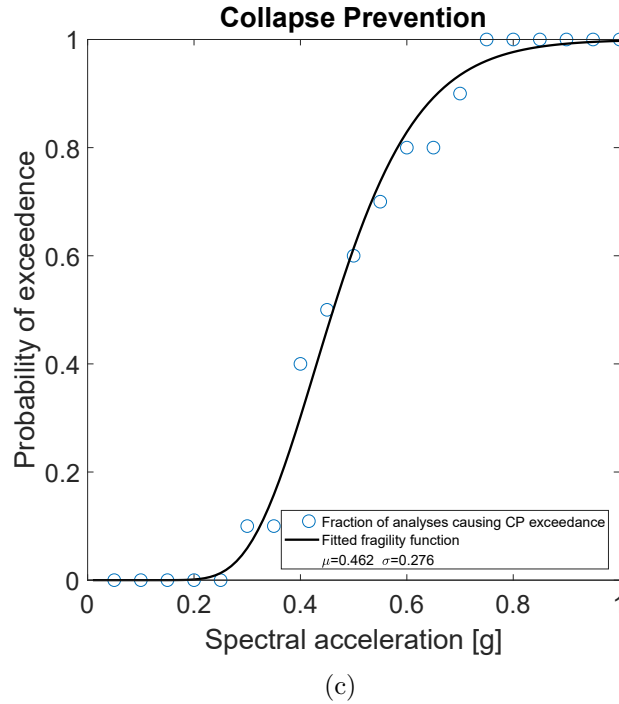


Figure 5.9: Observed fractions of exceedences and fitted fragility functions obtained using the maximum likelihood approach for Immediate Occupancy (a), Life Service (b) and Collapse Prevention performance levels (c) (cont.)

5.4 Accuracy of MPA-based fragility curves

In this section the accuracy of MPA-based approximate procedure is assessed by comparing the predicted fragility curves with the exact fragility curves determined by non-linear incremental dynamic analysis of the MDOFs models for both case studies. The non-linear RHA analyses were performed using Hilber-Hughes-Taylor numerical method ($\gamma = 0.5$; $\beta = 0.25$) with a time step of $0.01s$. A viscous damping of $\xi = 0.02$ was assumed and the geometric non-linearities $P-\Delta$ were accounted. Time history analyses were conducted for each ground motion, each intensity level for each building, resulting in 200 analyses for each building. Each N-RHA analysis was time consuming due to the large memory size of the numerical models especially for the Helix-Parking building model. This is the main reason why a larger number of records was not considered.

The approximate fragility curves estimated by the MPA-based approximate procedure for the SAC-9 building including three modes are presented in figure 5.10 together with the exact fragility curves determined by N-RHA. The parameters for the fitting log-normal functions are summarized in table 5.5. Comparison of the curves demonstrates that the MPA-based approximate fragility curves are fairly accurate over the entire range of ground motion intensity, even close to collapse.

Table 5.5: Approximate and exact values of fragility curves for both case studies.

Building	Limit state	Median		Standard deviation	
		MPA-based	Exact	MPA-based	Exact
SAC-9	IO	0.086	0.086	0.386	0.386
	LS	0.513	0.545	0.278	0.234
	CP	0.924	0.954	0.223	0.281
Helix-Parking	IO	0.0960	0.097	0.085	0.111
	LS	0.341	0.353	0.293	0.326
	CP	0.462	0.465	0.276	0.310

For the low range drift ratios, the estimated probability corresponds to the exact evaluation, while for the Life Service moderate damage the MPA method tends to slightly overestimate the actual probability of damage leading to a more conservative assessment. The accuracy does not deteriorate with regards to estimating structural capacities for the collapse prevention limit state.

The same conclusions can be drawn by analysing the comparison of the approximate and exact curves for the Helix-Parking, for which five modes were considered, shown in figure 5.11.

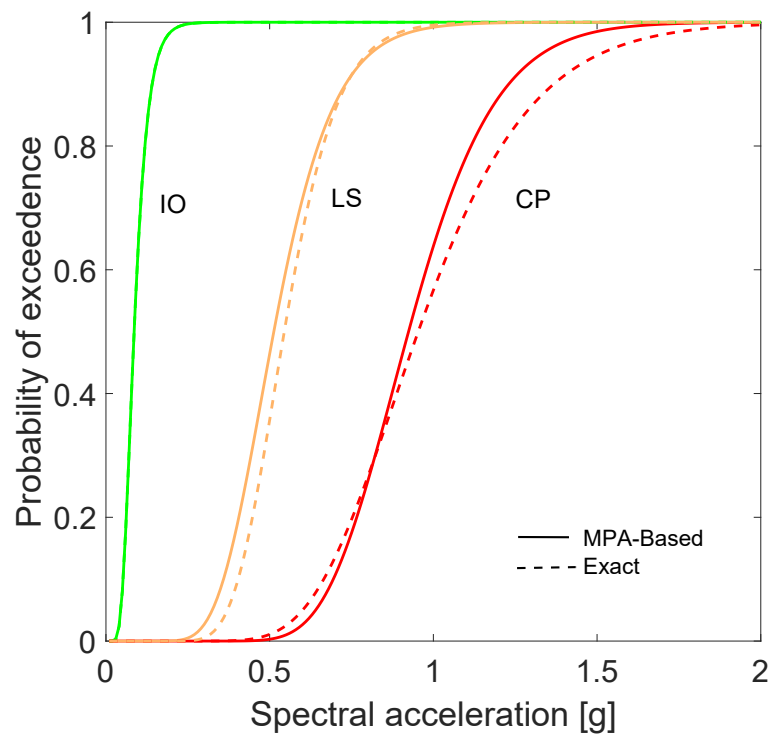


Figure 5.10: Immediate Occupancy, Life Service and Collapse Prevention fragility curves for SAC-9 building from N-RHA (exact) versus MPA-based approximate procedure.

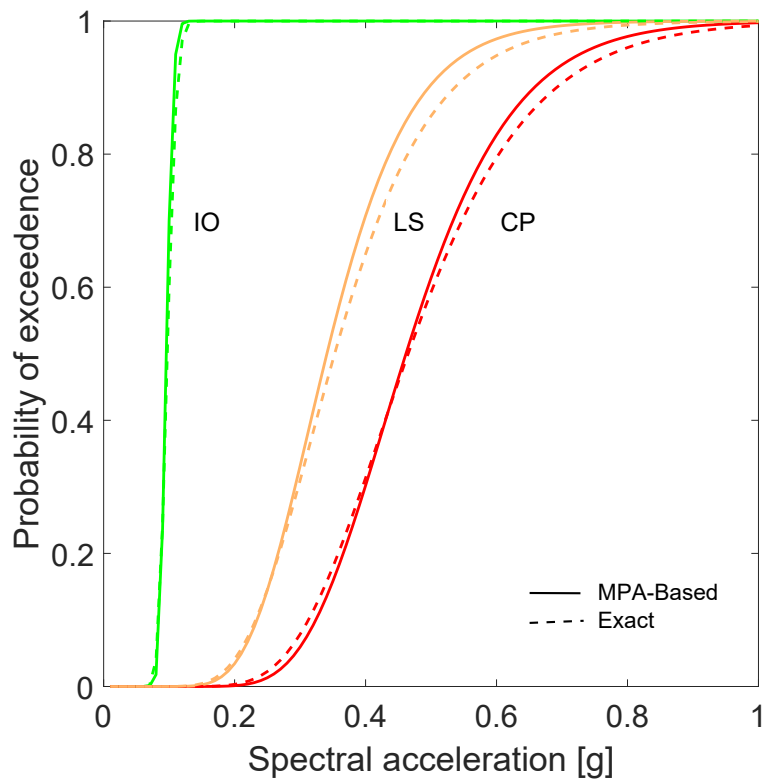


Figure 5.11: Immediate Occupancy, Life Service and Collapse Prevention fragility curves for Helix-Parking from N-RHA (exact) versus MPA-based approximate procedure..

Chapter 6

Conclusion

There is no disagreement that Non-linear response history analysis (N-RHA) is the most realistic seismic performance assessment method. However, N-RHA of practical structures is computationally extremely demanding and since that the structural analysis is not intended to predict accurately the exact structural behaviour but rather to get the necessary information for making design decisions, excessive sophistication in structural analysis is not justified. With this in mind, the Non-linear Static Procedures (NSPs) represent an alternative instrument for a rational yet practical assessment procedure for building structures for multiple performance objectives. This thesis was aimed toward the application of NSPs for the derivation of fragility curves and the evaluation of their accuracy by comparison with N-RHA. The investigation has led to the following conclusions:

1. The approximate Modal Pushover Analysis MPA , including a number of modes that mobilise more than 85% of the total seismic mass provides reliable results in terms of building's maximum displacement and inter-storey drift. In particular, while the first mode is generally sufficient in estimating the maximum displacement for regular buildings, it is not satisfactory when it comes to the evaluation of interstorey drift ratios for both regular and irregular structures. The inadequacy of the first mode alone in estimating drifts is mainly attributable to the translational character of the first mode shape while higher modes are generally weave modes, i.e they consist of a counter-phase oscillation of the storeys. First mode alone fails also to predict the maximum displacement of irregular space frames due the torsional effects.
2. Comparing to the MPA the N2 method with the same number of modes yielded more conservative results for both maximum displacement and inter-storey drift for the regular building and very close results for the irregular one.
3. Some d Incremental Dynamic curves of the equivalent SDOF systems exhibits a twisting behaviour, i.e the analysed systems exhibit at higher intensities, the same or even smaller responses to those showed at smaller seismic intensities. This counter-intuitive phenomenon, which has been already observed observed also for the MDOF systems, is more likely attributable to the scaling of the

ground motions. In more detail, scaling up of record may force early, usually weak waves to become strong enough to initiate yielding and yet change the structural response to the forthcoming stronger cycles. The earlier yielding make the system less responsive in later cycles that had previously caused higher response values.

4. For the probabilistic assessment of structures the first-mode spectral acceleration $Sa(T_1)$ is a way more efficient intensity measure comparing to the Peak ground acceleration PGA , since it simplifies the selection of appropriate ground motion records. In particular, for intermediate period structures, interstory drift as damage indicator and $Sa(T_1)$ as intensity measure, the median of the results obtained from records that have been scaled to some level intensity provide a reliable estimate of the median results of a set of unscaled ground motions with the same level of intensity measure.
5. The MPA-based approximate fragility curves are fairly accurate over the entire range of ground motion intensity, even close to collapse. For the low range drift ratios the estimated probability corresponds to the exact evaluation, while for the Life Service moderate damage the MPA method tends to slightly overestimate the actual probability of damage leading to a more conservative assessment. The accuracy does not deteriorate with regards to estimating structural capacities for the collapse prevention limit state.

Appendices

Appendix A

The First Appendix

A.1 Pushover curves parameters

A.1.1 SAC-9

A.1.2 Helix-Parking

Table A.1: Pushover curves values for the three equivalent SDOFs.

MODE 1		MODE 2		MODE 3	
d [m]	Vb [kN]	d [m]	Vb [kN]	d [m]	Vb [kN]
0.00	0	0.00	0	0.00	0
0.15	2879	0.08	4589	0.04	5058
0.30	5758	0.08	4652	0.04	5309
0.32	6176	0.11	5455	0.06	6325
0.38	7186	0.20	6348	0.13	7958
0.41	7399	0.24	6460	0.18	8499
0.52	7873	0.36	6629	0.25	8989
0.53	7884	0.48	6683	0.26	9064
0.64	8020	0.56	6717	0.36	9488
0.68	8042	0.66	6675	0.44	9861
0.70	8044	0.76	6633	0.46	9918
0.71	8043	0.80	6616	0.52	10011
0.86	7903	0.97	6339	0.60	10069
0.87	7896	1.07	6134	0.63	10026
1.10	7424	1.17	5884	0.76	9662
1.25	7102	1.27	5563	0.83	9422
1.43	6653	1.47	4897	0.91	9183
1.43	6698	1.57	4548	0.98	8943
1.43	6648	1.67	4200	1.06	8704
1.43	6655	1.77	3851	1.13	8465
1.49	6459	1.87	3503	1.21	8225

Table A.2: Pushover curves values for the five equivalent SDOFs.

Mode 1		Mode 2		Mode 3		Mode 4		Mode 5	
d [m]	Vb [kN]	d [m]	Vb [kN]	d [m]	Vb [kN]	d [m]	Vb [kN]	d [m]	Vb [kN]
0.0000	0.00	0.0000	0.00	0.0000	0.00	0.0000	0.00	0.0000	0.00
0.0081	662.24	0.0024	631.85	0.0028	765.09	0.0182	3483.23	0.0004	7076.63
0.0231	1226.56	0.0178	1992.90	0.0243	4760.69	0.0299	4274.58	0.0006	5870.29
0.0257	1155.90	0.0597	3698.74	0.0559	8034.78	0.0427	5178.62	0.0009	11123.02
0.0274	1128.86	0.1109	4862.74	0.0866	10389.74	0.0528	5904.24	0.0015	13848.09
0.0367	1445.23	0.1181	4808.54	0.1076	11760.78	0.0643	6822.30	0.0033	17550.64
0.0393	1444.41	0.1208	4871.62	0.1059	11356.49	0.0745	7641.38	0.0231	31470.23
0.0439	1456.04	0.1346	4976.09	-	-	-	-	-	-
0.0702	2071.09	0.1387	5062.13	-	-	-	-	-	-
0.0712	2048.14	0.1519	5139.04	-	-	-	-	-	-
0.0732	1940.56	0.2056	6247.59	-	-	-	-	-	-
0.1039	2514.59	0.2594	7350.78	-	-	-	-	-	-
0.1414	3025.81	0.3215	8618.59	-	-	-	-	-	-
0.1785	3415.93	0.3794	9797.40	-	-	-	-	-	-
0.2126	3757.50	0.4281	10786.99	-	-	-	-	-	-
0.2512	4135.46	0.4898	12034.97	-	-	-	-	-	-
0.2597	4185.04	0.5108	12457.96	-	-	-	-	-	-

A.2 IDA results

A.2.1 SAC-9

Table A.3: MPA-based IDA for the 295 record.

Sa	$d_{(1, max)}$	$d_{(2, max)}$	$d_{(3, max)}$	$d_{(1, max)} * \Gamma_1$	$d_{(1, max)} * \Gamma_2$	$d_{(1, max)} * \Gamma_3$	$drift_1$	$drift_2$	$drift_3$	MPA total drift
0.10	0.127	0.028	0.009	0.174	0.014	0.002	0.032	0.010	0.006	0.034
0.20	0.254	0.057	0.019	0.348	0.029	0.004	0.059	0.017	0.008	0.062
0.30	0.375	0.084	0.028	0.514	0.043	0.007	0.088	0.023	0.010	0.092
0.40	0.417	0.112	0.037	0.571	0.057	0.009	0.099	0.028	0.011	0.104
0.50	0.430	0.142	0.047	0.589	0.073	0.011	0.103	0.034	0.013	0.109
0.60	0.814	0.168	0.056	1.116	0.086	0.013	0.218	0.038	0.015	0.222
0.70	0.893	0.196	0.066	1.223	0.100	0.016	0.245	0.041	0.016	0.249
0.80	0.807	0.224	0.075	1.106	0.114	0.018	0.216	0.045	0.018	0.221
0.90	0.629	0.255	0.084	0.862	0.130	0.020	0.159	0.048	0.020	0.167
1.00	0.621	0.251	0.094	0.851	0.128	0.022	0.157	0.048	0.021	0.165
1.10	0.629	0.263	0.103	0.862	0.134	0.025	0.159	0.049	0.023	0.168
1.20	0.763	0.296	0.112	1.045	0.151	0.027	0.201	0.052	0.024	0.209
1.30	0.893	0.328	0.122	1.223	0.167	0.029	0.245	0.054	0.026	0.253
1.40	1.127	0.356	0.131	1.544	0.182	0.031	0.334	0.056	0.027	0.339
1.50	1.428	0.373	0.140	1.956	0.190	0.034	0.463	0.057	0.028	0.467
1.60	1.708	0.376	0.150	2.339	0.192	0.036	0.599	0.057	0.030	0.603
1.70	1.976	0.375	0.159	2.707	0.191	0.038	0.744	0.057	0.031	0.747
1.80	2.345	0.382	0.169	3.213	0.195	0.040	0.967	0.057	0.032	0.970
1.90	2.963	0.387	0.178	4.059	0.197	0.043	1.400	0.058	0.033	1.401
2.00	3.566	0.386	0.187	4.885	0.197	0.045	1.895	0.058	0.035	1.896

Table A.4: MPA-based IDA for the 239 record.

Sa	$d_{(1, max)}$	$d_{(2, max)}$	$d_{(3, max)}$	$d_{(1, max)} * \Gamma_1$	$d_{(1, max)} * \Gamma_2$	$d_{(1, max)} * \Gamma_3$	$drift_1$	$drift_2$	$drift_3$	MPA total drift
0.10	0.122	0.065	0.111	0.167	0.033	0.027	0.031	0.019	0.024	0.043
0.20	0.246	0.130	0.222	0.337	0.066	0.053	0.057	0.031	0.039	0.076
0.30	0.373	0.194	0.368	0.511	0.099	0.088	0.088	0.041	0.052	0.110
0.40	0.424	0.259	0.334	0.581	0.132	0.080	0.101	0.049	0.049	0.122
0.50	0.435	0.296	0.380	0.596	0.151	0.091	0.104	0.052	0.053	0.128
0.60	0.480	0.496	0.450	0.658	0.253	0.108	0.116	0.061	0.057	0.143
0.70	0.584	0.639	0.632	0.800	0.326	0.152	0.145	0.062	0.063	0.170
0.80	0.669	0.745	0.844	0.917	0.380	0.203	0.171	0.062	0.065	0.193
0.90	0.806	0.747	1.036	1.104	0.381	0.249	0.215	0.062	0.064	0.233
1.00	0.948	0.729	1.209	1.298	0.372	0.290	0.265	0.062	0.063	0.279
1.10	1.104	0.734	1.388	1.513	0.374	0.333	0.325	0.062	0.062	0.336
1.20	1.236	0.697	1.490	1.693	0.355	0.358	0.378	0.062	0.061	0.388
1.30	1.368	0.648	1.555	1.874	0.331	0.373	0.436	0.062	0.061	0.445
1.40	1.501	0.717	1.674	2.057	0.366	0.402	0.497	0.062	0.061	0.505
1.50	1.635	0.831	1.820	2.240	0.424	0.437	0.562	0.061	0.061	0.569
1.60	1.815	0.995	1.968	2.487	0.508	0.472	0.656	0.059	0.062	0.661
1.70	1.962	1.054	2.126	2.688	0.537	0.510	0.736	0.058	0.062	0.741
1.80	2.163	1.101	2.272	2.963	0.562	0.545	0.854	0.058	0.063	0.858
1.90	2.616	1.143	2.382	3.584	0.583	0.572	1.148	0.058	0.064	1.151
2.00	3.202	1.158	2.524	4.387	0.590	0.606	1.587	0.058	0.064	1.590

Table A.5: MPA-based IDA for the 123 record.

sa	$d_{(1, max)}$	$d_{(2, max)}$	$d_{(3, max)}$	$d_{(1, max)} * \Gamma_1$	$d_{(1, max)} * \Gamma_2$	$d_{(1, max)} * \Gamma_3$	$drift_1$	$drift_2$	$drift_3$	MPA total drift
0.10	0.127	0.222	0.222	0.174	0.113	0.053	0.032	0.045	0.039	0.067
0.20	0.254	0.337	0.337	0.348	0.172	0.081	0.060	0.055	0.050	0.095
0.30	0.519	0.539	0.540	0.711	0.275	0.130	0.128	0.062	0.061	0.154
0.40	0.655	0.665	0.587	0.897	0.339	0.141	0.168	0.062	0.062	0.190
0.50	0.795	0.730	0.564	1.090	0.372	0.135	0.214	0.062	0.061	0.231
0.60	0.850	0.782	0.776	1.164	0.399	0.186	0.232	0.061	0.065	0.249
0.70	0.931	0.947	1.012	1.275	0.483	0.243	0.262	0.060	0.065	0.276
0.80	0.937	1.214	1.265	1.284	0.619	0.304	0.264	0.057	0.063	0.277
0.90	0.950	1.307	1.519	1.301	0.667	0.364	0.269	0.057	0.061	0.281
1.00	0.981	1.226	1.724	1.345	0.625	0.414	0.280	0.057	0.061	0.293
1.10	1.013	1.101	1.943	1.387	0.562	0.466	0.292	0.058	0.061	0.304
1.20	1.039	1.024	2.160	1.423	0.522	0.518	0.302	0.059	0.062	0.314
1.30	1.064	1.132	2.383	1.457	0.577	0.572	0.312	0.058	0.064	0.324
1.40	1.087	1.313	2.512	1.489	0.670	0.603	0.321	0.057	0.064	0.333
1.50	1.172	1.720	2.627	1.605	0.877	0.630	0.356	0.057	0.064	0.366
1.60	1.132	2.126	2.713	1.550	1.084	0.651	0.339	0.056	0.064	0.350
1.70	1.396	2.494	2.804	1.912	1.272	0.673	0.454	0.050	0.064	0.461
1.80	1.821	2.629	2.865	2.495	1.341	0.688	0.669	0.047	0.064	0.674
1.90	3.127	2.726	2.937	4.284	1.390	0.705	1.557	0.045	0.064	1.559
2.00	5.325	4.428	3.050	7.295	2.258	0.732	3.832	-0.071	0.063	3.833

Table A.6: MPA-based IDA for the 336 record.

sa	$d_{(1, max)}$	$d_{(2, max)}$	$d_{(3, max)}$	$d_{(1, max)} * \Gamma_1$	$d_{(1, max)} * \Gamma_2$	$d_{(1, max)} * \Gamma_3$	$drift_1$	$drift_2$	$drift_3$	MPA total drift
0.10	0.131	0.134	0.067	0.180	0.068	0.016	0.033	0.032	0.017	0.049
0.20	0.263	0.244	0.133	0.360	0.124	0.032	0.061	0.047	0.027	0.082
0.30	0.350	0.289	0.200	0.479	0.147	0.048	0.082	0.051	0.036	0.103
0.40	0.367	0.319	0.268	0.503	0.163	0.064	0.086	0.054	0.044	0.111
0.50	0.450	0.393	0.364	0.616	0.200	0.087	0.108	0.058	0.052	0.133
0.60	0.573	0.479	0.315	0.785	0.244	0.076	0.142	0.061	0.048	0.162
0.70	0.722	0.581	0.362	0.989	0.296	0.087	0.188	0.062	0.051	0.204
0.80	1.654	0.667	0.459	2.267	0.340	0.110	0.572	0.062	0.057	0.578
0.90	3.855	0.662	0.623	5.282	0.337	0.149	2.158	0.062	0.063	2.160
1.00	3.898	0.701	0.643	5.341	0.358	0.154	2.198	0.062	0.063	2.200
1.10	3.448	0.695	0.591	4.724	0.354	0.142	1.792	0.062	0.062	1.794
1.20	3.448	0.914	0.583	4.724	0.466	0.140	1.792	0.060	0.062	1.794
1.30	3.689	0.926	0.613	5.054	0.472	0.147	2.004	0.060	0.063	2.006
1.40	4.174	0.904	0.645	5.719	0.461	0.155	2.467	0.060	0.063	2.468
1.50	3.759	0.904	0.680	5.150	0.461	0.163	2.068	0.060	0.064	2.070
1.60	4.194	0.864	0.720	5.746	0.441	0.173	2.487	0.061	0.064	2.488
1.70	3.797	0.812	0.762	5.202	0.414	0.183	2.103	0.061	0.065	2.105
1.80	4.546	0.884	0.847	6.228	0.451	0.203	2.852	0.060	0.065	2.853
1.90	5.601	0.958	0.962	7.673	0.489	0.231	4.092	0.059	0.065	4.093
2.00	21.567	1.042	1.116	29.547	0.531	0.268	49.604	0.059	0.064	49.604

Table A.7: MPA-based IDA for the 536 record.

sa	$d_{(1, max)}$	$d_{(2, max)}$	$d_{(3, max)}$	$d_{(1, max)} * \Gamma_1$	$d_{(1, max)} * \Gamma_2$	$d_{(1, max)} * \Gamma_3$	$dri ft_1$	$dri ft_2$	$dri ft_3$	MPA total drift
0.10	0.126	0.048	0.011	0.172	0.025	0.003	0.032	0.015	0.006	0.036
0.20	0.252	0.097	0.021	0.345	0.049	0.005	0.059	0.025	0.008	0.065
0.30	0.324	0.195	0.032	0.444	0.099	0.008	0.076	0.041	0.010	0.087
0.40	0.385	0.243	0.043	0.528	0.124	0.010	0.091	0.047	0.012	0.103
0.50	0.391	0.194	0.053	0.535	0.099	0.013	0.092	0.041	0.014	0.102
0.60	0.482	0.248	0.064	0.661	0.127	0.015	0.117	0.048	0.016	0.127
0.70	0.571	0.262	0.075	0.783	0.134	0.018	0.142	0.049	0.018	0.151
0.80	0.668	0.252	0.086	0.915	0.129	0.021	0.171	0.048	0.020	0.178
0.90	0.728	0.300	0.096	0.998	0.153	0.023	0.190	0.052	0.022	0.198
1.00	0.755	0.336	0.107	1.034	0.171	0.026	0.198	0.055	0.023	0.207
1.10	0.815	0.357	0.118	1.117	0.182	0.028	0.218	0.056	0.025	0.227
1.20	1.006	0.341	0.128	1.378	0.174	0.031	0.287	0.055	0.027	0.293
1.30	42.650	0.380	0.139	58.431	0.194	0.033	186.521	0.057	0.028	186.521
1.40	52.539	0.404	0.150	71.978	0.206	0.036	280.865	0.058	0.030	280.865
1.50	62.480	0.425	0.160	85.598	0.217	0.038	395.093	0.059	0.031	395.093
1.60	70.978	0.463	0.171	97.240	0.236	0.041	508.151	0.061	0.033	508.151
1.70	79.527	0.465	0.182	108.952	0.237	0.044	636.220	0.061	0.034	636.220
1.80	86.055	0.451	0.192	117.895	0.230	0.046	743.693	0.060	0.035	743.693
1.90	92.920	0.541	0.203	127.300	0.276	0.049	865.757	0.062	0.037	865.757
2.00	100.139	0.600	0.214	137.190	0.306	0.051	1004.115	0.062	0.038	1004.115

Table A.8: MPA-based IDA for the 6264 record.

sa	$d_{(1, max)}$	$d_{(2, max)}$	$d_{(3, max)}$	$d_{(1, max)} * \Gamma_1$	$d_{(1, max)} * \Gamma_2$	$d_{(1, max)} * \Gamma_3$	$drift_1$	$drift_2$	$drift_3$	MPA total drift
0.10	0.129	0.047	0.013	0.177	0.024	0.003	0.032	0.014	0.006	0.036
0.20	0.258	0.094	0.025	0.353	0.047	0.006	0.060	0.025	0.009	0.066
0.30	0.371	0.141	0.038	0.509	0.071	0.009	0.087	0.033	0.011	0.094
0.40	0.574	0.189	0.050	0.786	0.094	0.012	0.142	0.040	0.014	0.149
0.50	0.660	0.236	0.063	0.904	0.118	0.015	0.168	0.046	0.016	0.175
0.60	0.679	0.283	0.076	0.930	0.141	0.018	0.174	0.050	0.018	0.182
0.70	0.728	0.330	0.088	0.997	0.165	0.021	0.190	0.054	0.020	0.198
0.80	0.866	0.377	0.101	1.187	0.189	0.024	0.236	0.057	0.022	0.244
0.90	0.932	0.424	0.113	1.277	0.212	0.027	0.259	0.059	0.024	0.267
1.00	1.069	0.518	0.126	1.464	0.259	0.030	0.311	0.062	0.026	0.318
1.10	1.142	0.566	0.139	1.564	0.283	0.033	0.340	0.062	0.028	0.346
1.20	1.156	0.566	0.151	1.584	0.283	0.036	0.345	0.062	0.030	0.352
1.30	1.290	0.613	0.164	1.767	0.306	0.039	0.402	0.062	0.032	0.408
1.40	1.637	0.660	0.176	2.243	0.330	0.042	0.564	0.062	0.033	0.568
1.50	2.075	0.707	0.189	2.843	0.354	0.045	0.801	0.062	0.035	0.805
1.60	2.476	0.754	0.202	3.392	0.377	0.048	1.052	0.062	0.036	1.055
1.70	1.880	0.801	0.214	2.576	0.401	0.051	0.691	0.061	0.038	0.695
1.80	2.043	0.848	0.227	2.798	0.424	0.054	0.783	0.061	0.039	0.786
1.90	2.177	0.896	0.240	2.982	0.448	0.057	0.862	0.060	0.041	0.865
2.00	3.250	0.943	0.252	4.453	0.471	0.061	1.627	0.060	0.042	1.628

Table A.9: MPA-based IDA for the 196 record.

sa	$d_{(1, max)}$	$d_{(2, max)}$	$d_{(3, max)}$	$d_{(1, max)} * \Gamma_1$	$d_{(1, max)} * \Gamma_2$	$d_{(1, max)} * \Gamma_3$	$drift_1$	$drift_2$	$drift_3$	MPA total drift
0.10	0.095	0.108	0.103	0.130	0.055	0.025	0.025	0.028	0.023	0.044
0.20	0.255	0.219	0.205	0.349	0.112	0.049	0.059	0.044	0.037	0.083
0.30	0.335	0.256	0.269	0.459	0.131	0.065	0.078	0.048	0.044	0.102
0.40	0.539	0.511	0.327	0.738	0.260	0.078	0.132	0.062	0.049	0.154
0.50	0.576	0.615	0.407	0.790	0.314	0.098	0.143	0.062	0.054	0.165
0.60	0.594	0.599	0.425	0.814	0.306	0.102	0.148	0.062	0.055	0.170
0.70	0.682	0.677	0.427	0.934	0.345	0.102	0.175	0.062	0.056	0.194
0.80	0.736	0.808	0.463	1.008	0.412	0.111	0.192	0.061	0.057	0.210
0.90	0.857	0.909	0.605	1.174	0.464	0.145	0.233	0.060	0.062	0.248
1.00	0.892	1.088	0.761	1.221	0.555	0.183	0.245	0.058	0.065	0.260
1.10	0.849	1.448	0.834	1.163	0.739	0.200	0.230	0.057	0.065	0.246
1.20	0.975	1.779	0.701	1.335	0.907	0.168	0.275	0.057	0.064	0.288
1.30	1.098	1.493	0.645	1.504	0.762	0.155	0.322	0.057	0.063	0.333
1.40	1.221	1.212	0.748	1.673	0.618	0.180	0.372	0.057	0.065	0.382
1.50	1.389	1.150	1.075	1.902	0.587	0.258	0.445	0.058	0.064	0.453
1.60	1.459	1.158	1.481	1.999	0.590	0.355	0.478	0.058	0.061	0.485
1.70	1.644	1.230	1.885	2.253	0.627	0.452	0.567	0.057	0.061	0.573
1.80	1.917	1.305	2.257	2.626	0.666	0.542	0.711	0.057	0.063	0.716
1.90	2.151	1.383	2.482	2.946	0.705	0.596	0.846	0.057	0.064	0.851
2.00	3.496	1.461	2.761	4.789	0.745	0.663	1.833	0.057	0.064	1.835

Table A.10: MPA-based IDA for the 947 record.

sa	$d_{(1, max)}$	$d_{(2, max)}$	$d_{(3, max)}$	$d_{(1, max)} * \Gamma_1$	$d_{(1, max)} * \Gamma_2$	$d_{(1, max)} * \Gamma_3$	$driфт_1$	$driфт_2$	$driфт_3$	MPA total drift
0.10	0.126	0.117	0.031	0.173	0.060	0.007	0.032	0.029	0.010	0.044
0.20	0.252	0.235	0.062	0.346	0.120	0.015	0.059	0.046	0.016	0.076
0.30	0.333	0.227	0.093	0.456	0.116	0.022	0.078	0.045	0.021	0.092
0.40	0.398	0.375	0.124	0.545	0.191	0.030	0.094	0.057	0.026	0.113
0.50	0.450	0.414	0.155	0.616	0.211	0.037	0.108	0.059	0.030	0.127
0.60	0.504	0.409	0.186	0.690	0.209	0.045	0.123	0.059	0.034	0.140
0.70	0.623	0.446	0.217	0.853	0.228	0.052	0.157	0.060	0.038	0.172
0.80	0.856	0.546	0.248	1.173	0.278	0.059	0.232	0.062	0.042	0.244
0.90	1.115	0.580	0.281	1.528	0.296	0.067	0.329	0.062	0.045	0.338
1.00	1.296	0.611	0.316	1.776	0.312	0.076	0.404	0.062	0.048	0.412
1.10	1.255	0.641	0.404	1.719	0.327	0.097	0.387	0.062	0.054	0.395
1.20	1.206	0.670	0.506	1.653	0.342	0.121	0.366	0.062	0.059	0.376
1.30	1.109	0.697	0.566	1.520	0.356	0.136	0.327	0.062	0.061	0.338
1.40	1.137	0.854	0.607	1.557	0.436	0.146	0.338	0.061	0.062	0.349
1.50	0.942	0.910	0.639	1.291	0.464	0.153	0.263	0.060	0.063	0.277
1.60	2.989	1.035	0.695	4.095	0.528	0.167	1.420	0.059	0.064	1.422
1.70	6.614	1.158	0.729	9.061	0.591	0.175	5.490	0.058	0.064	5.491
1.80	4.784	1.347	0.769	6.554	0.687	0.185	3.112	0.057	0.065	3.113
1.90	9.772	0.872	0.843	13.387	0.445	0.202	11.143	0.060	0.065	11.143
2.00	10.406	0.905	0.851	14.256	0.462	0.204	12.514	0.060	0.065	12.514

Table A.11: MPA-based IDA for the 595 record.

sa	$d_{(1, max)}$	$d_{(2, max)}$	$d_{(3, max)}$	$d_{(1, max)} * \Gamma_1$	$d_{(1, max)} * \Gamma_2$	$d_{(1, max)} * \Gamma_3$	$drift_1$	$drift_2$	$drift_3$	MPA total drift
0.10	0.126	0.038	0.036	0.173	0.019	0.009	0.032	0.013	0.011	0.036
0.20	0.252	0.076	0.072	0.346	0.039	0.017	0.059	0.021	0.018	0.065
0.30	0.318	0.115	0.108	0.436	0.058	0.026	0.074	0.029	0.024	0.083
0.40	0.415	0.153	0.144	0.569	0.078	0.035	0.099	0.035	0.029	0.109
0.50	0.430	0.191	0.181	0.589	0.097	0.043	0.102	0.041	0.034	0.115
0.60	0.507	0.229	0.217	0.695	0.117	0.052	0.124	0.045	0.038	0.137
0.70	0.600	0.254	0.253	0.821	0.130	0.061	0.150	0.048	0.042	0.163
0.80	0.668	0.341	0.294	0.915	0.174	0.071	0.171	0.055	0.046	0.185
0.90	0.751	0.420	0.269	1.029	0.214	0.065	0.197	0.059	0.044	0.210
1.00	0.828	0.466	0.301	1.134	0.191	0.072	0.223	0.057	0.047	0.235
1.10	0.968	0.447	0.332	1.326	0.228	0.080	0.273	0.060	0.049	0.283
1.20	1.236	0.451	0.328	1.693	0.230	0.079	0.378	0.060	0.049	0.386
1.30	3.747	0.414	0.324	5.133	0.211	0.078	2.057	0.059	0.049	2.059
1.40	3.757	0.401	0.349	5.147	0.205	0.084	2.066	0.058	0.050	2.068
1.50	13.110	0.427	0.364	17.961	0.218	0.087	19.251	0.059	0.052	19.252
1.60	4.435	0.466	0.387	6.076	0.238	0.093	2.734	0.061	0.053	2.735
1.70	6.277	0.565	0.426	8.599	0.288	0.102	5.003	0.062	0.055	5.004
1.80	7.250	0.640	0.446	9.933	0.326	0.107	6.471	0.062	0.057	6.472
1.90	7.661	0.763	0.447	10.496	0.389	0.107	7.147	0.062	0.057	7.148
2.00	18.402	0.871	0.502	25.210	0.444	0.121	36.596	0.060	0.059	36.596

Table A.12: MPA-based IDA for the 244 record.

sa	$d_{(1, max)}$	$d_{(2, max)}$	$d_{(3, max)}$	$d_{(1, max)} * \Gamma_1$	$d_{(1, max)} * \Gamma_2$	$d_{(1, max)} * \Gamma_3$	$drift_1$	$drift_2$	$drift_3$	MPA total drift
0.10	0.099	0.063	0.041	0.135	0.032	0.010	0.026	0.018	0.012	0.034
0.20	0.201	0.127	0.082	0.275	0.065	0.020	0.047	0.031	0.019	0.060
0.30	0.318	0.190	0.123	0.436	0.097	0.030	0.074	0.041	0.026	0.089
0.40	0.394	0.255	0.164	0.539	0.130	0.039	0.093	0.048	0.032	0.110
0.50	0.479	0.278	0.205	0.656	0.142	0.049	0.116	0.050	0.037	0.131
0.60	0.670	0.367	0.247	0.918	0.187	0.059	0.171	0.057	0.041	0.185
0.70	1.084	0.490	0.270	1.485	0.250	0.065	0.317	0.061	0.044	0.325
0.80	1.528	0.576	0.280	2.094	0.294	0.067	0.510	0.062	0.045	0.516
0.90	2.199	0.659	0.356	3.012	0.336	0.085	0.876	0.062	0.051	0.879
1.00	2.785	0.748	0.406	3.815	0.382	0.097	1.268	0.062	0.054	1.270
1.10	3.062	0.834	0.437	4.194	0.426	0.105	1.476	0.061	0.056	1.478
1.20	3.513	0.904	0.462	4.813	0.461	0.111	1.848	0.060	0.057	1.850
1.30	4.193	1.042	0.487	5.745	0.532	0.117	2.485	0.058	0.058	2.487
1.40	4.668	1.336	0.471	6.395	0.681	0.113	2.984	0.057	0.058	2.985
1.50	4.819	1.524	0.476	6.602	0.777	0.114	3.152	0.057	0.058	3.153
1.60	4.238	1.649	0.482	5.806	0.841	0.116	2.531	0.057	0.058	2.532
1.70	4.254	1.848	0.585	5.828	0.942	0.140	2.547	0.057	0.062	2.548
1.80	4.032	2.049	0.666	5.524	1.045	0.160	2.326	0.057	0.064	2.328
1.90	3.665	2.208	0.746	5.022	1.126	0.179	1.983	0.055	0.065	1.985
2.00	3.134	2.236	0.844	4.294	1.140	0.203	1.533	0.055	0.065	1.535

Table A.13: Exact IDA for the ten records.

		Maximum drift									
Sa	295	239	123	336	536	6264	196	947	595	244	
0.1	0.0274	0.0515	0.0783	0.0650	0.0386	0.0305	0.0494	0.0492	0.0361	0.0303	
0.2	0.0551	0.0814	0.0841	0.0890	0.0710	0.0605	0.0901	0.0681	0.0696	0.0813	
0.3	0.0756	0.0912	0.1278	0.0900	0.1018	0.0885	0.1011	0.0795	0.0817	0.0979	
0.4	0.0903	0.1274	0.1461	0.1200	0.1175	0.0896	0.1032	0.0926	0.0951	0.1055	
0.5	0.0879	0.1738	0.1737	0.1500	0.1142	0.1068	0.1487	0.0968	0.1195	0.1152	
0.6	0.0912	0.2295	0.2363	0.1900	0.1274	0.1184	0.1507	0.1121	0.1454	0.1503	
0.7	0.0977	0.2870	0.2949	0.2310	0.1353	0.1436	0.2307	0.1373	0.1647	0.1955	
0.8	0.1144	0.3723	0.3406	0.4700	0.1390	0.1787	0.2500	0.1632	0.1828	0.2576	
0.9	0.1325	0.4458	0.3897	DI	0.1734	0.2067	DI	0.1849	0.1798	0.3114	
1	0.1666	0.4980	0.4276	DI	0.2160	0.2363	DI	0.2064	0.1465	0.3402	
1.1	0.1930	DI	DI	DI	0.2614	0.2613	DI	0.2228	0.1642	DI	
1.2	0.2246	DI	DI	DI	0.3521	0.2881	DI	0.2643	0.3870	DI	
1.3	0.2705	DI	DI	DI	0.4584	0.3141	DI	0.2701	DI	DI	
1.4	0.3235	DI	DI	DI	0.6787	0.3411	DI	0.2738	DI	DI	
1.5	0.4180	DI	DI	DI	DI	0.4003	DI	0.3048	DI	DI	
1.6	DI	DI	DI	DI	DI	DI	DI	DI	DI	DI	
1.7	DI	DI	DI	DI	DI	DI	DI	DI	DI	DI	
1.8	DI	DI	DI	DI	DI	DI	DI	DI	DI	DI	
1.9	DI	DI	DI	DI	DI	DI	DI	DI	DI	DI	
2	DI	DI	DI	DI	DI	DI	DI	DI	DI	DI	

A.2.2 Helix-Parking

Table A.14: IDA for both components of the record 295.

	Earthquake component												TOTAL DRIFT					
	X				Y				X						Y			
	ROOF DISPLACEMENT		DRIFT		ROOF DISPLACEMENT		DRIFT		ROOF DISPLACEMENT		DRIFT				ROOF DISPLACEMENT		DRIFT	
Sa	Y	X	Y	X	Y	X	Y	X	Y	X	Y	X	Y	X	Y	X _{tot}	Y _{tot}	
0.05	0.018	0.005	0.019	0.003	0.001	0.004	0.000	0.013	0.001	0.013	0.001	0.013	0.001	0.013	0.001	0.013	0.013	
0.1	0.028	0.008	0.029	0.004	0.002	0.006	0.001	0.020	0.002	0.020	0.002	0.020	0.002	0.020	0.002	0.020	0.021	
0.15	0.038	0.010	0.039	0.005	0.004	0.009	0.002	0.027	0.004	0.027	0.004	0.027	0.004	0.027	0.004	0.028	0.028	
0.2	0.047	0.013	0.048	0.006	0.005	0.011	0.002	0.033	0.006	0.033	0.006	0.033	0.006	0.033	0.006	0.034	0.034	
0.25	0.062	0.015	0.056	0.007	0.007	0.013	0.003	0.044	0.008	0.044	0.008	0.044	0.008	0.044	0.008	0.045	0.045	
0.3	0.071	0.018	0.061	0.008	0.008	0.015	0.004	0.050	0.009	0.050	0.009	0.050	0.009	0.050	0.009	0.052	0.052	
0.35	0.078	0.019	0.063	0.009	0.009	0.016	0.004	0.054	0.010	0.054	0.010	0.054	0.010	0.054	0.010	0.057	0.057	
0.4	0.085	0.022	0.072	0.010	0.011	0.018	0.005	0.060	0.012	0.060	0.012	0.060	0.012	0.060	0.012	0.063	0.063	
0.45	0.092	0.023	0.084	0.011	0.011	0.020	0.005	0.064	0.013	0.064	0.013	0.064	0.013	0.064	0.013	0.067	0.067	
0.5	0.101	0.026	0.095	0.012	0.013	0.022	0.006	0.071	0.015	0.071	0.015	0.071	0.015	0.071	0.015	0.074	0.074	
0.55	0.111	0.031	0.108	0.013	0.016	0.026	0.007	0.078	0.017	0.078	0.017	0.078	0.017	0.078	0.017	0.082	0.082	
0.6	0.119	0.035	0.120	0.013	0.018	0.029	0.007	0.083	0.020	0.083	0.020	0.083	0.020	0.083	0.020	0.088	0.088	
0.65	0.130	0.038	0.130	0.014	0.020	0.032	0.008	0.091	0.022	0.091	0.022	0.091	0.022	0.091	0.022	0.097	0.097	
0.7	0.140	0.041	0.141	0.015	0.022	0.034	0.009	0.098	0.024	0.098	0.024	0.098	0.024	0.098	0.024	0.104	0.104	
0.75	0.149	0.043	0.152	0.016	0.023	0.037	0.009	0.105	0.025	0.105	0.025	0.105	0.025	0.105	0.025	0.111	0.111	
0.8	0.159	0.046	0.162	0.017	0.025	0.039	0.010	0.111	0.027	0.111	0.027	0.111	0.027	0.111	0.027	0.118	0.118	
0.85	0.168	0.048	0.171	0.018	0.026	0.040	0.011	0.118	0.028	0.118	0.028	0.118	0.028	0.118	0.028	0.124	0.124	
0.9	0.175	0.050	0.179	0.018	0.028	0.043	0.011	0.123	0.030	0.123	0.030	0.123	0.030	0.123	0.030	0.130	0.130	
0.95	0.185	0.053	0.185	0.018	0.029	0.045	0.012	0.130	0.031	0.130	0.031	0.130	0.031	0.130	0.031	0.137	0.137	
1	0.198	0.055	0.191	0.019	0.031	0.047	0.013	0.139	0.033	0.139	0.033	0.139	0.033	0.139	0.033	0.147	0.147	

Table A.15: IDA for both components of the record 239

	Earthquake component												TOTAL DRIFT			
	X				Y				DRIFT						X _{tot}	Y _{tot}
	ROOF DISPLACEMENT		X		Y		DRIFT		X		Y					
Sa	Y	X	Y	X	Y	X	Y	X	Y	X	Y	X	Y	X _{tot}	Y _{tot}	
0.05	0.026	0.010	0.021	0.014	0.006	0.007	0.017	0.011	0.018	0.013						
0.1	0.044	0.018	0.034	0.029	0.015	0.019	0.002	0.022	0.015	0.030						
0.15	0.062	0.024	0.047	0.035	0.019	0.025	0.003	0.034	0.019	0.042						
0.2	0.075	0.027	0.055	0.042	0.023	0.031	0.004	0.042	0.023	0.052						
0.25	0.088	0.028	0.062	0.048	0.026	0.036	0.005	0.050	0.027	0.062						
0.3	0.098	0.033	0.073	0.053	0.029	0.040	0.006	0.057	0.030	0.070						
0.35	0.116	0.040	0.083	0.063	0.035	0.048	0.007	0.068	0.036	0.084						
0.4	0.135	0.045	0.097	0.073	0.041	0.057	0.008	0.081	0.042	0.099						
0.45	0.156	0.050	0.110	0.080	0.045	0.063	0.010	0.094	0.046	0.113						
0.5	0.173	0.056	0.126	0.087	0.049	0.069	0.011	0.105	0.051	0.125						
0.55	0.191	0.062	0.138	0.094	0.053	0.074	0.012	0.116	0.055	0.138						
0.6	0.210	0.067	0.153	0.100	0.057	0.080	0.014	0.128	0.059	0.151						
0.65	0.229	0.071	0.149	0.107	0.061	0.086	0.015	0.141	0.063	0.165						
0.7	0.243	0.074	0.159	0.114	0.065	0.092	0.016	0.150	0.067	0.175						
0.75	0.256	0.078	0.168	0.121	0.070	0.098	0.017	0.158	0.072	0.185						
0.8	0.267	0.083	0.176	0.127	0.073	0.103	0.018	0.165	0.075	0.194						
0.85	0.278	0.087	0.190	0.134	0.078	0.109	0.019	0.172	0.080	0.203						
0.9	0.288	0.091	0.204	0.137	0.079	0.111	0.019	0.178	0.081	0.210						
0.95	0.299	0.096	0.220	0.139	0.080	0.112	0.020	0.185	0.082	0.216						
1	0.312	0.100	0.236	0.149	0.086	0.121	0.021	0.194	0.089	0.228						

Table A.16: IDA for both components of the record 123.

	Earthquake component												TOTAL DRIFT		
	ROOF DISPLACEMENT				DRIFT										
	X		Y		X		Y		X		Y				X _{tot}
S _a	Y	X	Y	X	Y	X	Y	X	Y	X	Y	X	Y	X _{tot}	Y _{tot}
0.05	0.020	0.012	0.025	0.010	0.005	0.005	0.005	0.001	0.011	0.005	0.012	0.005	0.012	0.005	0.012
0.1	0.033	0.019	0.042	0.019	0.009	0.009	0.012	0.002	0.021	0.009	0.024	0.009	0.024	0.009	0.024
0.15	0.045	0.028	0.053	0.029	0.014	0.014	0.019	0.003	0.029	0.014	0.034	0.014	0.034	0.014	0.034
0.2	0.058	0.032	0.064	0.038	0.017	0.017	0.023	0.003	0.035	0.017	0.042	0.017	0.042	0.017	0.042
0.25	0.066	0.037	0.073	0.049	0.019	0.019	0.026	0.004	0.041	0.020	0.049	0.020	0.049	0.020	0.049
0.3	0.073	0.041	0.087	0.052	0.022	0.022	0.030	0.005	0.050	0.023	0.058	0.023	0.058	0.023	0.058
0.35	0.084	0.046	0.100	0.055	0.025	0.025	0.034	0.006	0.058	0.026	0.068	0.026	0.068	0.026	0.068
0.4	0.098	0.052	0.112	0.059	0.028	0.028	0.039	0.007	0.066	0.029	0.077	0.029	0.077	0.029	0.077
0.45	0.114	0.059	0.123	0.061	0.032	0.032	0.045	0.008	0.073	0.033	0.085	0.033	0.085	0.033	0.085
0.5	0.128	0.066	0.138	0.065	0.037	0.037	0.051	0.009	0.082	0.038	0.097	0.038	0.097	0.038	0.097
0.55	0.139	0.072	0.152	0.073	0.040	0.040	0.056	0.010	0.091	0.041	0.107	0.041	0.107	0.041	0.107
0.6	0.149	0.078	0.166	0.081	0.044	0.044	0.061	0.011	0.100	0.045	0.117	0.045	0.117	0.045	0.117
0.65	0.157	0.083	0.180	0.089	0.047	0.047	0.066	0.012	0.109	0.048	0.127	0.048	0.127	0.048	0.127
0.7	0.164	0.089	0.194	0.097	0.050	0.050	0.070	0.013	0.118	0.052	0.138	0.052	0.138	0.052	0.138
0.75	0.172	0.095	0.207	0.105	0.054	0.054	0.075	0.014	0.127	0.055	0.147	0.055	0.147	0.055	0.147
0.8	0.179	0.100	0.218	0.113	0.057	0.057	0.080	0.014	0.134	0.059	0.156	0.059	0.156	0.059	0.156
0.85	0.187	0.106	0.229	0.119	0.060	0.060	0.085	0.015	0.141	0.062	0.164	0.062	0.164	0.062	0.164
0.9	0.194	0.111	0.241	0.126	0.064	0.064	0.089	0.016	0.148	0.066	0.173	0.066	0.173	0.066	0.173
0.95	0.200	0.117	0.253	0.134	0.067	0.067	0.094	0.017	0.155	0.069	0.182	0.069	0.182	0.069	0.182
1	0.206	0.123	0.265	0.141	0.070	0.070	0.099	0.018	0.163	0.073	0.191	0.073	0.191	0.073	0.191

Table A.17: IDA for both components of the record 336.

	Earthquake component												TOTAL DRIFT			
	X				Y				DRIFT						X _{tot}	Y _{tot}
	ROOF DISPLACEMENT		X		Y		DRIFT		X		Y					
Sa	Y	X	Y	X	Y	X	Y	X	Y	X	Y	X	Y	X _{tot}	Y _{tot}	
0.05	0.026	0.009	0.019	0.011	0.003	0.005	0.001	0.011	0.003	0.012	0.003	0.011	0.003	0.003	0.012	
0.1	0.044	0.015	0.031	0.022	0.006	0.014	0.002	0.023	0.007	0.027	0.007	0.023	0.007	0.007	0.027	
0.15	0.061	0.021	0.042	0.032	0.010	0.022	0.003	0.033	0.011	0.040	0.011	0.033	0.011	0.011	0.040	
0.2	0.065	0.026	0.054	0.042	0.013	0.031	0.004	0.036	0.014	0.048	0.014	0.036	0.014	0.014	0.048	
0.25	0.084	0.029	0.063	0.049	0.015	0.037	0.005	0.048	0.015	0.061	0.015	0.048	0.015	0.015	0.061	
0.3	0.094	0.033	0.069	0.052	0.017	0.039	0.006	0.054	0.018	0.067	0.018	0.054	0.018	0.018	0.067	
0.35	0.100	0.038	0.078	0.055	0.020	0.041	0.006	0.058	0.021	0.071	0.021	0.058	0.021	0.021	0.071	
0.4	0.105	0.044	0.089	0.057	0.024	0.043	0.006	0.061	0.024	0.075	0.024	0.061	0.024	0.024	0.075	
0.45	0.110	0.048	0.103	0.064	0.026	0.050	0.007	0.065	0.027	0.081	0.027	0.065	0.027	0.027	0.081	
0.5	0.116	0.052	0.118	0.068	0.028	0.053	0.007	0.069	0.029	0.087	0.029	0.069	0.029	0.029	0.087	
0.55	0.122	0.055	0.130	0.072	0.031	0.056	0.008	0.072	0.031	0.091	0.031	0.072	0.031	0.031	0.091	
0.6	0.130	0.059	0.140	0.076	0.033	0.060	0.008	0.077	0.034	0.097	0.034	0.077	0.034	0.034	0.097	
0.65	0.136	0.063	0.149	0.083	0.035	0.065	0.009	0.081	0.036	0.104	0.036	0.081	0.036	0.036	0.104	
0.7	0.143	0.067	0.156	0.089	0.037	0.070	0.009	0.086	0.038	0.111	0.038	0.086	0.038	0.038	0.111	
0.75	0.151	0.071	0.163	0.095	0.040	0.076	0.010	0.091	0.041	0.118	0.041	0.091	0.041	0.041	0.118	
0.8	0.156	0.078	0.170	0.101	0.044	0.081	0.010	0.094	0.045	0.124	0.045	0.094	0.045	0.045	0.124	
0.85	0.167	0.084	0.177	0.107	0.047	0.086	0.011	0.101	0.048	0.132	0.048	0.101	0.048	0.048	0.132	
0.9	0.177	0.088	0.184	0.114	0.050	0.091	0.011	0.107	0.051	0.141	0.051	0.107	0.051	0.051	0.141	
0.95	0.183	0.093	0.191	0.120	0.053	0.097	0.012	0.111	0.054	0.148	0.054	0.111	0.054	0.054	0.148	
1	0.190	0.096	0.197	0.126	0.055	0.102	0.012	0.115	0.056	0.154	0.056	0.115	0.056	0.056	0.154	

Table A.19: IDA for both components of the record 6264.

	Earthquake component												TOTAL DRIFT		
	X		Y				X				Y				
	ROOF DISPLACEMENT		DRIFT				X		Y		X _{tot}	Y _{tot}			
Sa	Y	X	Y	X	Y	X	Y	X	Y	X	Y	X	Y	X _{tot}	Y _{tot}
0.05	0.018	0.005	0.014	0.003	0.000	0.003	0.000	0.006	0.000	0.003	0.000	0.006	0.000	0.000	0.007
0.1	0.027	0.007	0.021	0.007	0.002	0.006	0.000	0.012	0.000	0.006	0.000	0.012	0.002	0.002	0.013
0.15	0.037	0.010	0.027	0.010	0.003	0.009	0.001	0.018	0.001	0.018	0.003	0.018	0.003	0.003	0.020
0.2	0.043	0.012	0.033	0.014	0.005	0.012	0.001	0.022	0.001	0.022	0.005	0.022	0.005	0.005	0.025
0.25	0.047	0.015	0.039	0.017	0.006	0.015	0.002	0.024	0.002	0.024	0.007	0.024	0.007	0.007	0.029
0.3	0.050	0.017	0.046	0.021	0.008	0.018	0.002	0.027	0.002	0.027	0.008	0.027	0.008	0.008	0.032
0.35	0.056	0.020	0.053	0.024	0.009	0.021	0.003	0.030	0.003	0.030	0.010	0.030	0.010	0.010	0.037
0.4	0.064	0.021	0.057	0.028	0.010	0.023	0.003	0.035	0.003	0.035	0.010	0.035	0.010	0.010	0.043
0.45	0.071	0.022	0.063	0.031	0.011	0.026	0.003	0.040	0.003	0.040	0.011	0.040	0.011	0.011	0.048
0.5	0.072	0.024	0.070	0.034	0.012	0.029	0.004	0.041	0.004	0.041	0.012	0.041	0.012	0.012	0.050
0.55	0.074	0.025	0.079	0.038	0.013	0.032	0.004	0.042	0.004	0.042	0.013	0.042	0.013	0.013	0.053
0.6	0.076	0.026	0.088	0.042	0.013	0.035	0.005	0.043	0.005	0.043	0.014	0.043	0.014	0.014	0.056
0.65	0.081	0.028	0.095	0.048	0.014	0.041	0.006	0.046	0.006	0.046	0.015	0.046	0.015	0.015	0.062
0.7	0.087	0.030	0.104	0.055	0.015	0.046	0.006	0.050	0.006	0.050	0.017	0.050	0.017	0.017	0.068
0.75	0.092	0.032	0.112	0.060	0.017	0.051	0.007	0.053	0.007	0.053	0.018	0.053	0.018	0.018	0.074
0.8	0.096	0.034	0.119	0.065	0.018	0.055	0.007	0.056	0.007	0.056	0.019	0.056	0.019	0.019	0.078
0.85	0.100	0.036	0.126	0.067	0.019	0.056	0.008	0.059	0.008	0.059	0.021	0.059	0.021	0.021	0.081
0.9	0.104	0.038	0.135	0.068	0.020	0.057	0.008	0.061	0.008	0.061	0.022	0.061	0.022	0.022	0.084
0.95	0.108	0.040	0.143	0.069	0.022	0.058	0.009	0.064	0.009	0.064	0.023	0.064	0.023	0.023	0.086
1	0.113	0.042	0.147	0.069	0.023	0.058	0.009	0.066	0.009	0.066	0.024	0.066	0.024	0.024	0.088

Table A.21: IDA for both components of the record 947.

	Earthquake component												TOTAL DRIFT	
	X		Y				X				Y			
	ROOF DISPLACEMENT		X		Y		X		Y		X _{tot}	Y _{tot}		
Sa	Y	X	Y	X	Y	X	Y	X	Y	X	Y	X _{tot}	Y _{tot}	
0.05	0.020	0.007	0.019	0.004	0.002	0.002	0.002	0.000	0.009	0.002	0.009	0.002	0.009	
0.1	0.032	0.011	0.030	0.008	0.004	0.004	0.005	0.001	0.014	0.005	0.014	0.005	0.014	
0.15	0.044	0.016	0.041	0.012	0.007	0.007	0.007	0.002	0.019	0.007	0.019	0.007	0.020	
0.2	0.053	0.019	0.052	0.016	0.009	0.009	0.008	0.003	0.023	0.009	0.023	0.009	0.025	
0.25	0.067	0.023	0.060	0.021	0.011	0.011	0.010	0.004	0.031	0.012	0.032	0.012	0.032	
0.3	0.080	0.026	0.066	0.025	0.013	0.013	0.011	0.005	0.038	0.014	0.039	0.014	0.039	
0.35	0.084	0.028	0.070	0.029	0.014	0.014	0.012	0.005	0.040	0.015	0.042	0.015	0.042	
0.4	0.089	0.031	0.074	0.032	0.016	0.016	0.014	0.005	0.043	0.017	0.046	0.017	0.046	
0.45	0.090	0.034	0.080	0.034	0.018	0.018	0.015	0.005	0.044	0.019	0.047	0.019	0.047	
0.5	0.098	0.038	0.091	0.038	0.020	0.020	0.017	0.006	0.049	0.021	0.052	0.021	0.052	
0.55	0.107	0.042	0.102	0.040	0.023	0.023	0.019	0.006	0.055	0.023	0.058	0.023	0.058	
0.6	0.115	0.046	0.113	0.042	0.025	0.025	0.021	0.007	0.060	0.026	0.064	0.026	0.064	
0.65	0.121	0.050	0.123	0.044	0.027	0.027	0.022	0.007	0.064	0.028	0.068	0.028	0.068	
0.7	0.127	0.054	0.127	0.046	0.029	0.029	0.024	0.008	0.068	0.030	0.073	0.030	0.073	
0.75	0.132	0.058	0.130	0.048	0.032	0.032	0.026	0.008	0.072	0.033	0.077	0.033	0.077	
0.8	0.137	0.062	0.144	0.050	0.034	0.034	0.028	0.009	0.076	0.035	0.081	0.035	0.081	
0.85	0.140	0.066	0.155	0.053	0.037	0.037	0.030	0.009	0.078	0.038	0.083	0.038	0.083	
0.9	0.143	0.070	0.162	0.057	0.039	0.039	0.032	0.009	0.080	0.040	0.086	0.040	0.086	
0.95	0.146	0.074	0.169	0.060	0.042	0.042	0.034	0.009	0.083	0.043	0.089	0.043	0.089	
1	0.151	0.078	0.174	0.064	0.044	0.044	0.035	0.010	0.086	0.045	0.093	0.045	0.093	

Table A.22: IDA for both components of the 595 record.

Sa	Earthquake component												TOTAL DRIFT	
	ROOF DISPLACEMENT				DRIFT				TOTAL DRIFT					
	X		Y		X		Y		X		Y		X _{tot}	Y _{tot}
0.05	0.020	0.005	0.027	0.010	0.004	0.005	0.001	0.012	0.004	0.013	0.013	0.004	0.013	
0.1	0.031	0.009	0.043	0.020	0.009	0.007	0.002	0.022	0.010	0.023	0.023	0.010	0.023	
0.15	0.038	0.012	0.053	0.030	0.015	0.010	0.003	0.028	0.016	0.030	0.030	0.016	0.030	
0.2	0.044	0.015	0.061	0.037	0.019	0.013	0.003	0.034	0.020	0.036	0.036	0.020	0.036	
0.25	0.048	0.018	0.072	0.039	0.021	0.015	0.004	0.041	0.021	0.043	0.043	0.021	0.043	
0.3	0.053	0.020	0.077	0.042	0.023	0.017	0.004	0.043	0.023	0.047	0.047	0.023	0.047	
0.35	0.058	0.022	0.090	0.051	0.028	0.019	0.005	0.052	0.029	0.055	0.055	0.029	0.055	
0.4	0.065	0.023	0.105	0.061	0.034	0.020	0.006	0.062	0.035	0.065	0.065	0.035	0.065	
0.45	0.068	0.025	0.130	0.070	0.039	0.021	0.008	0.077	0.040	0.080	0.080	0.040	0.080	
0.5	0.076	0.026	0.160	0.080	0.045	0.022	0.010	0.096	0.046	0.099	0.099	0.046	0.099	
0.55	0.079	0.027	0.193	0.085	0.048	0.022	0.012	0.117	0.050	0.119	0.119	0.050	0.119	
0.6	0.083	0.027	0.225	0.090	0.051	0.023	0.015	0.138	0.053	0.140	0.140	0.053	0.140	
0.65	0.085	0.029	0.253	0.096	0.055	0.025	0.017	0.156	0.057	0.158	0.158	0.057	0.158	
0.7	0.090	0.031	0.281	0.101	0.057	0.027	0.019	0.174	0.060	0.176	0.176	0.060	0.176	
0.75	0.097	0.033	0.311	0.104	0.059	0.028	0.021	0.193	0.063	0.195	0.195	0.063	0.195	
0.8	0.103	0.035	0.339	0.107	0.061	0.030	0.023	0.210	0.065	0.212	0.212	0.065	0.212	
0.85	0.113	0.037	0.362	0.113	0.065	0.031	0.024	0.225	0.069	0.227	0.227	0.069	0.227	
0.9	0.123	0.039	0.384	0.116	0.067	0.033	0.026	0.239	0.071	0.241	0.241	0.071	0.241	
0.95	0.130	0.040	0.402	0.120	0.069	0.034	0.027	0.251	0.074	0.253	0.253	0.074	0.253	
1	0.137	0.041	0.418	0.127	0.073	0.035	0.028	0.261	0.078	0.263	0.263	0.078	0.263	

Table A.23: IDA for both components of the 244 record.

	Earthquake component												TOTAL DRIFT		
	X		Y				X				Y				
	ROOF DISPLACEMENT		X		Y		X		Y		X _{tot}	Y _{tot}			
Sa	Y	X	Y	X	Y	X	Y	X	Y	X	Y	X	Y	X _{tot}	Y _{tot}
0.05	0.020	0.006	0.021	0.005	0.001	0.004	0.000	0.013	0.001	0.013	0.001	0.001	0.013	0.001	0.013
0.1	0.031	0.009	0.034	0.010	0.003	0.009	0.001	0.021	0.001	0.021	0.003	0.003	0.023	0.003	0.023
0.15	0.039	0.013	0.046	0.016	0.005	0.013	0.002	0.029	0.002	0.029	0.005	0.005	0.030	0.005	0.030
0.2	0.043	0.016	0.054	0.021	0.007	0.017	0.003	0.034	0.003	0.034	0.008	0.008	0.036	0.008	0.036
0.25	0.053	0.018	0.062	0.026	0.009	0.022	0.003	0.039	0.003	0.039	0.009	0.009	0.043	0.009	0.043
0.3	0.064	0.021	0.070	0.031	0.010	0.026	0.004	0.045	0.004	0.045	0.011	0.011	0.047	0.011	0.047
0.35	0.077	0.021	0.077	0.039	0.010	0.033	0.004	0.049	0.004	0.049	0.011	0.011	0.055	0.011	0.055
0.4	0.092	0.022	0.088	0.039	0.010	0.033	0.005	0.056	0.005	0.056	0.012	0.012	0.065	0.012	0.065
0.45	0.106	0.024	0.103	0.043	0.012	0.036	0.006	0.066	0.006	0.066	0.013	0.013	0.080	0.013	0.080
0.5	0.117	0.026	0.115	0.046	0.013	0.039	0.007	0.073	0.007	0.073	0.015	0.015	0.099	0.015	0.099
0.55	0.128	0.028	0.123	0.046	0.014	0.038	0.008	0.078	0.008	0.078	0.016	0.016	0.119	0.016	0.119
0.6	0.140	0.030	0.135	0.046	0.016	0.039	0.008	0.086	0.008	0.086	0.018	0.018	0.140	0.018	0.140
0.65	0.129	0.033	0.128	0.050	0.017	0.042	0.008	0.082	0.008	0.082	0.019	0.019	0.158	0.019	0.158
0.7	0.133	0.036	0.129	0.053	0.019	0.044	0.008	0.082	0.008	0.082	0.021	0.021	0.176	0.021	0.176
0.75	0.135	0.038	0.137	0.055	0.020	0.047	0.009	0.087	0.009	0.087	0.022	0.022	0.195	0.022	0.195
0.8	0.137	0.041	0.145	0.060	0.022	0.050	0.009	0.093	0.009	0.093	0.024	0.024	0.212	0.024	0.212
0.85	0.140	0.043	0.155	0.064	0.023	0.054	0.010	0.098	0.010	0.098	0.025	0.025	0.227	0.025	0.227
0.9	0.144	0.045	0.165	0.067	0.024	0.057	0.011	0.105	0.011	0.105	0.027	0.027	0.241	0.027	0.241
0.95	0.147	0.047	0.174	0.070	0.025	0.059	0.011	0.111	0.011	0.111	0.028	0.028	0.253	0.028	0.253
1	0.154	0.049	0.186	0.075	0.026	0.063	0.012	0.118	0.012	0.118	0.029	0.029	0.263	0.029	0.263

Table A.24: Exact IDA for the records considered

S _a	295		239		123		336		536	
	X	Y	X	Y	X	Y	X	Y	X	Y
0.05	0.0017	0.0119	0.0067	0.0130	0.0054	0.0114	0.0066	0.0123	0.0017	0.0087
0.1	0.0026	0.0188	0.0142	0.0226	0.0102	0.0177	0.0128	0.0197	0.0030	0.0152
0.2	0.0058	0.0405	0.0272	0.0338	0.0193	0.0304	0.0240	0.0506	0.0054	0.0229
0.3	0.0090	0.0631	0.0410	0.0523	0.0290	0.0458	0.0357	0.0816	0.0079	0.0381
0.4	0.0108	0.0875	0.0589	0.0765	0.0384	0.0609	0.0502	-0.1119	0.0101	0.0554
0.5	0.0142	0.1108	0.0672	0.1018	0.0482	0.0788	0.0610	0.1518	0.0121	0.0697
0.6	0.0121	0.1267	0.0901	0.1256	0.0618	0.1008	0.0707	0.1789	0.0149	0.0651
0.7	0.0138	0.1363	0.0987	0.1538	0.0717	0.1120	0.0833	0.2209	0.0157	0.0764
0.8	0.0151	0.2054	0.1177	0.1841	0.0867	0.1394	0.0944	0.2538	0.0189	0.0927
0.9	0.0190	0.2719	0.1454	0.2143	0.1031	0.1537	0.1068	0.2815	0.0198	0.0701
1	0.0215	0.3414	0.1641	0.2456	0.1189	0.1834	0.1191	0.3038	0.0252	0.0824

Table A.25: Exact IDA for the records considered (cont.)

Sa	6264		196		947		595		244	
	X	Y	X	Y	X	Y	X	Y	X	Y
0.05	0.0016	0.0096	0.0048	0.0100	0.0026	0.0087	0.0030	0.0127	0.0021	0.0095
0.1	0.0025	0.0137	0.0083	0.0147	0.0049	0.0134	0.0043	0.0187	0.0038	0.0163
0.2	0.0035	0.0223	0.0185	0.0366	0.0085	0.0201	0.0072	0.0362	0.0075	0.0336
0.3	0.0046	0.0325	0.0298	0.0590	0.0113	0.0299	0.0096	0.0469	0.0116	0.0438
0.4	0.0063	0.0427	0.0485	0.1037	0.0144	0.0385	0.0138	0.0572	0.0144	0.0528
0.5	0.0085	0.0540	0.0545	0.1098	0.0173	0.0469	0.0211	0.0544	0.0168	0.0533
0.6	0.0107	0.0659	0.0707	0.1092	0.0201	0.0502	0.0138	0.0571	0.0185	0.0558
0.7	0.0126	0.0719	0.0845	0.1439	0.0230	0.0578	0.0250	0.0784	0.0196	0.0758
0.8	0.0148	0.0862	0.1013	0.1925	0.0259	0.0650	0.0283	0.0827	0.0210	0.0752
0.9	0.0167	0.0930	0.1120	0.1992	0.0276	0.0715	0.0284	0.1370	0.0231	0.0944
1	0.0184	0.0941	0.1340	0.2401	0.0308	0.0902	0.0291	0.1318	0.0266	0.1209

Bibliography

- [1] Thierry Camelbeeck, Kris Vanneste, and Pierre Alexandre. L'europe occidentale n'est pas a' l'abri d'un grand tremblement de terre. *Ciel et Terre*.
- [2] Paul Melchior. *Seismic activity in Western Europe: with particular consideration to the Liège earthquake of November 8, 1983*, volume 144. Springer Science & Business Media, 2012.
- [3] JD Renard. Seismic reassessment of the structures of the tihange 1 nuclear power plant. *WORKING MATERIAL*, page 659, 1993.
- [4] Price Code. Eurocode 8: Design of structures for earthquake resistance-part 1: general rules, seismic actions and rules for buildings. 2005.
- [5] British Standard. Eurocode 8: Design of structures for earthquake resistance. *Part, 1:1998-1*, 2005.
- [6] G Michele Calvi, Rui Pinho, Guido Magenes, Julian J Bommer, L Fernando Restrepo-Vélez, and Helen Crowley. Development of seismic vulnerability assessment methodologies over the past 30 years. *ISET journal of Earthquake Technology*, 43(3):75-104, 2006.
- [7] Carlos Bhatt and Rita Bento. Comparison of nonlinear static methods for the seismic assessment of plan irregular frame buildings with non seismic details. *Journal of Earthquake Engineering*, 16(1):15-39, 2012.
- [8] Maja Kreslin and Peter Fajfar. The extended n2 method considering higher mode effects in both plan and elevation. *Bulletin of Earthquake Engineering*, 10(2):695-715, 2012.
- [9] Anil K Chopra and Rakesh K Goel. A modal pushover analysis procedure for estimating seismic demands for buildings. *Earthquake Engineering & Structural Dynamics*, 31(3):561-582, 2002.
- [10] Miriam Colombi, Barbara Borzi, Helen Crowley, Mauro Onida, Fabrizio Meroni, and Rui Pinho. Deriving vulnerability curves using italian earthquake damage data. *Bulletin of Earthquake Engineering*, 6(3):485-504, 2008.

- [11] Robert V Whitman, John W Reed, and ST Hong. Earthquake damage probability matrices. In *Proceedings of the Fifth World conference on earthquake engineering*, volume 2, pages 2531–2540. Rome, Italy: Palazzo DEI CONGRESSI (EUR), 1973.
- [12] F Braga, M Dolce, and D Liberatore. A statistical study on damaged buildings and an ensuing review of the msk-76 scale. In *Proceedings of the 7th European Conference on Earthquake Engineering, Athens*, volume 7, pages 431–450, 1982.
- [13] Sonia Giovinazzi and Sergio Lagomarsino. Una metodologia per l’analisi di vulnerabilità sismica del costruito. In *Proceedings of the X Congresso Nazionale on L Ingegneria Sismica in Italia, Potenza-Matera, Italy, Paper*, number 121, 2001.
- [14] RJS Spence, AW Coburn, A Pomonis, and S Sakai. Correlation of ground motion with building damage: the definition of a new damage-based seismic intensity scale. In *Proceedings of the Tenth World Conference on Earthquake Engineering, Madrid, Spain*, volume 1, pages 551–56, 1992.
- [15] Giampiero Orsini. A model for buildings’ vulnerability assessment using the parameterless scale of seismic intensity (psi). *Earthquake Spectra*, 15(3):463–483, 1999.
- [16] F Sabetta, A Goretti, and A Lucantoni. Empirical fragility curves from damage surveys and estimated strong ground motion. In *11th European Conference on Earthquake Engineering*, number 3, 1998.
- [17] T Rossetto and A Elnashai. Derivation of vulnerability functions for european-type rc structures based on observational data. *Engineering structures*, 25(10):1241–1263, 2003.
- [18] Masanobu Shinozuka, Stephanie E Chang, Ronald T Eguchi, Daniel P Abrams, Howard HM Hwang, and Adam Rose. Advances in earthquake loss estimation and application to memphis, tennessee. *Earthquake Spectra*, 13(4):739–758, 1997.
- [19] Ajay Singhal and Anne S Kiremidjian. Method for probabilistic evaluation of seismic structural damage. *Journal of Structural Engineering*, 122(12):1459–1467, 1996.
- [20] Mauro Dolce, Angelo Masi, Maria Marino, and Marco Vona. Earthquake damage scenarios of the building stock of potenza (southern italy) including site effects. *Bulletin of Earthquake Engineering*, 1(1):115–140, 2003.
- [21] Gian Michele Calvi. A displacement-based approach for vulnerability evaluation of classes of buildings. *Journal of Earthquake Engineering*, 3(03):411–438, 1999.

-
- [22] Comité Européen De Normalisation. Eurocode 8—design of structures for earthquake resistance—part 1: General rules, seismic actions and rules for buildings. *European Standard NF EN*, 1:2005, 1998.
- [23] FEMA Mitigation Directorate. Hazus® 99 estimated annualized earthquake losses for the united states. *Washington, DC: Federal Emergency Management Agency*, 2001.
- [24] Masanobu Shinozuka, Maria Q Feng, Ho-Kyung Kim, and Sang-Hoon Kim. Nonlinear static procedure for fragility curve development. *Journal of engineering mechanics*, 126(12):1287–1295, 2000.
- [25] Anil K Chopra et al. *Dynamics of structures*, volume 3. Prentice Hall New Jersey, 1995.
- [26] Peter Fajfar et al. Capacity spectrum method based on inelastic demand spectra. *Earthquake engineering and structural dynamics*, 28(9):979–994, 1999.
- [27] Juan C Reyes and Anil K Chopra. Three-dimensional modal pushover analysis of buildings subjected to two components of ground motion, including its evaluation for tall buildings. *Earthquake Engineering & Structural Dynamics*, 40(7):789–806, 2011.
- [28] Anil K Chopra and Chatpan Chintanapakdee. Inelastic deformation ratios for design and evaluation of structures: single-degree-of-freedom bilinear systems. *Journal of structural engineering*, 130(9):1309–1319, 2004.
- [29] Sigmund A Freeman. Development and use of capacity spectrum method. In *Proceedings of the 6th US national conference on earthquake engineering*. EERI Seattle, WA, 1998.
- [30] H Krawinkler. New trends in seismic design methodology. In *New trends in seismic design methodology*. EUROPEAN CONFERENCE ON EARTHQUAKE ENGINEERING, 1995.
- [31] Tomaž Vidic, Peter Fajfar, and Matej Fischinger. Consistent inelastic design spectra: strength and displacement. *Earthquake Engineering & Structural Dynamics*, 23(5):507–521, 1994.
- [32] Prestandard FEMA. Commentary for the seismic rehabilitation of buildings. *FEMA-356, Federal Emergency Management Agency, Washington, DC*, 2000.
- [33] Akshay Gupta and Helmut Krawinkler. *Seismic demands for the performance evaluation of steel moment resisting frame structures*. PhD thesis, Stanford University Stanford, California, 1999.
- [34] Chiara Smerzini, Carmine Galasso, Iunio Iervolino, and Roberto Paolucci. Ground motion record selection based on broadband spectral compatibility. *Earthquake Spectra*, 30(4):1427–1448, 2014.

- [35] Masanobu Shinozuka, Maria Q Feng, Jongheon Lee, and Toshihiko Naganuma. Statistical analysis of fragility curves. *Journal of engineering mechanics*, 126(12):1224–1231, 2000.
- [36] Oreste S Bursi and David Wagg. *Modern testing techniques for structural systems: dynamics and control*, volume 502. Springer Science & Business Media, 2009.
- [37] Dimitrios Vamvatsikos and C Allin Cornell. Incremental dynamic analysis. *Earthquake Engineering & Structural Dynamics*, 31(3):491–514, 2002.
- [38] Paolo Bazzurro, C Allin Cornell, Nilesh Shome, and Jorge E Carballo. Three proposals for characterizing mdof nonlinear seismic response. *Journal of Structural Engineering*, 124(11):1281–1289, 1998.
- [39] NN Ambraseys, J Douglas, B Margaris, R Sigbjörnsson, P Smit, and P Suhadolc. Isesd—internet site for european strong-motion data, 2002.
- [40] Oh-Sung Kwon and Amr Elnashai. The effect of material and ground motion uncertainty on the seismic vulnerability curves of rc structure. *Engineering structures*, 28(2):289–303, 2006.
- [41] Dimitrios Vamvatsikos and C Allin Cornell. Incremental dynamic analysis. *Earthquake Engineering & Structural Dynamics*, 31(3):491–514, 2002.